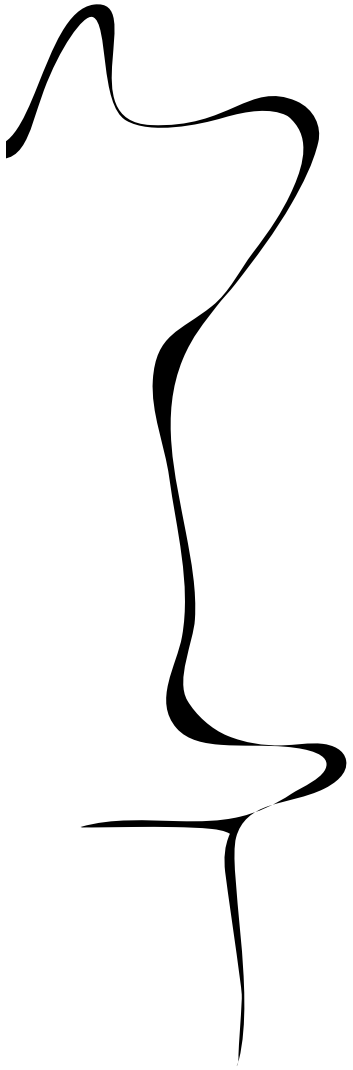


UNIVERSITY OF TWENTE.

Faculty of Science and Technology

Using lung-on-a-chip model to study the differences in translocation of nanoplastics through lung epithelium



Edward Katgert
Bachelor thesis
August 2, 2021



Supervisors:

prof. dr. ir. S. Le Gac

dr. ir. K.M. Pondman

dr. K. Broersen

AMBER Group

Faculty of Science and Technology

Biomedical Engineering

Abstract

Plastic pollution is a problem from the modern era, studies have found that plastics can be broken down via bio and non-biodegradation into small sizes of plastics, called nanoplastics and microplastics. These plastics can travel through air and end up in the human lungs. Possible effects of presence of these plastics in the lungs are inflammation reactions, oxidative stress and immune dysfunction. In this study we will focus on nanoplastics which have proven to be able to be taken up through active and passive transport in alveolar epithelium. The aims of this research are to build a lung-on-a-chip which mimics the alveolar structure and has Collagen 1 as a foundation. The other aim is to examine whether and how nanoplastics could transfer through tubular alveolar epithelium in the established device. At last, we want to determine if nanoplastics could disturb the tight junctions of alveolar epithelium, since this has not been researched for a tubular alveolar epithelial structure.

The device that is used in this research was made from polydimethylsiloxaan which is a soft elastomer after curing in a 3D printed mold. After, inlets and outlets were punched and the chip was prepared for cell seeding of Calu-3 and A549 cells and incubation of green fluorescent nanoplastics with the sizes 50 and 100 nm. The following concentrations of nanoplastics were used 10, 100 and 1000 $\mu\text{g}/\text{mL}$. Staining the nuclei, cell membrane and ZO-1 proteins resulted in determination of where the nanoplastics had traveled to in the device.

Samenvatting

Plasticvervuiling is een probleem uit de moderne tijd, studies hebben uitgewezen dat plastic via biologische- en niet-biologische afbraak kan worden afgebroken tot kleine stukjes plastic, nanoplastics en microplastics genoemd. Deze plastics kunnen zich door de lucht verplaatsen en in de longen van de mens terecht kunnen komen. Mogelijke effecten van de aanwezigheid van deze plastics in de longen zijn ontstekingsreacties, oxidatieve stress en immuundisfunctie. In dit onderzoek zullen we ons richten op nanoplastics waarvan is aangetoond dat ze door actief en passief transport in alveolaire epitheelcellen kunnen worden opgenomen. De doelstellingen van dit onderzoek zijn het bouwen van een long-op-een-chip apparaat dat de alveolaire structuur nabootst en Collageen 1 als basis heeft. Het andere doel is na te gaan of en hoe nanoplastics door tubulair alveolair epitheel kunnen worden getransporteerd in de gebouwde chip. Tenslotte willen we bepalen of nanoplastics de tight junctions van het alveolair epithelium kunnen verstoren, aangezien dit nog niet is onderzocht voor een tubulaire alveolaire epitheliale structuur.

The chip dat in dit onderzoek is gebruikt, wordt gemaakt van polydimethylsiloxaan, een zacht elastomeer dat na uitharding in een 3D-geprinte mal is geprint. Daarna werden ingangen en uitgangen geponst en werd de chip voorbereid voor het zaaien van A549-cellen en incubatie van groen fluorescerende nanoplastics met de afmetingen 50 en 100 nm. De volgende concentraties nanoplastics werden gebruikt 10, 100 en 1000 $\mu\text{g}/\text{mL}$. Door kleuring van de kernen, het celmembraan en de ZO-1 eiwitten kon worden bepaald waar de nanoplastics naartoe waren verplaatst.

Contents

1	Introduction	4
1.1	Nanoplastics in the environment and their impact on the human health	4
1.2	Translocation mechanisms of nanoplastics	5
1.3	Lung-on-a-chip models	6
1.4	Types of alveolar epithelial cell types	7
1.5	Research goals	8
2	Materials and methods	9
2.1	Fabrication of the PDMS device	9
2.2	Lumen formation: viscous finger patterning technique (VFPT)	9
2.3	Cell culture in culture flasks	10
2.4	Seeding cells in the chip	11
2.5	Optimisation of the tubular structure from Calu-3 and A549 cells	11
2.6	Determining adherence time of A549 cells	11
2.7	Nanoplastic exposure to A549 cells	11
2.7.1	Preparation of nanoplastics	11
2.7.2	Cell seeding, addition of nanoplastics and staining of cells	12
3	Results	14
3.1	Optimisation of the tubular cell structure	14
3.2	Determine adherence time of A549 cells	16
3.3	Nanoplastic exposure	17
3.3.1	Differences in viability of A549 cells after exposure to nanoplastics	17
3.3.2	Translocation of nanoplastics in the channels and the well plate	18
4	Discussion	23
4.1	Overlapping spectra of the stains	23
4.2	Compromises of the lung-on-a-chip	25
4.3	Translocation mechanisms of NPs	25
4.4	Determining viability in a more specific way	27
4.5	Future perspectives and recommendations	27
5	Conclusion	28
6	Acknowledgements	29
	References	30
A	Appendix	34

1 Introduction

1.1 Nanoplastics in the environment and their impact on the human health

Globally, plastics are extremely popular for their use in a lot of products like packaging material and clothing, which are discarded after use. Governments try to persuade people to separate plastic waste, but only 9% of plastics ever made has been recycled and 60% has been dumped [1]. It is estimated that if we continue to use plastics until 2050, we will have discarded 12,000 million metric tons of plastic waste in landfills or in the natural environment [2]. Plastic waste that is not disposed correctly often ends up in the nature and gets broken down via biodegradation and/or non-biodegradation into smaller particles. Examples for biodegradation and/or non-biodegradation are UV light, wind and mechanical abrasion. If waited long enough microplastics (MPs) and nanoplastics (NPs) occur which present respectively a diameter of smaller than 5 mm and 0.1 μm [3]. These plastics are very light, can easily travel by wind and be inhaled in the human lungs. In fact, Parisian atmosphere research has shown that plastics with sizes from 50 nm to 1400 nm were present in the form of fibers [4]. In other cities, sizes varied from 2 nm to 5000 nm and shapes differed from fibers, fragments, films and foams/granules. Most found materials were polyethylene terephthalate (PET), polyvinyl chloride (PVC), polyethylene (PE), ethylvinyl acetate (EVA) copolymers and polystyrene (PS) which originated from plastic items like bottles, bags and clothing. It has been shown that PS can translocate through rat alveolar epithelial cells and cause damage to intracellular structures [5] [6]. In general, particles smaller than 10 μm can end up in the alveolar region [7]. MPs and NPs can, depending on size and shape be taken up into circulation, see figure 1. A lot of factors can affect absorption of plastic particles into the human body, like their size, density, surface charge and hydrophobicity and the smaller the particles the better they are distributed in the body [4]. Particles which are larger than 10 μm are mostly filtered by the nasal and upper respiratory tract, particles with a diameter of around 100 nm are deposited in the alveolar region and particles of around 1 nm in the tracheobronchial region. Particles with a diameter between 1 and 100 nm tend to behave like gas molecules, which makes it easy for them to end up in the alveolar region and affect the gas exchange. If these particles end up in the lungs, they can also damage them as was researched in animals [8]. For this reason we elaborate further on the effect of NPs on alveolar epithelial cells.

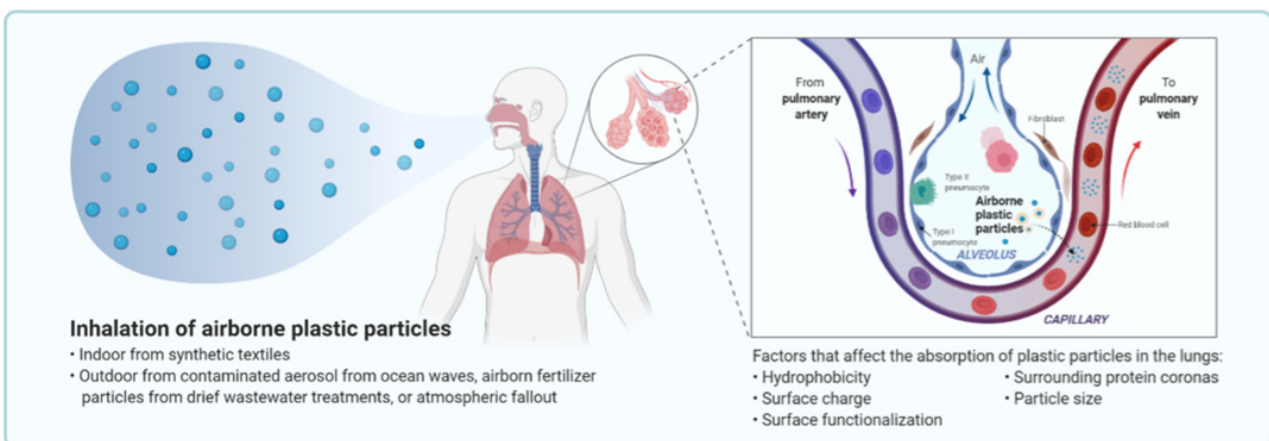


Figure 1: Inhalation route that plastic particles take from the air to the blood, picture was taken from [3]. Airborne MPs and NPs enter the lungs through the mouth, nose and trachea and are filtered according to their size. Particles larger than 10 μm are filtered by nose, cilia and mucous membranes and due to their larger size they remain most of the time in the upper respiratory tract. Coughing and sneezing eliminates these particles, but particles smaller than 10 μm end up in the alveoli.

Observational studies state that dyspnea is one of the consequences of MPs [8]. Other effects of exposure to MPs and NPs for the alveolar epithelium are asthma, wheezing and coughing [4].

These consequences are due to dust overload, oxidative stress, cytotoxicity and translocation [8]. Research done by Dong et al. found that the effect of plastics on human cells were inflammation reactions. Tissue necrosis factor- α (TNF- α) and IL-8 expression had risen in A549 human lung cells with addition of larger particles (202 nm and 535 nm) when compared to smaller particles (64 nm). IL-6 and IL-8 expression also rose according to increasing concentration for normal lung BEAS-2B cells [9]. Exposure to high concentrations of PS MPs has been reported to increase the risk for chronic obstructive pulmonary disease (COPD), meanwhile low concentrations can disrupt the pulmonary barrier by phosphorylating zonula occludens (ZO) proteins which decreases the functionality of the barrier tightness [9]. Another problem is that plastics contain chemicals or additives which can leach into organs and tissues with possibly even worse consequences, like endocrine disruption [3].

1.2 Translocation mechanisms of nanoplastics

Translocation of NPs through the alveolar epithelium may occur in three ways. The first one is via phagocytosis, since macrophages are the first line of defence against for example NPs. Macrophages generally clear surfactants and cell debris from lung surface. So, NPs could be phagocytized; however NPs which are not removed by macrophages remain in the alveoli and could be taken up by the alveolar epithelium. So, the second way of uptake is endocytosis and via diffusion [10]. The third way of translocation is via paracellular transport through disrupted tight junctions [10]. However, there has been no research done on this topic with alveolar epithelial cells, but it was done on intestinal cells where was seen that tight junctions were disturbed which led to a higher permeability. Research done by Zhang et al. in mouse models with 50 and 500 nm NPs in intestinal cells resulted in an increase of reactive oxygen species (ROS) and apoptosis for 50 nm NPs compared to 500 nm NPs [11]. This caused a higher cell membrane permeability and more translocation of 50 nm than 500 nm NPs through the intestinal barrier. Mahler et al. did transepithelial electrical resistance (TEER) measurements in which they found that respectively low (2×10^9 and 1.25×10^8 nm particles/mL) and medium (2×10^{11} and 1.25×10^{10} nm particles/mL) concentrations of 50 and 200 nm PS NPs would not decrease TEER values, but high concentrations (2×10^{13} and 1.25×10^{12} nm particles/mL) would [12]. This means that the permeability of the intestinal barrier was higher for high concentrations of NPs. Paracellular translocation of NPs was investigated for alveolar type 1 cells, but tight junctions were not disrupted and NPs did not reach further than the apical side regarding 50 and 100 nm NPs which had no functionalization or carboxyl- and amine-groups at the NPs [10]. Overall, literature stated that 60 nm PS NPs were cytotoxic in BEAS-2B cells from a concentration higher than 10 $\mu\text{g/mL}$ [13]. Also, 44 and 100 nm PS NPs with a 10 $\mu\text{g/mL}$ concentration in gastric cells were observed to have respectively lower viability and higher viability. A minor cytotoxicity was observed for 50 and 100 nm PS NPs at a concentration of 100 $\mu\text{g/mL}$. Mixtures of NPs sizes made a difference in translocation rates, because a higher amount of ROS was generated when 50 and 500 nm PS NPs were introduced to the intestinal barrier of mouse. This resulted in apoptosis and severely damaged and dysfunctional intestine which in turn increased absorption rates of NPs of 50 and 500 nm in size [11].

Surface modification of polystyrene

PS with surface modification has been used widely for research on uptake of NPs by macrophages or epithelial cells. There are a few surface modifications for PS possible, like amino groups (cationic) or carboxyl groups (anionic) to the NPs [10]. Uptake by alveolar type 1 cells of amine-modified polystyrene NPs (amine PS) was the highest and unmodified polystyrene NPs (unmodified PS) had the lowest uptake, see figure 2. However, the disadvantage of amine PS is that it was able to create holes in the cell membrane of alveolar type 1 cells [14]. Since we are interested if translocation of NPs could happen through tight junctions, carboxyl-modified polystyrene (carboxyl PS) NPs are a good compromise between the unmodified PS and amine PS NPs, because its greater uptake tends to give a higher chance to be monitored as compared

to unmodified PS. Also, there seems to be no negative influence from carboxyl PS known in literature. As for amine PS, it can create holes in cells which would interfere with our experiment to discover whether NPs could disturb tight junctions.

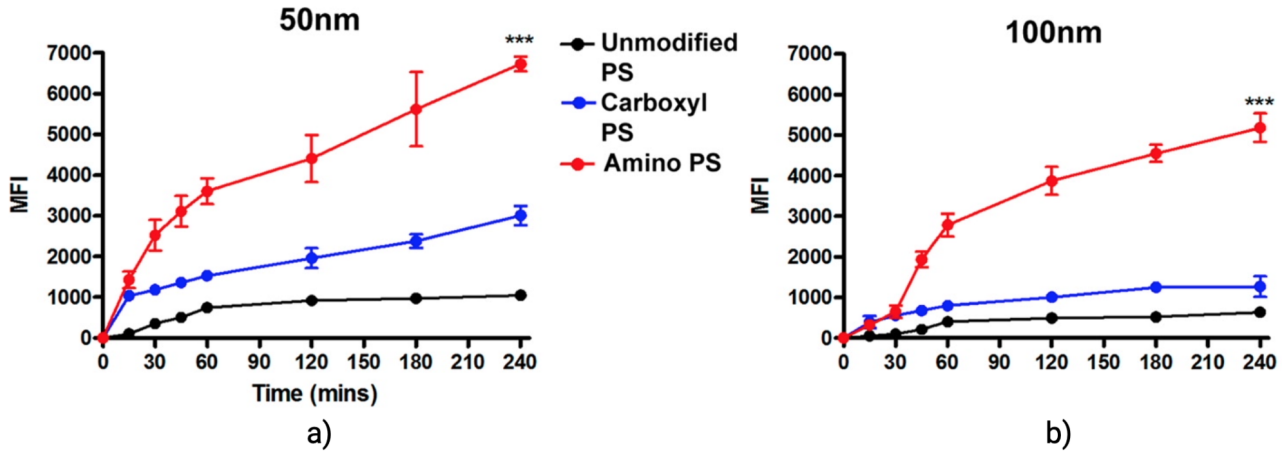


Figure 2: Image was reprinted from [10]. Amine PS NPs are internalized to a greater degree and faster than carboxyl or unmodified PS NPs for the sizes 50 nm 100 nm. Also, 50 nm NPs are more internalized than 100 nm NPs. It is hypothesised that 50 nm PS NPs are able to translocate via passive diffusion and endocytosis, whereas 100 nm PS NPs largely translocate via endocytosis [10].

1.3 Lung-on-a-chip models

Not long ago cell culture experiments were only done using 2D models, but with modern innovations models have evolved to be more realistic and to support for instance mechanical stress and/or fluid flows [15]. Fluidical shear stresses for instance provide a more realistic model of for example uptake through cells, because lack of flow can cause NPs to sediment on the epithelial layer which could increase NP uptake and is less realistic in that way [16]. Some chips have proven its advantage over 2D models, for instance drugs responsiveness was more realistic and signalling pathways could be captured better. Lung-on-a-chip models are small devices that operate using microfluidics to mimic the physiological environment and cellular architecture of the lung. These devices are relatively new and are constantly being tailored to the desired form and function to mimic specific disease condition [17]. These chips used to be made from glass and silicon, but silicon is optically opaque and expensive and glass can be difficult to form a chip with, since it has to be molten before it can be put in a mold. Nowadays, soft lithography using poly-dimethylsiloxane (PDMS) is used to form chips. It is optically transparent, has a low toxicity, is a soft elastomer and has a high permeability for O₂ and CO₂.

Two types of models for a lung-on-a-chip

There are different lung-on-a-chip models, an example is the model that has been developed by the Wyss Institute which has lung cells on one side of the membrane and capillary cells on the other side. These cells are grown on a porous elastomere membrane. Stretching of cells like in human alveoli is mimicked with stretching of this membrane, which is realised by the cyclic pumping vacuum channels at the sides of the membrane, see figure 3 [17]. This stretching movement is important, since stretching of human alveolar epithelial cells led to a greater uptake of 12 nm silica nanoparticles compared to a static experiment [18]. Marcinkiewicz et al. determined that surfactant proteins in air-liquid interface culture systems remained at the same level, meanwhile these proteins dissipated over time for submerged culture systems [19]. The presence of surfactants on the cells plays an important role in NP uptake as will be discussed in the paragraph *Types of alveolar epithelial cell types*. At the AMBER group at the University of Twente a chip with 5 channels is used for research on tubular alveolar epithelium, see figure 4b in the *Materials and Methods*. In research, most often non biological materials are used to grow cells on, like growing cells on a plastic petridish, but behaviour of cells can change significantly

when Collagen 1 is used as a basis for the cells to grow on. Collagen is a representative material to let the cells grown on, since it is a very important and frequent protein in extracellular matrices [20]. Collagen 1 and the viscous finger patterning technique (discussed in paragraph *Lumen formation: viscous finger patterning technique (VFPT)*) are used to create the curvature and natural environment which is present in alveoli. At the AMBER group the choice is made to only look at translocation of NPs through epithelial cells. If indeed a whole lung model needs to be made, the model from the Wyss Institute could be representative because its support for natural stretching of cells. However, since an artificial membrane is being used for that model, cells are not growing on the same surface which they are used to grow on. This is however the case for the model from the AMBER group, next to that cells are submerged in culture medium.

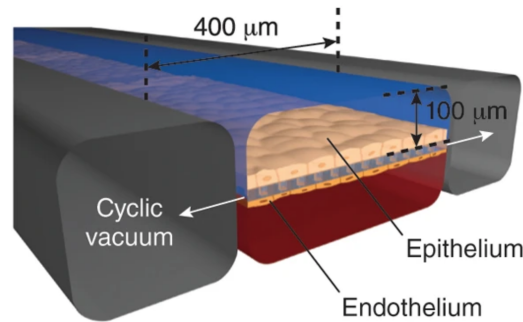


Figure 3: Image was reprinted from [15]. Lung-on-a-chip model created by the Wyss Institute; this chip contains alveolar cells on one side of the membrane and endothelial cells on the other side. Cyclic stretching is provided through vacuum chambers on both sides to create a more realistic lung-on-a-chip model [15].

1.4 Types of alveolar epithelial cell types

As mentioned by Foster et al. a healthy alveolar epithelium is made up of multiple cell types and contains pore sizes ranging from 2.6 to 87 Å. Other studies even suggested the presence of pores larger than 80 Å that are used for the diffusion of large molecules. This means that human alveolar epithelium is very complex to recreate. Taking this information, we looked at cell types that can mimic the alveolar epithelial barrier and narrowed it down to a few cell types that are often used in vitro to create a representative model including uptake of NPss of the alveolar epithelium, like A549, 16HBE and Calu-3 cells [21]. Calu-3 cells tend to form a stronger monolayer than 16HBE and A549 cells as was proven with TEER experiments, they were also seeded in a static channel [22] [23] [24]. However, the A549 cells have a faster growth rate than Calu-3 cells [25]. If we look at the uptake of NPs a difference can be seen between alveolar cell types I and II, since the first cell type had proven to take up significant amounts of NPs, while uptake in the second cell type was nearly undetectable [10] [23]. However, alveolar type I cells cover around 96% of the surface area of the alveolar epithelium, meanwhile type II cells are present in a larger number and have functions, like producing surfactants [26] [27]. Bonding of opsonizing SP-A and SP-D surfactant to nanoparticles has shown to be important for the uptake of nanoparticles, since magnetite nanoparticles that were treated with surfactant SP-A gave an increase in uptake by alveolar macrophages [28]. In a study that has been done by Radiom et al. was found that due to pulmonary surfactants uptake of positively charged silica nanoparticles in A549 cells was reduced by an order of two [29]. One could suggest that in a more realistic setting A549 cells are cocultured with alveolar macrophages. This has been done by Rothen-Rutishauser et al.; they discovered that the uptake of 1 µm nanoparticles was greater for alveolar macrophages than A549 cells [30]. They saw that particles which were not removed by alveolar macrophages were taken up by A549 cells; 24 hours later more nanoparticles were found in alveolar macrophages and A549 cells.

1.5 Research goals

Modern technologies give us the opportunity to create a lung-on-a-chip that has a foundation which cells are used to grow on, namely collagen. Moreover, the chip has a channel in which the cells can grow. With the natural foundation and curvature of the channel, cells are given the opportunity to grow and behave in a realistic and natural way. The research question is: How do NPss translocate through alveolar epithelium in a lung-on-a-chip device?

To produce the base of the chip soft lithography with PDMS has to be used. Next, poly-dopamine and Collagen 1 will be added to the channel using the viscous finger patterning technique. Cells have to create a tubular structure in the channels which has to be optimised, so different concentrations per cell type will be used. After a confluent tubular structure is achieved translocation of NPs will have to be analysed, for which we will have to dilute NPs in culture medium with two sizes and three concentrations. The analysis will be done using the Zeiss 880 confocal laser microscope.

2 Materials and methods

The experimental part of this report will be highlighted in this chapter. The way in which the chip is fabricated and how polydopamine and Collagen 1 work together to create a foundation for the cells to bond to will be elaborated. Next optimisation of a tubular structure will be discussed and it will be determined how long A549 cells take to attach to a collagen layer. Finally, the incubation of NPs solution in channels and wells and staining the cells will be discussed.

2.1 Fabrication of the PDMS device

First, a mold with 5 channels with a channel length of 1 cm and a width of 0.6 mm was made using a 3D printer, see figure 4a. Next a mixture of polydimethylsiloxane (PDMS, Sylgard™ 184 Silicone Elastomer base) and hardener (Sylgard™ 184 Silicone Elastomer Curing Agent) was prepared in a volume ratio of 10:1. Air bubbles were removed in the desiccator after thoroughly mixing. Thereafter, PDMS was poured onto the 3D printed mold and put under the desiccator to ensure all air bubbles were removed from the PDMS after which it was put in the oven to cure overnight at 67 °C. The next day inlets and outlets were punched with punchers of, respectively, 1 and 1.5 mm. Finally the PDMS chip and a glass slide were bonded together using air plasma at 500 mTorr, 50 W for 70 s with the Femto Science Cute plasma system. A finished device is shown in figure 4b.

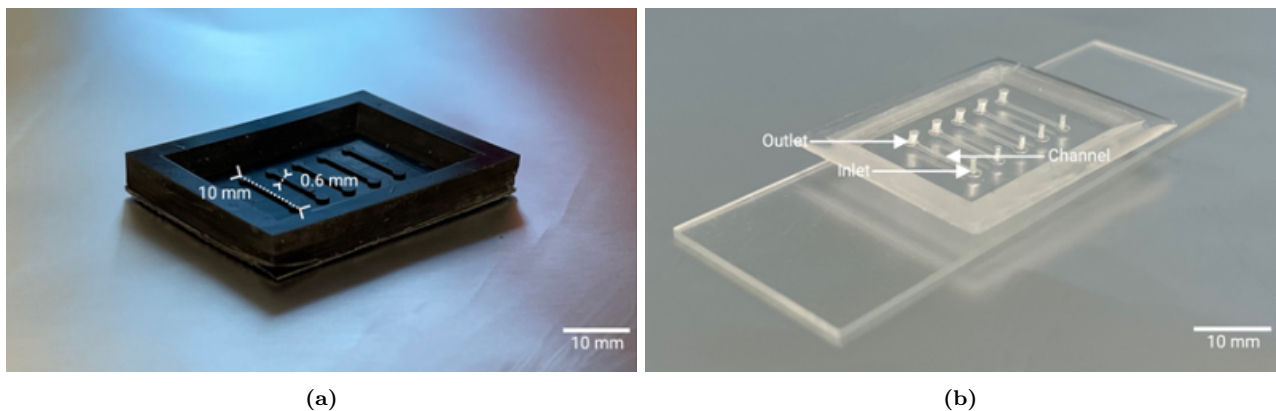


Figure 4: The pictures in figure 4a and 4b were taken from the used 3D printed mold and the PDMS chip bonded on a glass slide. Figure 4a provides the 3D printed mold on which the PDMS is poured and figure 4b shows the PDMS chip on a glass slide after plasma bonding containing inlets, outlets and channels. These images were edited using Biorender.com.

2.2 Lumen formation: viscous finger patterning technique (VFPT)

Since cells had to adhere to a collagen structure which did not bond to the PDMS, channels had to be coated with polydopamine. Next, collagen was added to the channels after which the VFPT was used to create a channel through the collagen. VFPT works following the passive pumping method where the surface energy of a PBS droplet creates a pumping effect which creates a round channel through the added collagen [31]. An overview of the VFPT can be seen in figure 5.

To start, a hydrophilic polydopamine solution was prepared consisting of 2 mg/mL polydopamine (Sigma) mixed in Tris-HCl buffer pH: 8.5 (Sigma). 10 μ L of the solution was added to the channels to ensure droplets were present at the outlets. The channels were then incubated for 30 minutes at room temperature under the flow hood. Demiwater and 70% ethanol were used to wash the channels after which the chip was put in the oven for 1 hour at 67 °C. After, the channels were washed again with ethanol and let air dry. The next step was to form the lumen using a Collagen 1 (Corning) mixture of which the substituents V_f , $V_{PBS,10X}$, $V_{i,collagen}$,

V_{NaOH} , V_{PBS} were calculated using respectively the following formulas 5, 6, 7, 8, 9, where V_f is the total volume of collagen mixture, n_{channels} is the amount of channels that need to be prepared, C_f is the final concentration of Collagen 1 in the mixture for which we used 5 mg/mL and C_i is the initial concentration of the collagen stock which is 10.57 mg/mL. Depending on the amount of channels that needed to be prepared, the final volume and the substituents could be altered to suit the needs. After slowly mixing (Collagen 1 is very viscous) 10 μ L of the collagen mixture was then added to the channels and 20 μ L of 1X Phosphate Buffered Saline (PBS, Gibco) was added to the outlet and 20 μ L of the smallest possible droplets were added drop by drop with a 10 μ L micropipet (Eppendorf) to the inlet following the viscous finger patterning technique. It is important to note that above standing steps need to be finished per channel, since solidification of collagen might occur which would mean that a lumen cannot be created.

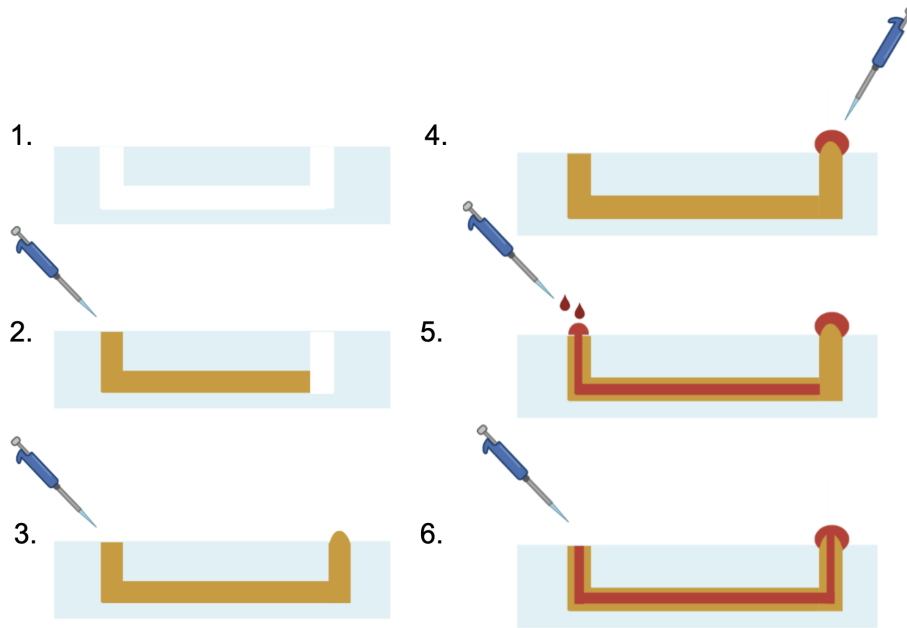


Figure 5: The viscous finger patterning technique is displayed in this scheme. First, we started at step 1 2 where an empty channel was filled with a prepared Collagen 1 mixture. After this, the mixture came out of the outlet at step 3, a PBS droplet was added to the outlet at step 4. Next, small PBS droplets were added to the inlet to create a channel through the collagen using the VFPT. This image was designed by R.P.F.Maia. using Biorender.com.

2.3 Cell culture in culture flasks

Calu-3 cells

Calu-3 cells (gift from RIVM) were cultured and maintained in a T75 cell culture flask (Greiner) with 12 mL Eagle's Minimal Essential Medium (EMEM, Gibco) enriched with 10% FBS (Gibco), 100 units/mL penicillin (Gibco), 100 μ g/mL streptomycin (Gibco) and 200 mM GlutaMAX (Gibco) and medium was refreshed after 3 to 4 days. Incubation happened at 37°C and with 5% CO₂. After the cells had reached 85% confluence medium was removed and cells were washed with 8 mL PBS which was then removed to be substituted with 2 mL 0.25% trypsin (Gibco). The trypsin was incubated less than 5 minutes until cells had come loose and fresh medium was added to neutralise the trypsin. The suspension was centrifuged (Eppendorf Centrifuge 5810 R) at room temperature and 300g for 4 minutes and medium was removed after which enough medium was added to create the desired concentrations. The volume of cell suspension that was not used was put back into culture for future experiments. The total amount of cells in 1 mL of medium was calculated using formula 1, where cells were counted in 4 quadrants of 1 mm² using the Bürker-Türk counting chamber.

$$n_{\text{cells/mL}_{\text{cellsuspension}}} = \frac{n_{\text{cells}/4\text{mm}^2}}{4} \cdot 10000 \quad (1)$$

A549 cells

Culture of A549 cells (ECACC, lot: 14b005) was nearly the same as for the Calu-3 cells, the difference was that A549 cells were cultured in a T175 cell culture flask (Greiner) and they used Dulbecco's Modified Eagle's Medium (DMEM, Gibco) enriched with 10% FBS (Gibco), 100 units/mL penicillin (Gibco), 100 µg/mL streptomycin (Gibco) and 200 mM GlutaMAX (Gibco) as a culture medium. Since A549 cells grew to confluence within 5 days instead of more than a week for Calu-3 cells these were let to grow to 100% confluence instead of 85% from the Calu-3 cells.

2.4 Seeding cells in the chip

Seeding of the chip began with flushing the channels of the chip with the corresponding culture medium after which cell suspension was prepared with the correct concentration (see below) following the method in paragraph *Cell culture in culture flasks*. Subsequently, 5 µL of cell suspension was added to fill the channels. 20 µL drops of medium onto the inlets and outlets prevented the cells from drying. The chip was incubated at 37°C with 5% CO₂ for 24 hours to make sure that the cells were fully adhered to the collagen structure after which the channels were flushed gently with culture medium to ensure adhered cells would not become loose due to too high fluid pressure. Next, cell suspension at the same concentration was added, but now the chip was flipped with the top-side facing downwards to ensure cells would also adhere to the top-side of the channels. The chip was incubated again for 24 hours. The chips with Calu-3 and A549 cells were maintained for respectively three days and six days by changing medium once a day.

2.5 Optimisation of the tubular structure from Calu-3 and A549 cells

Since Calu-3 and A549 cells differ from each other regarding phenotype and growth rate various cell concentrations for both cell lines were tested to see which would give the best achievable tubular structure following the above standing seeding method. For Calu-3 cells concentrations ranging from 1 to 1.5, 4 and 6 million cells/mL were incubated for three days in the channels. For A549 cells concentrations of 1 to 3, 5, 7, 9, 10, 12 and 15 million cells/mL were used and were incubated for six days.

2.6 Determining adherence time of A549 cells

To prevent cells from coming loose as a result of premature rinsing with culture medium it should be determined how long seeded channels need to be incubated per side for the A549 cells to bond to a collagen layer. An experiment was set up where a density of 0.6 million cells/mL was added to a collagen layer in a 96 well cell culture plate F-bottom (Greiner), as a control A549 cells were added to three wells without a layer of collagen. Every hour attachment of the cells was recorded to see after how much time cells would adhere.

2.7 Nanoplastic exposure to A549 cells

2.7.1 Preparation of nanoplastics

Carboxyl-modified Dragon green NPs were ordered from Bangs Laboratories in the sizes 50 ± 10 nm and 100 ± 10 nm, these bottles were placed in an ultrasonic bath for 1 minute before being diluted with culture medium for the A549 cells such that we ended up with the following concentrations C_{NP} : 10, 100 and 1000 µg/mL. The density of polystyrene averages at 1.005 g/cm³ and following formulas were used to determine the quantity of NPs per mL.

$$V_{NP} = \frac{4}{3} \cdot \pi \cdot r_{NP}^3 \quad (2)$$

$$m_{NP} = \rho_{polystyrene} \cdot V_{NP} \quad (3)$$

$$particles/mL = \frac{C_{NP}}{m_{NP}} \quad (4)$$

2.7.2 Cell seeding, addition of nanoplastics and staining of cells

Chip

A549 cells were cultured in duplo in the channels with a concentration of 10 million cells/mL for six days till 'islands' of cells appeared. Subsequently, the 30 channels were washed and the NPs solutions were placed in a glass tube in an ultrasonic bath for 1 minute and were added to fill the channels to be incubated for 24 hours at 37°C with 5% CO₂. Table 1 presents the layout and stains that were used for the chips and well plate. Two types of control were used, the positive control contained cells with 20 ng/mL TNF- α , (Thermo Fisher scientific) in culture medium and was incubated for 30 minutes at 37°C with 5% CO₂. The negative control contained culture medium only. After incubation of NPs channels were washed three times with PBS. Next, to determine the viability of the cells after coming in contact with the NPs half of the chips were stained with the live/dead assay: ethidium homodimer-1 and calcein-AM (Thermo Fisher scientific) which were incubated at 37°C with 5% CO₂ for 30 minutes. Subsequently, since cells were not fixed nuclei were stained using Hoechst solution (Thermo Fisher scientific) for 20 minutes at room temperature. These three stains gave us an indication of the number of cells that were still alive which was expressed in the viability of the cells per condition. The other half of the chips were stained with DID (Thermo Fisher scientific) 1:200 in PBS to stain the cell membranes for 20 minutes. After, cells were fixed with 4% Paraformaldehyde (PFA, Sigma) and incubated for 45 minutes under the flow hood. Cells were washed afterwards with PBS containing 0.25% Triton X-100 (Sigma) and incubated for 10 minutes. Furthermore cells were washed three times with PBS and blocking solution (BSA, Sigma) was incubated in the channels for 20 minutes at room temperature. Afterwards, the ZO-1 proteins were incubated with mouse anti-ZO-1 (Thermo Fisher scientific) which was added in a 1:200 ratio with BSA and incubated overnight at 4°C. Cells were washed three times using PBS and Goat-anti-mouse-Alexa549 (Thermo Fisher scientific) was added in the same 1:200 ratio in BSA and incubated for one hour at room temperature under protected from any light source. Next, cells were washed three times with PBS and since the cells were fixed this time, nuclei were stained using 4',6-diamidino-2-fenylindool (DAPI, Thermo Fisher scientific) in a ratio of 1:100 in BSA and incubated at room temperature for 5 minutes still protected from any light source. Channels and wells were analysed using confocal laser microscopy (Zeis 880) with excitation lasers of 405 (DAPI), 488 (NPs), 561 (ZO-1) and 633 (DID) nm. Detector ranges were respectively 410-520, 493-587, 585-650, 654-710 nm. The natural excitation and emission spectra of each stain can be seen in figure 25. The outline of the nanoplastic experiment is shown in figure 6.

96 Well plate

As a 2D control cells were also seeded in a 96 well plate for three days to ensure a monolayer was created. Afterwards, the same protocol was used here as explained in paragraph [Chip](#).

Table 1: Layout of the nanoplastic densities 10, 100 and 1000 $\mu\text{g}/\text{mL}$ in the sizes of 50 and 100 nm. This duplo experiment was stained with a live/dead assay of ethidium homodimer-1 and calcein-AM, nucleus staining with Hoechst (only for non fixed cells) and DAPI (only for fixed cells). Staining of the cell membrane was done with DID and ZO-1 proteins were stained for the tight junction staining.

	50 nm				100 nm			
Concentration nanoplastics incubated in channels and wells ($\mu\text{g}/\text{mL}$)	10	10	10	10	10	10	10	10
	100	100	100	100	100	100	100	100
	1000	1000	1000	1000	1000	1000	1000	1000

- Live/dead assay (ethidium homodimer-1 + calcein-AM) + Hoechst
- DID + ZO-1 + DAPI

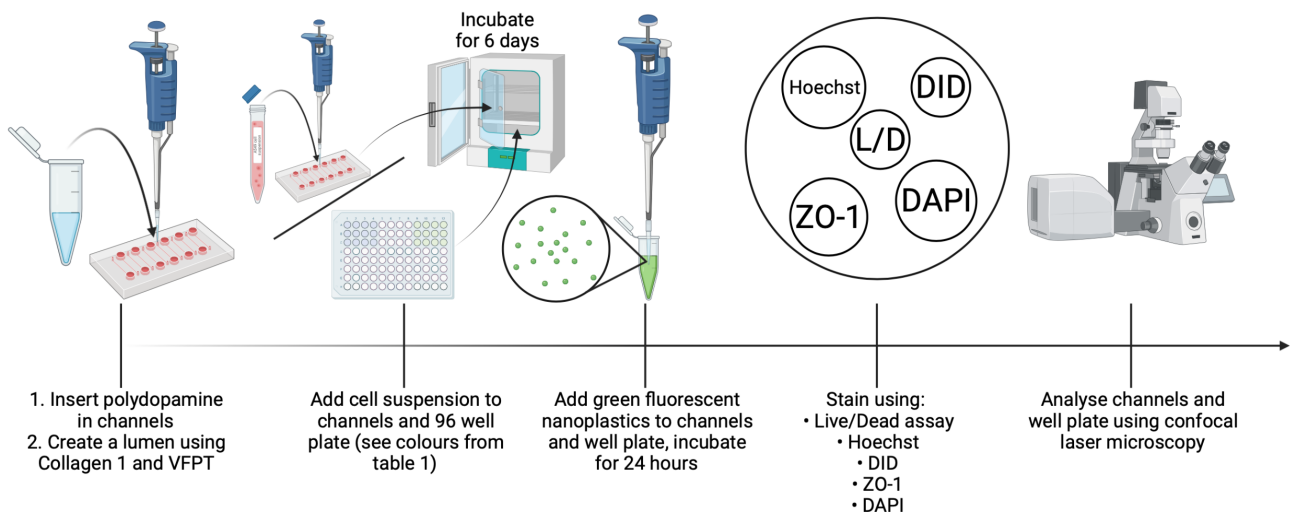


Figure 6: Overview of the nanoplastic experiment. First polydopamine was added to the channels following with Collagen 1 suspension to prepare the lumens using VFPT. Subsequently, channels were washed with culture medium (not shown) and cell suspension with 10 million A549 cells/mL was added inside the channels and in the well plate (see colour coding from table 1). After six days of incubation nanoplastics were added and incubated for 24 hours which was followed with the live/dead assay and following stains: Hoechst, DID, ZO-1 and DAPI. At last, cells were imaged using confocal microscopy. This image was made using Biorender.com.

3 Results

This section provides the obtained data from the seeding densities of Calu-3 and A549 cells in channels which were used to try to acquire a tubular cell structure. Also, the time period in which A549 cells attach to the collagen will be analysed. At last, the nanoplastic exposure experiments will be fully analysed to understand what happened with the viability of the cells and the translocation the nanoplastics. All data were acquired using the EVOS transmission microscope (Thermo Fisher scientific) and confocal laser microscopy (Zeiss 880).

3.1 Optimisation of the tubular cell structure

To determine which cell type would give the best results in becoming an alveolar epithelial tubular structure in the channels, we seeded both cell types in the channels on the top- and bottom-sides of the channels and let the Calu-3 cells grow for three days and the A549 cells for six days. The idea was that the cells would grow from the top- and bottom-side to the sides to create a tubular structure. Calu-3 cells at a concentration of 6 million cells/mL (figure 7) created twice as fast a structure on the bottom-side compared to every used concentration of A549 cells. Furthermore, Calu-3 cells grew slowly in the culture flask and in the channels, since they took about 10 days to grow confluent in the flask. Cells grew slowly in the channels and in particular cells with the concentration of 1.5 million cells/mL, see figure 20 and 21 took 14 days to form a structure on the bottom of the channel at transmission microscopic images. If the structure contained cells which had formed a tight junctioned barrier has not been verified using stains under the confocal laser microscope. Overall, it seemed that Calu-3 cells liked to grow with more cells together instead of alone, since we only saw patches of cells in the culture flask and no lonely cells. If we look back at the channels, the Calu-3 cells created patches that eventually formed islands in three days. However, the cells on the top-side of the channels did not seemed to realise a layer, as few cells seemed to attach to the top-side of the channels, see figure 8a for the bottom-side of the channel and figure 8b for the top-side of the channel.

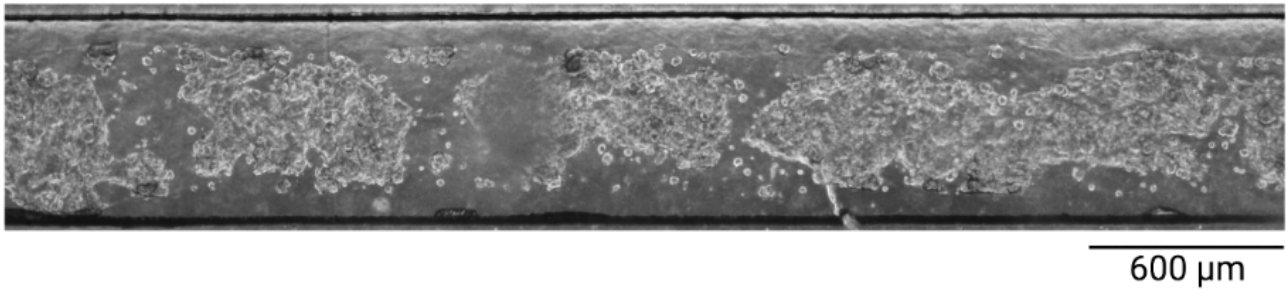


Figure 7: Top view of a channel with 6 million cells/mL Calu-3 cells after 3 days of culture which creates a structure at the bottom-side of the channel after three days of incubation. This structure is non continuous since islands of cells spread through the channels. This picture was made with the EVOS transmission microscope (Thermo Fisher scientific).

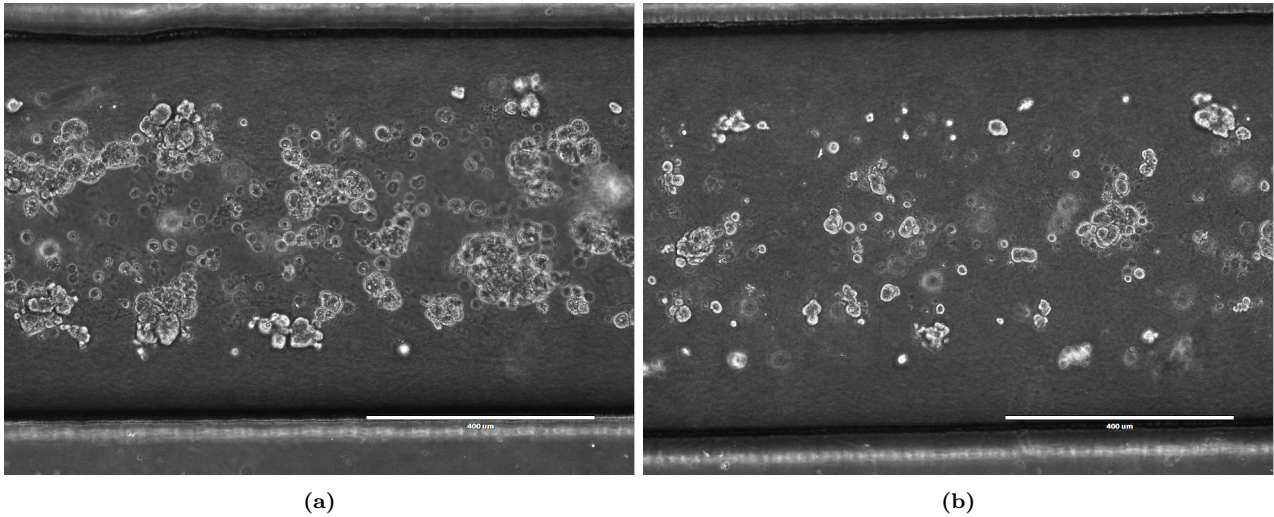


Figure 8: Top view of a channel with 4 million A549 cells/mL which were incubated for six days. Figure 8a shows the denser bottom-side of cells in the channel and figure 8b shows the top-side of the same channel, however less cells were visible. These pictures were made with the EVOS transmission microscope (Thermo Fisher scientific).

Concentrations of 10, 12 and 15 million cells/mL for A549 cells can be seen respectively in figure 9a, 9b and 9c. Figure 9a with 10 million cells/mL gave the the best structure on the bottom-side of the channel, since almost no individual cells were found and the structure is as good as closed for the middle part. The borders of the structure still provided some discontinuity. If we take a look at figure 9b and c, one can see that 12 million cells/mL only provide patches of cells and for the 15 million cells/mL we predominantly see individual cells. We found the same here as for the Calu-3 cells, since the cells did not grow in a tubular structure and only grew on the bottom side of the channel.

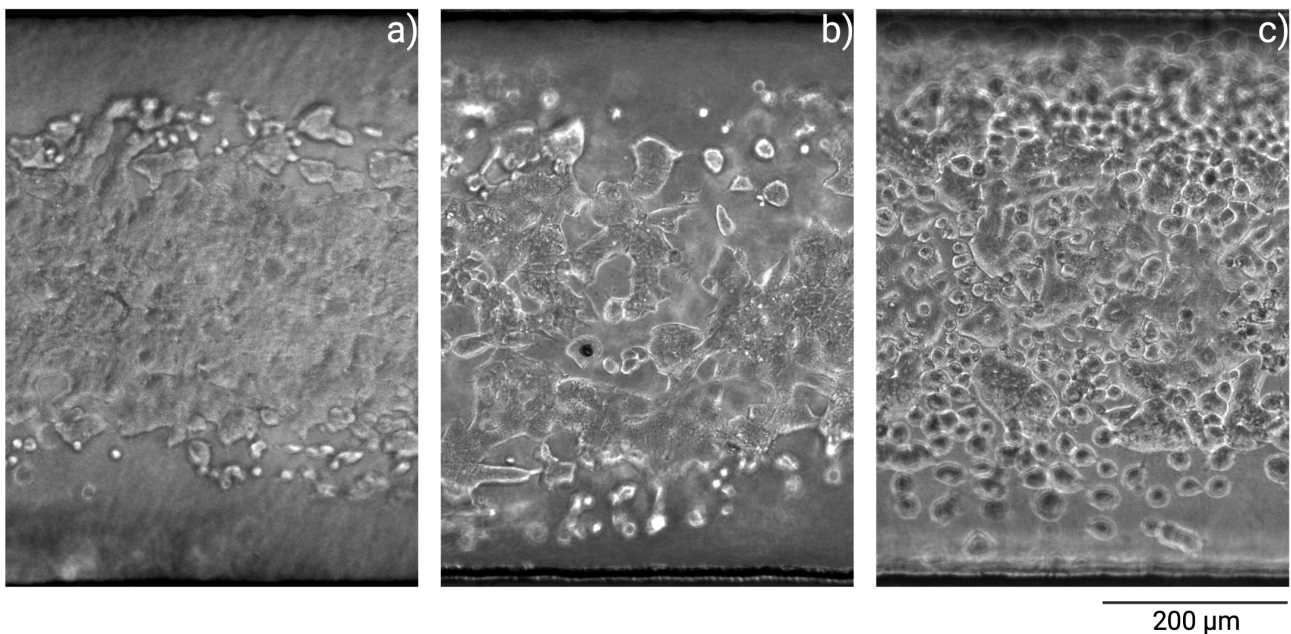


Figure 9: Top view of the channels with a) 10 million cells/mL, b) 12 million cells/mL and c) 15 million cells/mL which were incubated for six days. The concentration in a) gives the best continuous structure with only discontinuity at the borders, however this result is not consistent for each channel seeded with this concentration. These pictures were made with the EVOS transmission microscope (Thermo Fisher scientific).

The barrier shown in figure 9a may not be entirely representative for each channel seeded with 10 million cells/mL, since the same seeding is also shown in figure 10 where red areas are places where A549 cells did not create a fully closed barrier. However, out of the tested seeding densities, 10 million cells/mL seems to give the best structure.

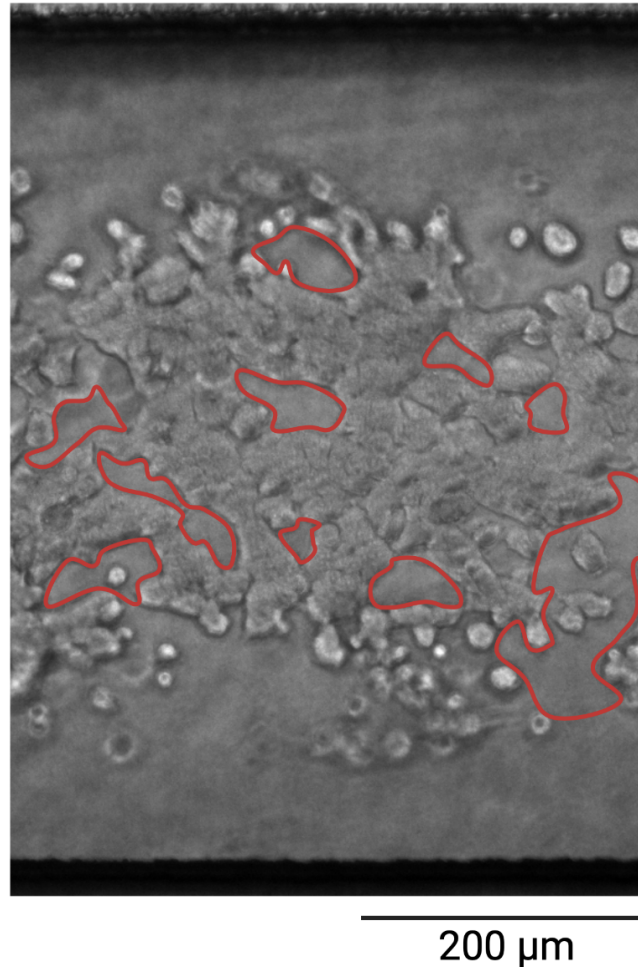


Figure 10: Top view of a channel with 10 million A549 cells/mL which was incubated for six days. Red circled areas are fields where cells did not reach, which means that the structure is broken at these points. Obviously, the structures were not consistent at the top and bottom of the channel, as can be seen by the discontinuity at the top and bottom of the picture. This picture was made with the EVOS transmission microscope (Thermo Fisher scientific). Biorender.com was used for editing the image.

3.2 Determine adherence time of A549 cells

Getting to know after how much time cells adhere to the collagen is very important to determine the time needed between seeding in the channels. This is why adherence of A549 cells is recorded per hour which can be seen in figure 22 for the collagen treated wells and figure 23 shows the results for the control wells. After 1 hour cells in the control and collagen treated wells looked the same with no adherence to the bottom of the wells or at the collagen layer. There were also cells at different depths present in the wells. After 2 hours, cells of the negative control seemed to have sedimented at the bottom of the well. Meanwhile, the cells in the collagen treated wells remained at different depths. The third hour we noticed that cells had also sedimented at the collagen layer for the collagen wells and they also seemed to be spreading more than the control. For the fourth hour this continued further. At the sixth hour, cells from the collagen wells were adhering better than the control, still there were unattached cells left. Cells from the control had also started to spread and attach to the well. 24 hours after seeding, cells in the collagen wells had fully attached. However, this was not the case for the control, as a lot of unattached cells were still present.

3.3 Nanoplastic exposure

3.3.1 Differences in viability of A549 cells after exposure to nanoplastics

Since NPs are known for possibly affecting cell viability as discussed in *chapter 1* we did a duplet live/dead assay on A549 cells which were exposed to different sizes and concentrations of NPs. Pictures were taken from the conditions from which a representative square area of 215 X 215 pixels and an average of 239 cells per picture were selected to count the total cells and the dead cells, as can be seen in figure 11. The viability per condition was determined from this selection. Also, since size and amount of NPs/mL could mean a higher or lower toxicity, the amount of NPs/mL in the solution is determined and is presented in figure 24 and table 2. At first glance, one could suggest that the viability lies around the same value for every condition, in which the negative control has the highest viability as can be seen in tables 3 and 4. The viability diagram in figure 12 shows that the viability for 1000 $\mu\text{g/mL}$ is slightly lower than for 10 $\mu\text{g/mL}$. This is because the average viability of 10 and 1000 $\mu\text{g/mL}$ is respectively 97.3% and 95.3%. What stands out is that error margins are becoming larger with increasing concentration. Another thing that stands out is the deviating low viability of 100 $\mu\text{g/mL}$ for the 50 nm NPs in the chip, unfortunately no duplet data were available so this has to be taken into account for the discussion. The viability of the negative controls were 99%.

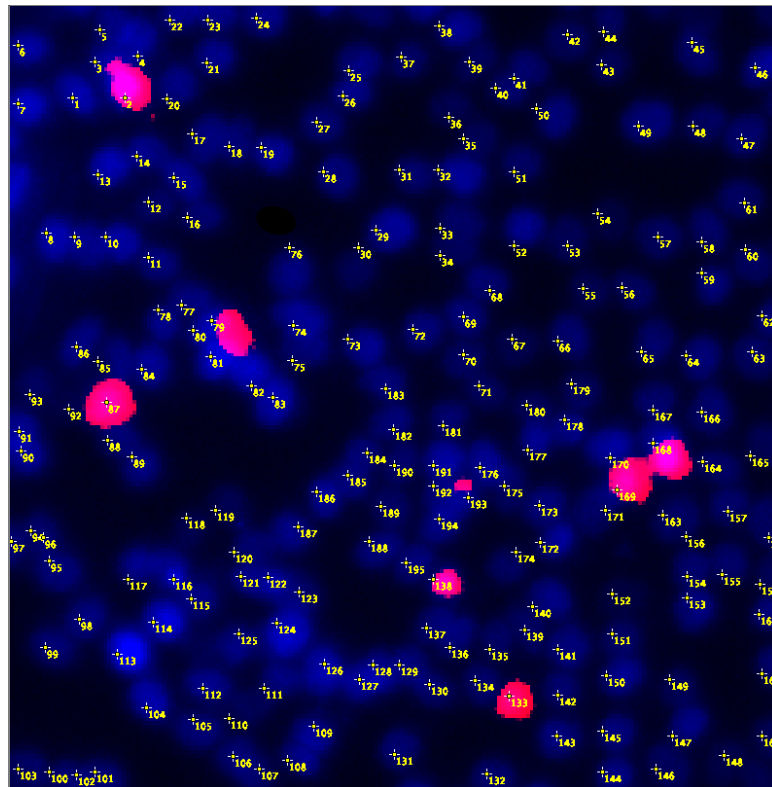


Figure 11: Picture of all the counted nuclei (blue) and dead cells (red).

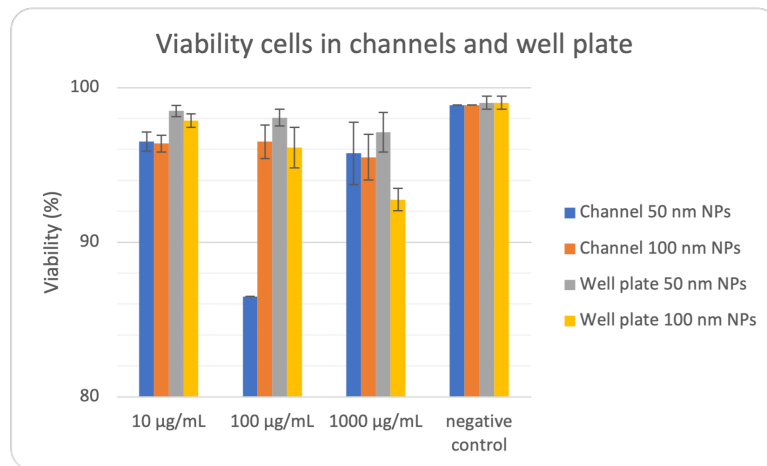


Figure 12: Diagram presenting the viability of cells in the channels and well plate.

3.3.2 Translocation of nanoplastics in the channels and the well plate

In general can be said that NPs were taken up by cells to different extents. Also, every condition showed signs of NPs adhering to the cell membranes while scrolling through different heights in the confocal images. It also seemed that cells had a difficulty in taking up aggregates.

Controls

Figure 13 represents the control images from the channels and well plate after incubation of A549 cells for respectively 6 and 3 days. a) presents the negative control of the channel, b) the positive control, c) presents the negative control of the well plate and d) the positive control. The figure shows that the ZO-1 proteins are stained more for the positive control as compared to the negative control. This is the case for the channels and the well plate. In general can be seen that the cell membranes are stained more for the positive controls as compared to the NPs conditions. A difference between the controls for the well plate and channels can be seen in the fact that the well plate shows more ZO-1 staining for both controls. This staining also is more consistent over the whole cell layer.

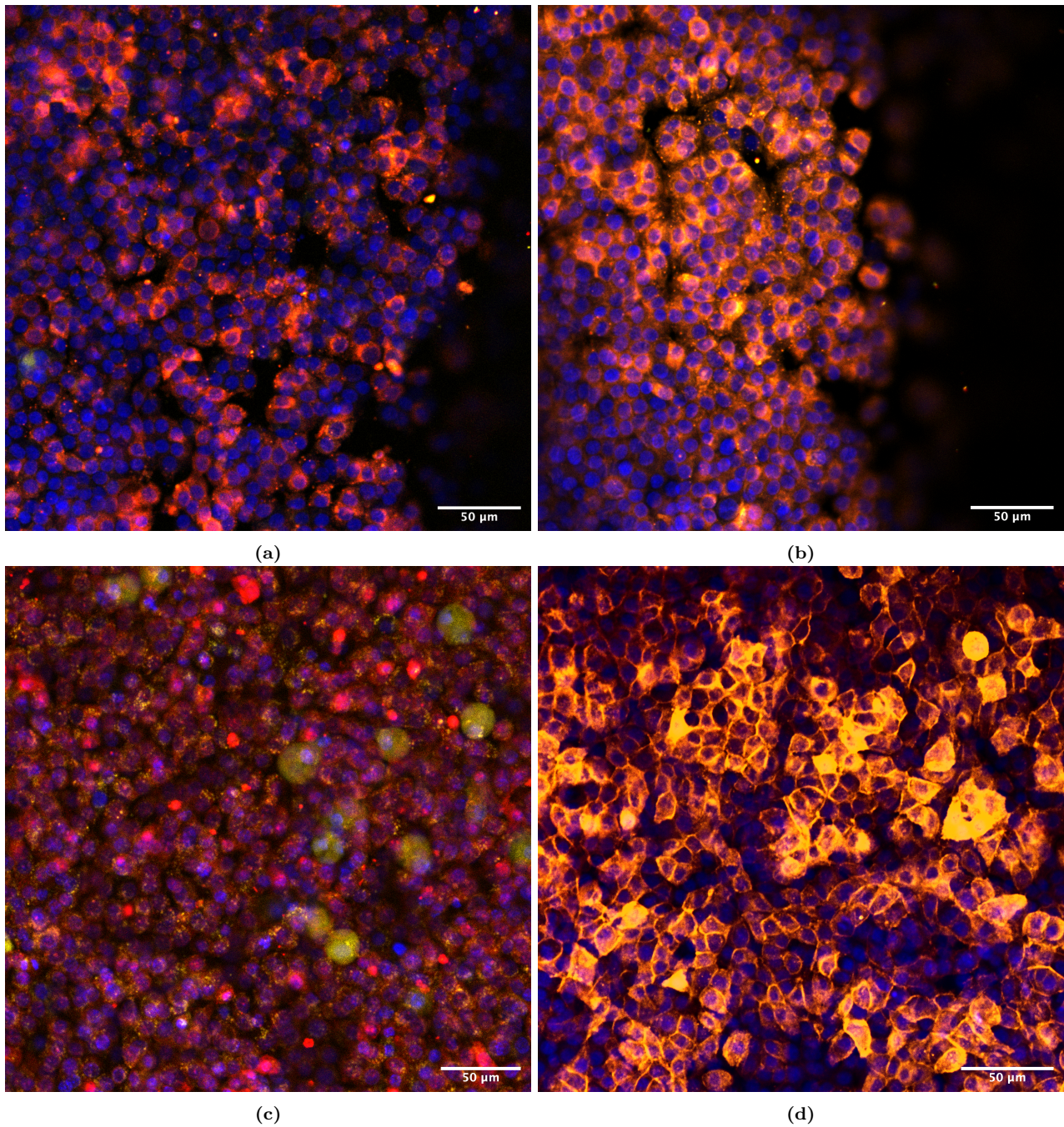


Figure 13: The figure represents the confocal images that were taken from the controls after the A549 cells were incubated for 6 days (channels) and 3 days (well plate). a) represents the negative control of a channel, b) the positive control, c) represents the negative control in the well plate and d) the positive control. These pictures were made with the confocal laser microscope (Zeiss 880).

Chip

After incubating for 24 hours cells were fixated and stained with the stains as discussed in *chapter 2*. However, it must be said that no channel contained a continuous structure, since islands of cells were present, comparable to the channel shown in figure 10. Also, the stainings for the cell membrane and ZO-1 proteins had overlapping spectra. The following figures were made using confocal laser microscopy and the colour blue stands for DAPI (nucleus), red/yellow for ZO-1 and cell membrane staining since the two stains were overlapping with each other. Finally, green stands for the NPs. Figure 14 contains 50 nm NPs with the following concentrations: a) 10 $\mu\text{g}/\text{mL}$, b) 100 $\mu\text{g}/\text{mL}$ and c) 1000 $\mu\text{g}/\text{mL}$. Overall can be seen that NPs predominantly were present near cells, but not in the open areas where cells did not exist but collagen did. If we look closer at figure 14a one could see that NPs were present mostly inside the cells, however

a little amount of cells had taken up multiple NPs. Z-stacks of the concentration 10 $\mu\text{g}/\text{mL}$ also provided proof that NPs did not translocate further than the cells for 10 $\mu\text{g}/\text{mL}$ as can be seen in figure 26. The Z-stack also showed that NPs were visible in a few cells, see figure 27. b) shows roughly the same result as for a), since NPs were clearly mostly present inside the cells as can be seen with the arrows, however a Z-stack shows a little a few NPs in the collagen layer behind the cells, see figure 28. The Z-stack also showed that NPs were present in a lot of cells, but not all, see figure 29. NPs in figure 14c also started to become visible outside the cells, still most NPs were visible inside the A549 cells as can be seen for instance with the three arrows. The difference in concentration was also visible between figures 14 a), b) and c), since an increasing amount of NPs could be seen with increasing concentration. Something that stood out was that almost every A549 cell had taken up NPs for each condition as could be seen in figures 38, 39 and 40.

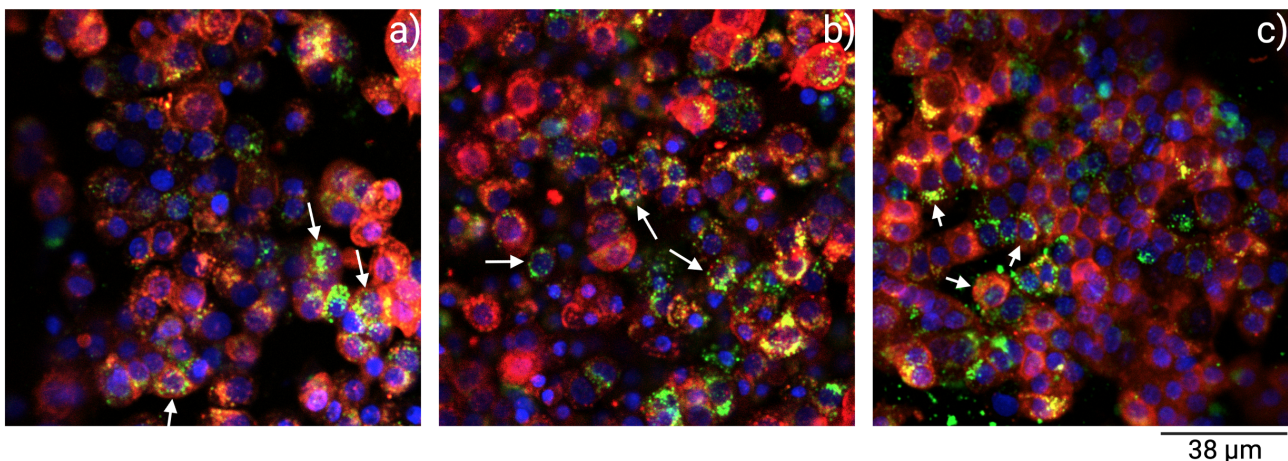


Figure 14: This figure presents A549 cells exposed to 50 nm NPs in channels. The cells were incubated for 6 days after which the NPs were incubated for 24 hours. a) contained NPs at a concentration of 10 $\mu\text{g}/\text{mL}$, b) NPs at a concentration of 100 $\mu\text{g}/\text{mL}$ and c) NP at a concentration of 1000 $\mu\text{g}/\text{mL}$. Arrows show cells which clearly contained NPs. Blue: nuclei staining (DAPI), Green: NPs, Red/Orange: cell membrane and ZO-1 staining. The arrows show for all three figures cells which clearly contain NPs inside the cells. This image was made using confocal laser microscopy (Zeiss 880) and edited using Imagej.

100 nm NPs with the concentrations of 10, 100 and 1000 $\mu\text{g}/\text{mL}$ are presented respectively in figure 15 a), b) and c). It was noticed that a haze was visible in figure 15c which made the picture less clear than for the other concentrations. Moreover, 100 nm NPs started to aggregate more compared to 50 nm NPs. The same principle as explained for 50 nm NPs applies for the 100 nm NPs, since NPs mostly did not translocate further than the cells themselves. However, few NPs were found to be behind the cells as could be seen in the Z-stack of the concentrations 100 and 1000 $\mu\text{g}/\text{mL}$ which are presented in figure 30 and 32. So, NPs translocated to the cells for all three concentrations and most NPs could be seen to be present inside the cells. Again, at the arrows cells were visible which clearly showed NPs inside the cells for a). This was also the case for b), but it must be noted that looking at the missing nuclei in some spaces, the structure from b) is less continuous than the structures from a) and c) which had less holes in the structure b) also had NPs in a lot of cells as shown in the Z-stack in figure ?? . c) also shows NPs inside the cells, but here NPs started to aggregate more compared to the other 50 and 100 nm NPs in the channels. In figure 31 can be seen that less cells contained NPs compared to b). It was also noted that during confocal imaging some NPs adhered to the outer cell membrane which was more present for the two higher concentrations. Original pictures of the NP uptake can be seen in figure 41, 42 and 43.

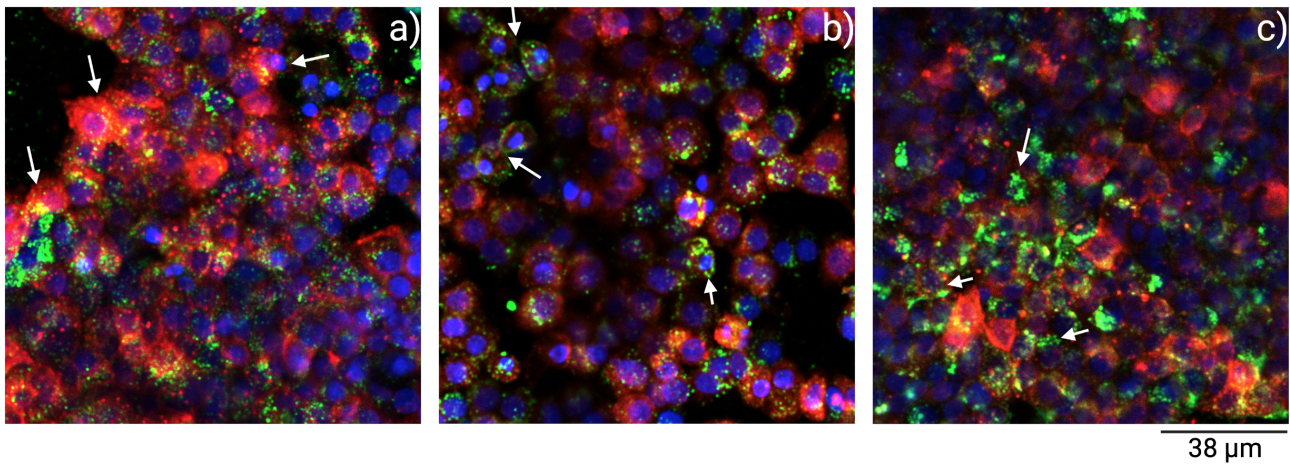


Figure 15: This figure presents A549 cells exposed to 100 nm NPs in channels. The cells were incubated for 6 days after which the NPs were incubated for 24 hours. a) contained NPs at a concentration of 10 $\mu\text{g}/\text{mL}$, b) NPs at a concentration of 100 $\mu\text{g}/\text{mL}$ and c) NP at a concentration of 1000 $\mu\text{g}/\text{mL}$. Arrows show cells which clearly contained NPs. Blue: nuclei staining (DAPI), Green: NPs, Red/Orange: cell membrane and ZO-1 staining. The arrows show for all three figures cells which clearly contain NPs inside the cells. This image was made using confocal laser microscopy (Zeiss 880) and edited using Imagej.

Well plate

The same protocol for the A549 cells in the well plate was used as for the channels. The only difference was that the cells were incubated for three days instead of six days. This was because a confluent monolayer was achieved twice as fast. Figure 16 represents exposure of 50 nm NPs to A549 cells in a well plate. If we look closer at figure 16a which represents 10 $\mu\text{g}/\text{mL}$ NPs, we can see that a lot of NPs were visible inside the cells, but not every cell had NPs in them as could be seen in the Z-stack shown in figure ???. It cannot be proven that all NPs were inside the cells. The Z-stack in figure 34 let's us see that no NPs were found inside the collagen. b) contains NPs with a concentration of 100 $\mu\text{g}/\text{mL}$ and shows the same principle as in a), since a lot of NPs were found inside the cells. The cells marked with the arrow clearly indicate uptake of NPs. We also see for this concentration and for the 10 $\mu\text{g}/\text{mL}$ concentration that NPs tend to be closer to the nucleus which can be predominantly seen at the most right arrow in b). c) has a NPs concentration of 1000 $\mu\text{g}/\text{mL}$ and in the image can be seen that the concentration of NPs was really high compared to a) and b). This created a aggregation of NPs and a haze in the image. This made it hard to locate the NPs, however during confocal microscopy could be seen that a lot of NPs adhered to the outer cell membrane.

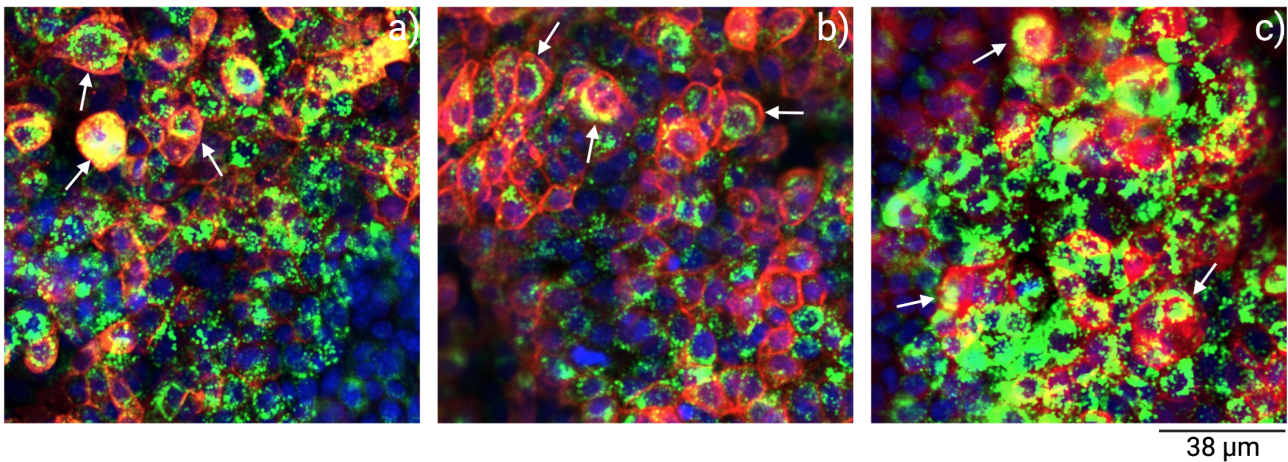


Figure 16: This figure presents A549 cells exposed to 50 nm NPs in a well plate. The cells were incubated for 3 days after which the NPs were incubated for 24 hours. a) contained NPs at a concentration of 10 µg/mL, b) NPs at a concentration of 100 µg/mL and c) NP at a concentration of 1000 µg/mL. Arrows show cells which clearly contained NPs. Blue: nuclei staining (DAPI), Green: NPs, Red/Orange: cell membrane and ZO-1 staining. The arrows show for all three figures cells which clearly contain NPs inside the cells. This image was made using confocal laser microscopy (Zeiss 880) and edited using Imagej.

Figure 17 represents the exposure of 100 nm NPs at the concentrations of 10 µg/mL, 100 µg/mL and 1000 µg/mL in respectively a), b) and c) to A549 cells in a well plate. a) shows uptake of NPs by most cells. The arrows indicate cells in which clear uptake of NPs could be seen. The Z-stack in figure 36 shows us that a few NPs were visible underneath the cells. It looks like to be the opposite, but the most NPs that are visible were from an upper level of the Z-stack, since they are unsharp. The Z-stack in figure 37 shows us a lot of cells have taken up NPs. b) shows uptake of NPs, with many NPs inside the cells, however there are also cells which do not have NPs inside them. Again, we can see that NPs tended to reside closer to the nucleus. In c) we can see a similar haze as in figure 16c. There was also more aggregation visible which made it hard to locate the NPs. The arrows indicate cells that showed clear uptake of NPs and the most left arrows showed NPs which were located close to the nucleus.

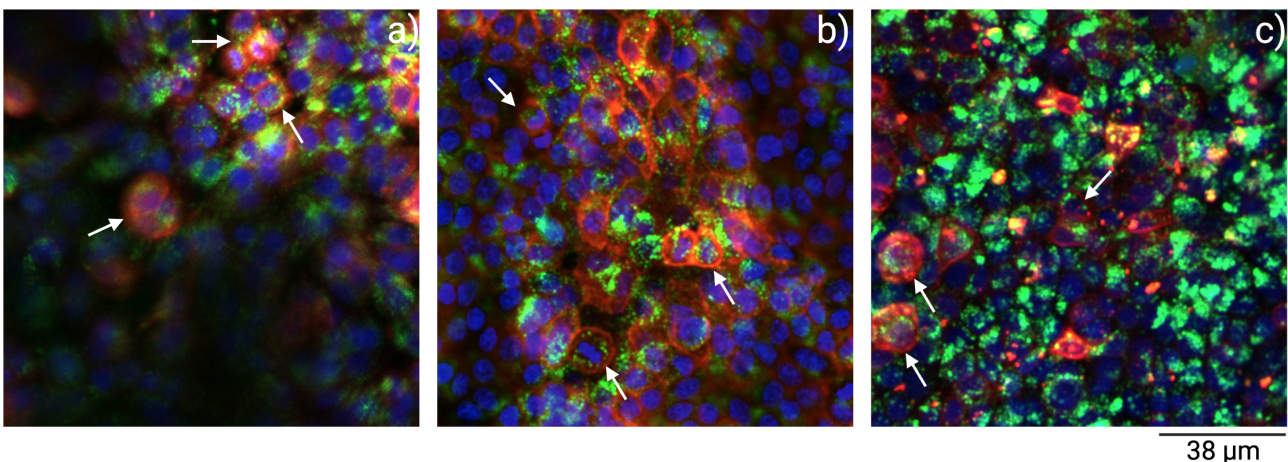


Figure 17: This figure presents A549 cells exposed to 100 nm NPs in a well plate. The cells were incubated for 6 days after which the NPs were incubated for 24 hours. a) contained NPs at a concentration of 10 µg/mL, b) NPs at a concentration of 100 µg/mL and c) NP at a concentration of 1000 µg/mL. Arrows show cells which clearly contained NPs. Blue: nuclei staining (DAPI), Green: NPs, Red/Orange: cell membrane and ZO-1 staining. The arrows show for all three figures cells which clearly contain NPs inside the cells. This image was made using confocal laser microscopy (Zeiss 880) and edited using Imagej.

4 Discussion

4.1 Overlapping spectra of the stains

First of all as seen in figure 25 overlap between exciting and emitting wavelengths of DID and ZO-1 and are clearly present. This means that when either of those are excited the other stain will be excited too and will emit. This makes it hard drawing a conclusion from whether tight junctions were disturbed. However, as can be seen in the splitted channels in figure 18 there are minor differences visible between a) and b), since b) presents the outline of cells that are at the same depth and thus seem to lie next to each other. These cells might have tight junctions. This effect is less visible for a), since a) predominantly presents staining of the cell membrane in general and b) presents also staining of the cells which possibly have tight junctions. The ZO-1 protein is one of the members of the tight junction family, but the tight junction family consists of many proteins. In general the proteins can be divided into claudin, occludin, junctional adhesion molecules, cytosolic scaffold proteins and the zonulae occludens 1 (ZO-1) protein [32]. To get a completer picture of the state of the tight junctions after coming in contact with the NPs, more proteins, like occludin, E-cadherin and β -catenin could be stained alongside the ZO-1 protein as was done by Carterson et al. [33]. However, the cell membrane should not be stained to avoid spectrum overlap between stains.

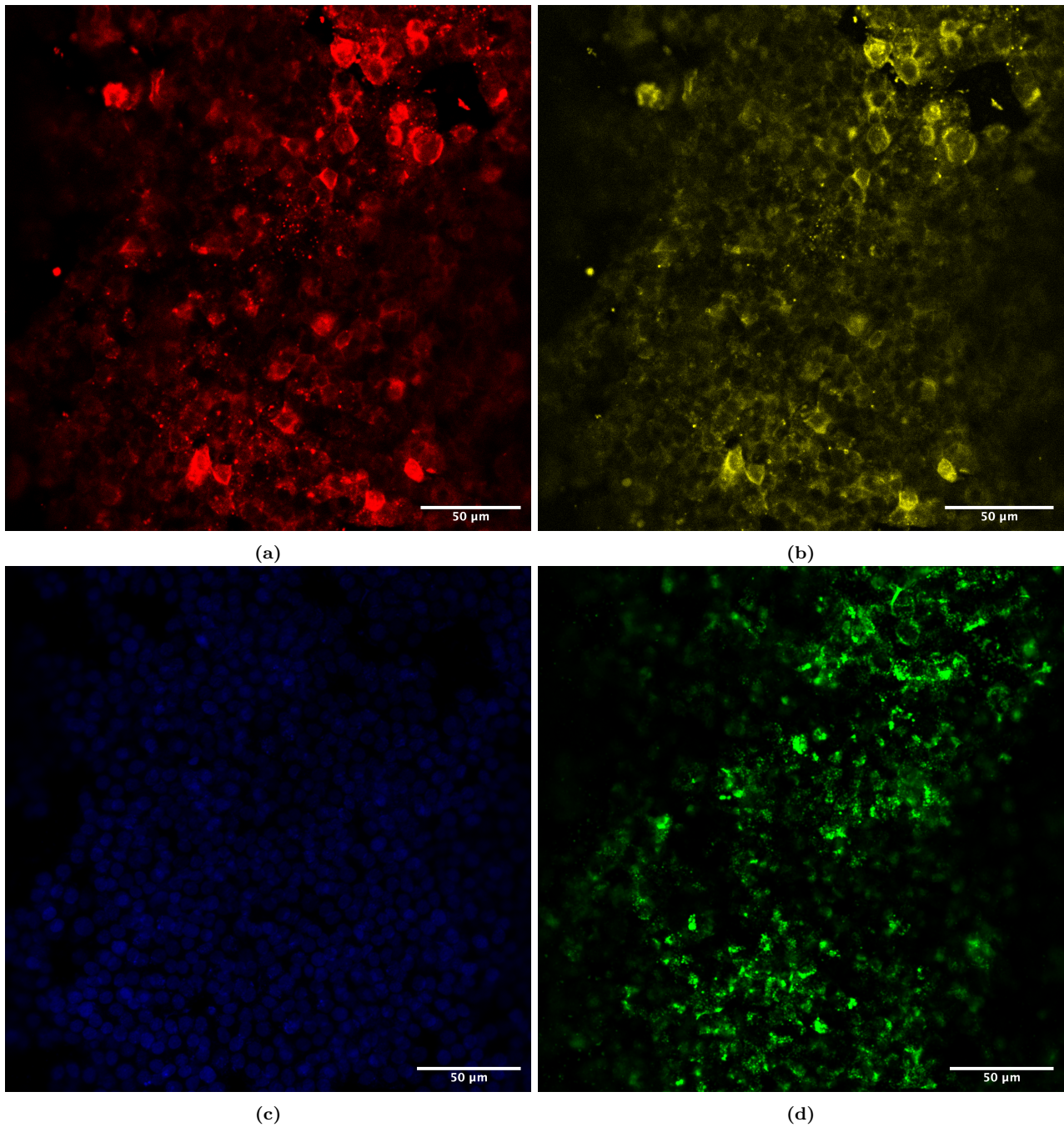


Figure 18: The figure represents 100 nm NPs with the concentration 1000 $\mu\text{g}/\text{mL}$ which were incubated for 24 hours in A549 cells in channels. The A549 cells were incubated for six days. a) represents the cell membrane staining (DID), b) is the tight junction staining (ZO-1), c) is the nuclei staining (DAPI) and d) are the NPs. These pictures were made with the confocal laser microscope (Zeiss 880).

As could be seen in *chapter 3* the controls did not give us information about the condition of the tight junctions. It was expected the negative control would give cells with the cell membranes clearly visible. However, this worked out a bit different since not all cell membranes had an equal intensity on the confocal images. On the contrary, this same effect was visible for the positive control and for every condition that was used. The positive control was expected to show no cell membranes. These controls should also have been stained with the addition of above standing stains to properly analyse the controls. Now that we do not have a result from the controls we cannot verify what the effect of NPs and $\text{TNF-}\alpha$ is on A549 cells.

4.2 Compromises of the lung-on-a-chip

The experiments with channels offer only a layer of cells on the bottom of the channels. As discussed in paragraph *Seeding the chip* cells only provided a layer on the bottom side of the channel, but consistently did not populate the top side of the channel. A possible explanation for this could be that the collagen in the 24 hours time period that the bottom layer of cells was seeded has become unfavourable for the second seeding of cells to attach and grow on. To determine if the collagen has degraded, we could use a Collagen Degradation/Zymography Assay Kit (abcam). Non degraded collagen would be presented with the release of fluorophores and the opposite for degraded collagen.

Both cell lines Calu-3 and A549 did not successfully create a closed barrier. As we saw in *chapter 3* Calu-3 cells like to grow in patches and achieved a layer of cells as could be seen under the transmission microscope. The concentration of 6 million cells/mL created a layer which had islands of closed barriers, possibly even better results could have been achieved if higher concentrations were used, since more islands of Calu-3 cells could be present which could stimulate Calu-3 cells to form a barrier that is closed over the whole channel. However, as was seen with the concentrations of 10, 12 and 15 million A549 cells the optimal concentration was 10 million cells/mL, so one should be careful to find the right concentration, since too high concentrations could give the opposite effect as was demonstrated with A549 cells. Regarding the holes in the barrier of A549 cells, it was known that A549 cells do not like to grow a barrier, since TEER values did not rise in experiments as discussed in the introduction [22]. This could mean that tight junctions were not formed for our A549 cells, however this is not provable with the experiments we have done, since we only used ZO-1 protein staining to see if tight junctions have formed, but this stain has overlap with DID which makes pulling conclusion on tight junctions of A549 cells debatable. Next to this was the achieved cell layer in the channels that did not have a tubular structure despite the goal to achieve this. The extent to how much difference in interaction of cells with NPs a confluent tubular structure would create has not been researched.

Currently, models from a lung-on-a-chip are made using submerged cell cultures of tumor or immortalised cell lines. Even though these types of cultures do not represent real lung air interfaces they come the closest to reality to what is achievable nowadays. Additionally, long-term culture of alveolar epithelial type II cells is difficult and unattainable [34]. In this same research was discussed that differentiating alveolar epithelial type II cells to an in vivo like phenotype had not been achieved. Unfortunately, this mechanism has not yet been added to our chip, since we used a static environment in which NPs in solution was incubated in the channels with cells. Adding an air flow to our chip would be the first thing to add after optimising tubular cell structure, since the presence of surfactants plays an important role in the uptake of NPs. Marcinkiewicz et al. has determined that surfactant proteins in air-liquid interface culture systems remained at the same level, meanwhile these proteins dissipated over time for submerged culture systems [19].

4.3 Translocation mechanisms of NPs

As discussed in *chapter 1* the three ways of NP uptake could be through phagocytosis, endocytosis or diffusion or translocation through disrupted tight junctions. It was clear that generally no NP was seen in the collagen, meanwhile they were visible inside the cells which would be remarkable, since the cell membrane is negative as are the NPs. This would mean that NPs were taken up through diffusion or endocytosis as described in the introduction. To find out what mechanism has played a role in the translocation we could have used for instance lysotrackers which stain lysosomes. In the normal pathway of endocytosis NPs would be taken up and they would end up in lysosomes [35]. So, staining lysosomes to see whether NPs have translocated

to the cells via endocytosis or diffusion would give us very useful information since in that case uptake would have only occurred via endocytosis. Staining lysosomes with lysotracker has been successfully done with NPs inside cells of zebrafish larvae [36].

The confocal images were not analysed in a statistical way which would be the proper way to determine how many cells per condition had taken up NPs and to determine which condition the largest uptake had. However, due to the relatively low image quality and short time span in which these confocal images had to be analysed it was chosen to not do the statistical analysis.

In the well plate, a few cells clearly demonstrated that NPs were placed around the nucleus for the conditions 50 nm with the concentrations 10 and 100 $\mu\text{g}/\text{mL}$ and 100 nm with the concentrations 100 $\mu\text{g}/\text{mL}$ and 1000 $\mu\text{g}/\text{mL}$. The same principle has been seen with negatively charged nanoparticles which even interacted with the cell nucleus [37]. The fact that a lot of cells had taken up NPs could be explained by the same reason that negatively charged NPs like to interact with the nucleus and for that they have to be inside the cells.

Differences between alveolar type I and type II cells in general were explained in *chapter 1* in which a clear difference was found between NP uptake where the type I did take up NPs meanwhile the type II did not. However, despite the fact that A549 cells express themselves mostly as alveolar type II cells they do take up NPs as was proven in *chapter 3*. This corresponds with the research from Rothen-Rutishauser et al.

For this research it is hypothesised that the tight junctions of intestinal cell act largely the same as for alveolar epithelial cells. We could not find any research article about the interaction of NPs with tight junctions for alveolar epithelial cells, so we looked at intestinal cells instead. Here, we found that NPs could disturb the tight junctions and that paracellular translocation was possible.

As stated in *chapter 1* surfactants can opsonize nanoparticles to be taken up by macrophages, on the contrary A549 cells were protected from uptake of positively charged silica nanoparticles by surfactants. However in our experiment negatively charged polystyrene nanoplastics were used and we do not know if A549 cells would interact differently than was found in the above mentioned research. Nevertheless, to determine presence of SP-A and SP-D electrophoresis could be executed as was done in the research of Kankavi et al. [38]

In *chapter 1* is described that NPs can result in ROS production and inflammation reactions with higher expression of TNF- α , IL-6 and IL-8 levels. Since ROS can let cells go in apoptosis NPs can pass through the barrier. However, since almost all NPs were taken up by cells, NPs were not found in the collagen and viability levels had not dropped significantly one could expect that high levels of ROS are not present. Though, this cannot be proofed without a dedicated assay for ROS and pro-inflammation cytokines. Presence of pro-inflammation cytokines like IL-6 and IL-8 could be tested for using the Inflammation 20-Plex Human ProcartaPlex™ Panel (Thermo Fisher scientific). For detection of ROS a Total Reactive Oxygen Species (ROS) Assay Kit 520 nm (Thermo Fisher scientific) could be used.

Also the NPs have a size margin of ± 10 nm, however since no difference in translocation mechanism was seen and since all cells had taken up both sizes NPs and no NPs were found behind the cell layer we suggest that this error margin might not play a big role in translocation mechanism.

4.4 Determining viability in a more specific way

The viability assay was done using the live/dead assay with ethidium homodimer-1 and calcein-AM, but because NPs were already green and calcein also is we only looked at the total amount of nuclei and dead cells. This gave us a basic indication of the percentage cells that were alive, however this is not much specific, since we did not have information about the condition of the cells apart from being alive or dead. That is why a proper live/dead assay might be used for future research. The MTT assay (sigmaaldrich) for instance was successfully used for A549 cells over three days [39]. However, plastics could adsorb the chemicals used in this assay. It must also be noted that we only had one measurement from the 50 nm NPs with a concentration of 100 µg/mL in a channel. This is unfortunate, since this is not very scientific. However, we can see that the viability is a lot lower than for every other condition. This leads us to suggest that this one reading was unfortunate, however it cannot be proven. The overall lower viability for cells that were exposed to NPs compared to the controls could be due to the NPs hindering gas exchange and metabolism, since NPs were found inside and outside the cells.

4.5 Future perspectives and recommendations

In the future, optimisation of the tubular cell structure should be the number one priority. Also, one could think about trying to create a co-culture of A549 cells with macrophages a tubular cell structure, since this might give more representative data. After this, the lung-on-a-chip device could be expanded with first of all an air flow for which NPs have to be mixed with air which could possibly be done using the Venturi effect. Next, stretching of cells gives a much more representative image of what is happening in real alveoli. This all can be realised by first seeding cells in the inner channel as can be seen in the drawing in figure 19. After cells have become confluent across the whole tubular structure of the channel an air mixture with NPs could be added, alongside the addition of a pumping motion realised by the vacuum pump (not shown) and chamber. This pumping motion is supposed to stretch the cells in a natural breathing frequency.

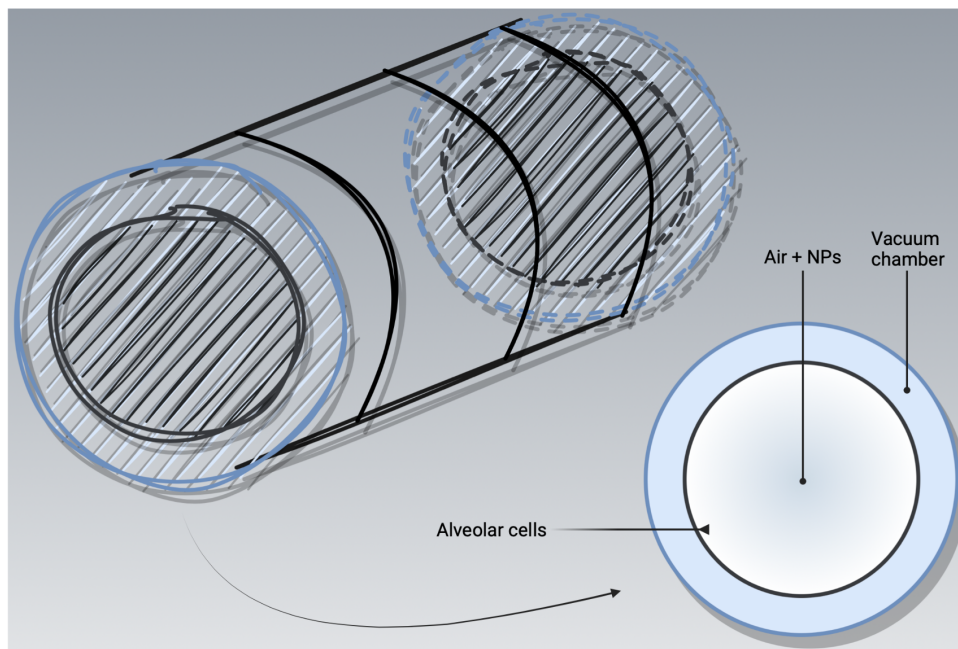


Figure 19: This drawing shows what a lung-on-a-chip device in the future could look like. With at the inner tube attached alveolar epithelial cells and the outer tube provides a vacuum chamber which is attached to a vacuum pump (not shown). The stretching of cells can be mimicked with the same frequency as in the body. This image is made using diagrams.net and BioRender.com.

5 Conclusion

For this project, the translocation of NPs through alveolar epithelium was studied.

To conclude this research, we found that we failed to create a tubular structure of either Calu-3 or A549 cells, since the cell layer had holes in it and the cells were almost not visible at the top of the channel.

The presence of NPs inside or around the cells did not seem to influence the viability of the A549 cells in a great way. However, margins of the viability consistently became greater as the concentration of NPs increased. This leads us to conclude that the viability must have suffered in some way from the presence of NPs in or near the cells.

We also found that NPs have a high likelihood to have translocated through diffusion or endocytosis. Neither of which is proven. However, what we did find was that NPs did not translocate through the cells.

We also determined that almost no NP was found inside the collagen which made us to conclude that the NPs were either inside the cells or that they were stuck to the outer cell membrane. This last point was especially visible in the well plate, since aggregates of NPs adhered to the outer cell membrane. An increment in the concentration of NPs meant an increasing amount of NPs that were not taken up by the epithelial cells.

6 Acknowledgements

This project would not have been possible without the help of people that were willing to help me. From the small things like pointing me where things were located in the lab to people that offered me to work for them.

Firstly, I would like to thank prof.dr.ir. S. Le Gac who gave me the opportunity to be a part of this project. I enjoyed every day working on this project till the last days. She also pushed me to deliver a report of which I am proud.

Secondly, big thanks goes out to dr.ir. K.M. Pondman who guided me in the right direction at the most critical points.

A special thanks goes out to msc. C.A. Paggi and dr.ing. A. Zuchowska who helped me in a lot of ways to realise things like setting up experiments and preparing a presentation.

Renata Patrícia Faria Maia, Tomas van Dorp and Simon Stevers were also very important in my project, since they were ready to help me every time I had a question.

Dr. K. Broersen helped me to realise that there were more aspects from this project than I first thought, so I would like to thank her for providing me these insights.

Last but not least, I would like to thank the DBE and AMBER members, since the nice work environment was because of you.

References

1. Gibb BC. Plastics are forever. *Nature Chemistry* 2019 11:5 2019 Apr; 11:394–5. DOI: 10.1038/s41557-019-0260-7. Available from: <https://www.nature.com/articles/s41557-019-0260-7>
2. Geyer R, Jambeck JR, and Law KL. Production, use, and fate of all plastics ever made. *Science Advances* 2017 Jul; 3:e1700782. DOI: 10.1126/SCIADV.1700782. Available from: <https://advances.sciencemag.org/content/3/7/e1700782> <https://advances.sciencemag.org/content/3/7/e1700782.abstract>
3. Yee MSL, Hii LW, Looi CK, Lim WM, Wong SF, Kok YY, Tan BK, Wong CY, and Leong CO. Impact of microplastics and nanoplastics on human health. 2021 Feb. DOI: 10.3390/nano11020496. Available from: <https://doi.org/10.3390/nano11020496>
4. Zhang Y, Kang S, Allen S, Allen D, Gao T, and Sillanpää M. Atmospheric microplastics: A review on current status and perspectives. 2020 Apr. DOI: 10.1016/j.earscirev.2020.103118
5. Yacobi NR, DeMaio L, Xie J, Hamm-Alvarez SF, Borok Z, Kim KJ, and Crandall ED. Polystyrene nanoparticle trafficking across alveolar epithelium. *Nanomedicine: Nanotechnology, Biology and Medicine* 2008 Jun; 4:139–45. DOI: 10.1016/J.NANO.2008.02.002
6. Geiser M, Rothen-Rutishauser B, Kapp N, Schürch S, Kreyling W, Schulz H, Semmler M, Im Hof V, Heyder J, and Gehr P. Ultrafine particles cross cellular membranes by nonphagocytic mechanisms in lungs and in cultured cells. *Environmental Health Perspectives* 2005 Nov; 113:1555–60. DOI: 10.1289/ehp.8006. Available from: <http://dx.doi.org/>
7. Yang JW, Shen YC, Lin KC, Cheng SJ, Chen SL, Chen CY, Kumar PV, Lin SF, Lu HE, and Chen GY. Organ-on-a-Chip: Opportunities for Assessing the Toxicity of Particulate Matter. *Frontiers in Bioengineering and Biotechnology* 2020; 8:1–13. DOI: 10.3389/fbioe.2020.00519
8. Prata JC. Airborne microplastics: Consequences to human health? 2018 Mar. DOI: 10.1016/j.envpol.2017.11.043
9. Dong CD, Chen CW, Chen YC, Chen HH, Lee JS, and Lin CH. Polystyrene microplastic particles: In vitro pulmonary toxicity assessment. *Journal of Hazardous Materials* 2020 Mar; 385:121575. DOI: 10.1016/J.JHAZMAT.2019.121575
10. Thorley AJ, Ruenraroengsak P, Potter TE, and Tetley TD. Critical determinants of uptake and translocation of nanoparticles by the human pulmonary alveolar Epithelium. *ACS Nano* 2014 Nov; 8:11778–89. DOI: 10.1021/nn505399e. Available from: </pmc/articles/PMC4246006/> <https://www.ncbi.nlm.nih.gov/pmc/articles/PMC4246006/?report=abstract> <https://www.ncbi.nlm.nih.gov/pmc/articles/PMC4246006/>
11. Liang B, Zhong Y, Huang Y, Lin X, Liu J, Lin L, Hu M, Jiang J, Dai M, Wang B, Zhang B, Meng H, Lelaka JJJ, Sui H, Yang X, and Huang Z. Underestimated health risks: polystyrene micro- and nanoplastics jointly induce intestinal barrier dysfunction by ROS-mediated epithelial cell apoptosis. *Particle and Fibre Toxicology* 2021 Dec; 18:1–19. DOI: 10.1186/s12989-021-00414-1. Available from: <https://doi.org/10.1186/s12989-021-00414-1>
12. Mahler GJ, Esch MB, Tako E, Southard TL, Archer SD, Glahn RP, and Shuler ML. Oral exposure to polystyrene nanoparticles affects iron absorption. *Nature Nanotechnology* 2012 Feb; 7:264–71. DOI: 10.1038/nnano.2012.3. Available from: www.nature.com/naturenanotechnology
13. Banerjee A and Shelver WL. Micro- and nanoplastic induced cellular toxicity in mammals: A review. *Science of The Total Environment* 2021 Feb; 755:142518. DOI: 10.1016/J.SCITOTENV.2020.142518

14. Ruenraroengsak P, Novak P, Berhanu D, Thorley AJ, Valsami-Jones E, Gorelik J, Korchev YE, and Tetley TD. Respiratory epithelial cytotoxicity and membrane damage (holes) caused by amine-modified nanoparticles. <http://dx.doi.org/10.3109/17435390.2011.558643> 2012 Feb; 6:94–108. DOI: 10.3109/17435390.2011.558643. Available from: <https://www.tandfonline.com/doi/abs/10.3109/17435390.2011.558643>
15. Bhatia SN and Ingber DE. Microfluidic organs-on-chips. *Nature Biotechnology* 2014 32:8 2014 Aug; 32:760–72. DOI: 10.1038/NBT.2989. Available from: <https://www-nature-com.ezproxy2.utwente.nl/articles/nbt.2989>
16. Lu RXZ and Radisic M. Organ-on-a-chip platforms for evaluation of environmental nanoparticle toxicity. *Bioactive Materials* 2021 Sep; 6:2801–19. DOI: 10.1016/J.BIOACTMAT.2021.01.021
17. Shrestha J, Razavi Bazaz S, Aboulkheyr Es H, Yaghobian Azari D, Thierry B, Ebrahimi Warkiani M, and Ghadiri M. Lung-on-a-chip: the future of respiratory disease models and pharmacological studies. 2020 Feb. DOI: 10.1080/07388551.2019.1710458. Available from: <https://www.tandfonline.com/action/journalInformation?journalCode=ibty20>
18. Huh D, Matthews BD, Mammoto A, Montoya-Zavala M, Hsin HY, and Ingber DE. Reconstituting Organ-Level Lung Functions on a Chip. *Science* 2010 Jun; 328:1662–8. DOI: 10.1126/SCIENCE.1188302. Available from: <https://science-sciencemag-org.ezproxy2.utwente.nl/content/328/5986/1662%20https://science-sciencemag-org.ezproxy2.utwente.nl/content/328/5986/1662.abstract>
19. Marcinkiewicz MM, Baker ST, Wu J, Hubert TL, and Wolfson MR. A Novel Approach for Ovine Primary Alveolar Epithelial Type II Cell Isolation and Culture from Fresh and Cryopreserved Tissue Obtained from Premature and Juvenile Animals. *PLoS ONE* 2016 Mar; 11:152027. DOI: 10.1371/JOURNAL.PONE.0152027. Available from: </pmc/articles/PMC4801353/%20/pmc/articles/PMC4801353/?report=abstract%20https://www.ncbi.nlm.nih.gov/pmc/articles/PMC4801353/>
20. Kanta J. Collagen matrix as a tool in studying fibroblastic cell behavior. *Cell Adhesion & Migration* 2015; 9:308. DOI: 10.1080/19336918.2015.1005469. Available from: </pmc/articles/PMC4594574/%20/pmc/articles/PMC4594574/?report=abstract%20https://www.ncbi.nlm.nih.gov/pmc/articles/PMC4594574/>
21. Capel V, Vllasaliu D, Watts P, and Stolnik S. Insight into the relationship between the cell culture model, cell trafficking and siRNA silencing efficiency. *Biochemical and Biophysical Research Communications* 2016 Aug; 477:260–5. DOI: 10.1016/j.bbrc.2016.06.054. Available from: </pmc/articles/PMC4948577/%20/pmc/articles/PMC4948577/?report=abstract%20https://www.ncbi.nlm.nih.gov/pmc/articles/PMC4948577/>
22. Hirakata Y, Yano H, Arai K, Endo S, Kanamori H, Aoyagi T, Hirotani A, Kitagawa M, Hatta M, Yamamoto N, Kunishima H, Kawakami K, and Kaku M. Monolayer Culture Systems with Respiratory Epithelial Cells for Evaluation of Bacterial Invasiveness. *Tohoku J. Exp. Med* 2010; 220:15–9. DOI: 10.1620/tjem.220.15
23. Bachler G, Losert S, Umehara Y, Goetz N von, Rodriguez-Lorenzo L, Petri-Fink A, Rothen-Rutishauser B, and Hungerbuehler K. Translocation of gold nanoparticles across the lung epithelial tissue barrier: Combining in vitro and in silico methods to substitute in vivo experiments. *Particle and Fibre Toxicology* 2015 12:1 2015 Jun; 12:1–18. DOI: 10.1186/s12989-015-0090-8. Available from: <https://particleandfibretoxicology.biomedcentral.com/articles/10.1186/s12989-015-0090-8>
24. Meerten PVPV. 3D cell culture in a lung-on-a-chip system. 2019

25. Foster KA, Oster CG, Mayer MM, Avery ML, and Audus KL. Characterization of the A549 Cell Line as a Type II Pulmonary Epithelial Cell Model for Drug Metabolism. *Experimental Cell Research* 1998 Sep; 243:359–66. DOI: 10.1006/EXCR.1998.4172
26. Castranova V, Rabovsky J, Tucker JH, and Miles PR. The alveolar type II epithelial cell: A multifunctional pneumocyte. *Toxicology and Applied Pharmacology* 1988 May; 93:472–83. DOI: 10.1016/0041-008X(88)90051-8
27. Koval M and Sidhaye VK. Introduction: The Lung Epithelium. *Lung Epithelial Biology in the Pathogenesis of Pulmonary Disease* 2017 Jan :xiii–xviii. DOI: 10.1016/B978-0-12-803809-3.00023-3
28. Ruge CA, Kirch J, Cañadas O, Schneider M, Perez-Gil J, Schaefer UF, Casals C, and Lehr CM. Uptake of nanoparticles by alveolar macrophages is triggered by surfactant protein A. *Nanomedicine: Nanotechnology, Biology and Medicine* 2011 Dec; 7:690–3. DOI: 10.1016/J.NANO.2011.07.009
29. Radiom M, Sarkis M, Brookes O, Oikonomou EK, Baeza-Squiban A, and Berret JF. Pulmonary surfactant inhibition of nanoparticle uptake by alveolar epithelial cells. *Scientific Reports* 2020 Dec; 10. DOI: 10.1038/S41598-020-76332-7. Available from: /pmc/articles/PMC7655959/%20/pmc/articles/PMC7655959/?report=abstract%20https://www.ncbi.nlm.nih.gov/pmc/articles/PMC7655959/
30. Rothen-Rutishauser B, Clift MJ, Jud C, Fink A, and Wick P. Human epithelial cells in vitro – Are they an advantageous tool to help understand the nanomaterial-biological barrier interaction? *Euro Nanotox Letters* 2012 Jun; 4:1–20. Available from: http://ihcp.jrc.ec.europa.eu/our%7B%5C_%7Dactivities
31. Walker GM and Beebe DJ. A passive pumping method for microfluidic devices. *Lab on a Chip* 2002 Aug; 2:131–4. DOI: 10.1039/B204381E. Available from: https://pubs-rsc-org.ezproxy2.utwente.nl/en/content/articlehtml/2002/lc/b204381e%20https://pubs-rsc-org.ezproxy2.utwente.nl/en/content/articlelanding/2002/lc/b204381e
32. Shea-Donohue T. Gut Barrier: Adaptive Immunity. *Physiology of the Gastrointestinal Tract: Sixth Edition* 2018 Jan; 1-2:641–61. DOI: 10.1016/B978-0-12-809954-4.00026-8
33. Carterson AJ, Bentrup KH zu, Ott CM, Clarke MS, Pierson DL, Vanderburg CR, Buchanan KL, Nickerson CA, and Schurr MJ. A549 Lung Epithelial Cells Grown as Three-Dimensional Aggregates: Alternative Tissue Culture Model for *Pseudomonas aeruginosa* Pathogenesis. *Infection and Immunity* 2005 Feb; 73:1129. DOI: 10.1128/IAI.73.2.1129-1140.2005. Available from: /pmc/articles/PMC547019/%20/pmc/articles/PMC547019/?report=abstract%20https://www.ncbi.nlm.nih.gov/pmc/articles/PMC547019/
34. Wu J, Wang Y, Liu G, Jia Y, Yang J, Shi J, Dong J, Wei J, and Liu X. Characterization of air-liquid interface culture of A549 alveolar epithelial cells. *Brazilian Journal of Medical and Biological Research* 2017 Dec; 51. DOI: 10.1590/1414-431X20176950. Available from: http://www.scielo.br/j/bjmb/a/q4qVMmQkPnM8vvwsv4R5HJQ/?lang=en
35. Schneider YJ, Octave JN, and Trouet A. Chapter 10 The Role of Endocytosis and Lysosomes in Cell Physiology. *Current Topics in Membranes and Transport* 1985 Jan; 24:413–58. DOI: 10.1016/S0070-2161(08)60332-9

36. Irene Brandts, Marlid Garcia-Ordoñez, Lluís Tort, Mariana Teles, and Nerea Roher. Polystyrene nanoplastics accumulate in ZFL cell lysosomes and in zebrafish larvae after acute exposure, inducing a synergistic immune response in vitro without affecting larval survival in vivo. *Environmental Science: Nano* 2020 Aug; 7:2410–22. DOI: 10.1039/D0EN00553C. Available from: <https://pubs.rsc.org/en/content/articlehtml/2020/en/d0en00553c>
<https://pubs.rsc.org/en/content/articlelanding/2020/en/d0en00553c>
37. Jung YK, Shin E, and Kim BS. Cell Nucleus-Targeting Zwitterionic Carbon Dots. *Scientific Reports* 2015 5:1 2015 Dec; 5:1–9. DOI: 10.1038/srep18807. Available from: <https://www.nature.com/articles/srep18807>
38. Kankavi O and Roberts MS. Detection of surfactant protein A (SP-A) and surfactant protein D (SP-D) in equine synovial fluid with immunoblotting. *Canadian Journal of Veterinary Research* 2004 Apr; 68:146. Available from: </pmc/articles/PMC1142159/>
<https://www.ncbi.nlm.nih.gov/pmc/articles/PMC1142159/>
39. Ramezanpour M, Burke da Silva K, and Sanderson BJ. Differential susceptibilities of human lung, breast and skin cancer cell lines to killing by five sea anemone venoms. *Journal of Venomous Animals and Toxins Including Tropical Diseases* 2012; 18:157–63. DOI: 10.1590/S1678-91992012000200005

A Appendix

Formulas viscous finger patterning technique

$$V_f = n_{channels} \cdot 10 + 20 \quad (5)$$

$$V_{PBS,10X} = \frac{V_f}{10} \quad (6)$$

$$V_{i,collagen} = V_f \cdot \frac{C_f}{C_i} \quad (7)$$

$$V_{NaOH} = 0.009 \cdot V_{i,collagen} \quad (8)$$

$$V_{PBS} = V_f - V_{PBS,10X} - V_{i,collagen} - V_{NaOH} \quad (9)$$

Seeding channels

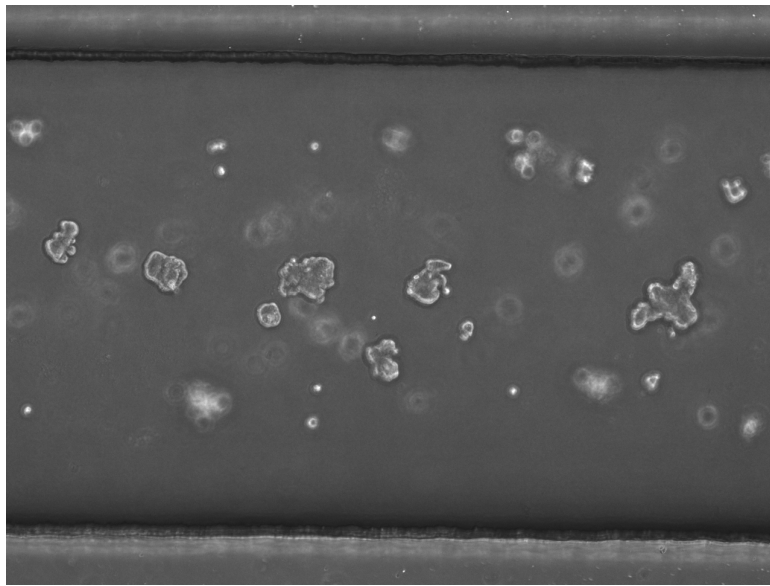


Figure 20: One day after seeding 1.5 million Calu-3 cells/mL which grow in small patches together.

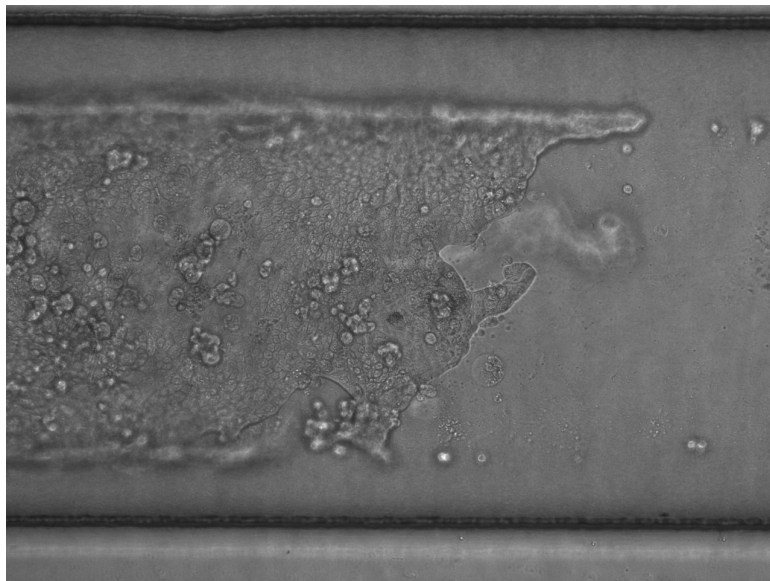


Figure 21: Fourteen days after seeding 1.5 million Calu-3 cells/mL which now created a barrier.

Determine adherence time of A549 cells

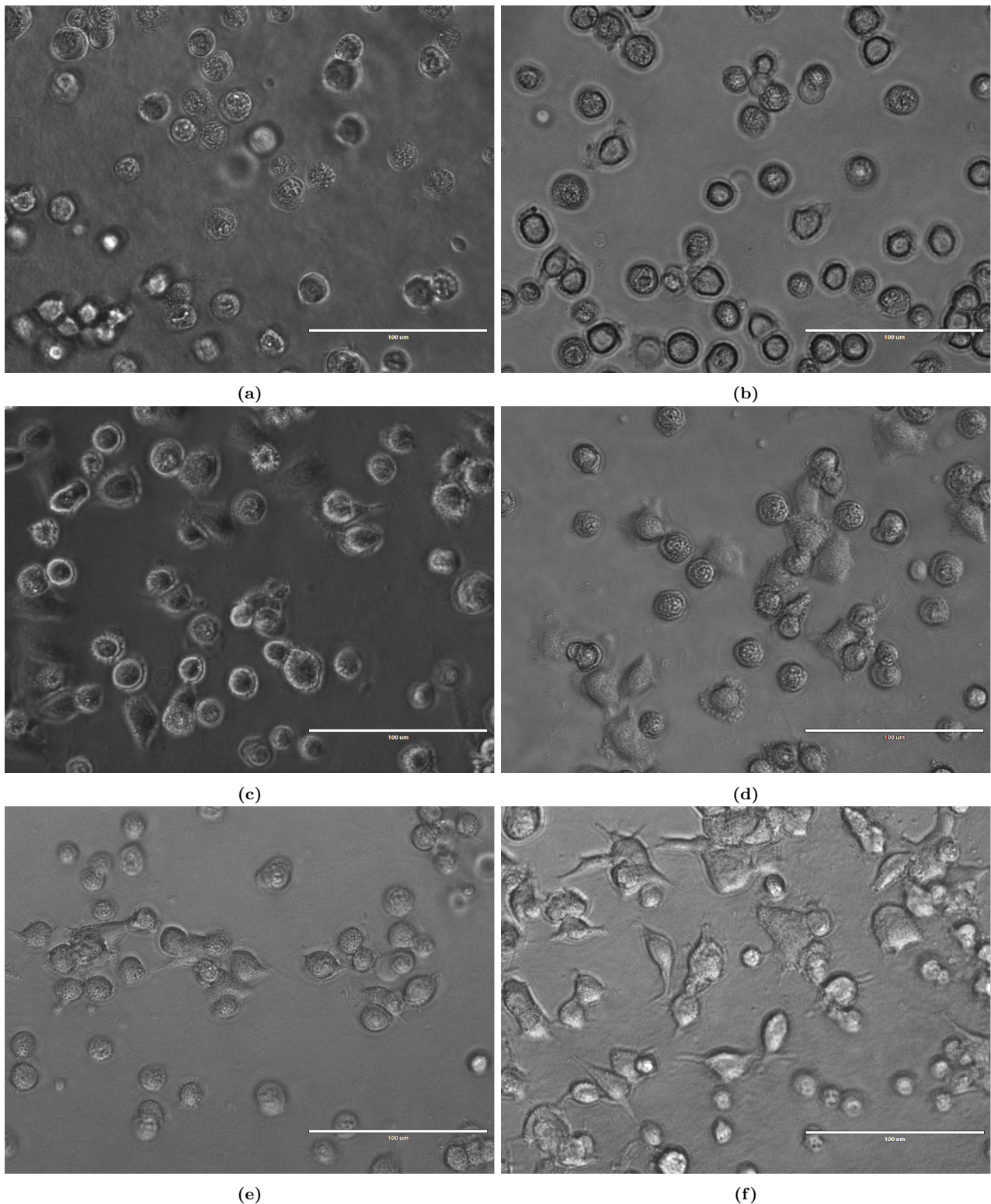


Figure 22: A) shows A549 cells seeded on a collagen layer in a well after 1 hour. Figure b) is after 2 hours, c) 3 hours, d) 4 hours, e) 6 hours and f) 24 hours. These pictures were made with the EVOS transmission microscope (Thermo Fisher scientific).

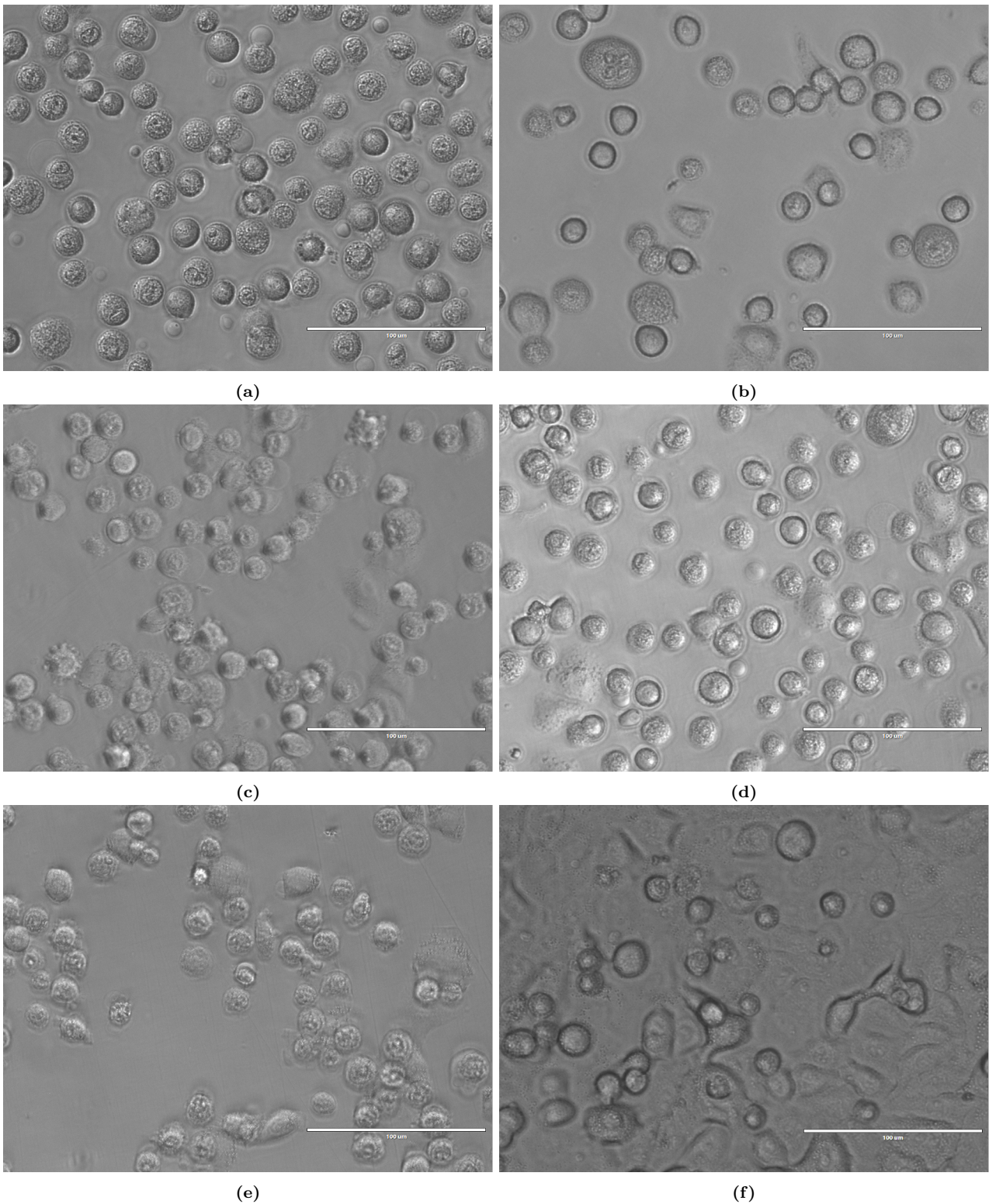


Figure 23: A) shows A549 cells seeded in a well after 1 hour. Figure b) is after 2 hours, c) 3 hours, d) 4 hours, e) 6 hours and f) 24 hours. These pictures were made with the EVOS transmission microscope (Thermo Fisher scientific).

Amount of nanoplastics in solution

The total amount of NPs/mL per condition is shown in figure 24 where a logarithmic relationship is chosen to display the particles per mL. These are theoretical values based on data given by the manufacturer Bangs Laboratories. A table of the NPs per mL is shown in table 2.

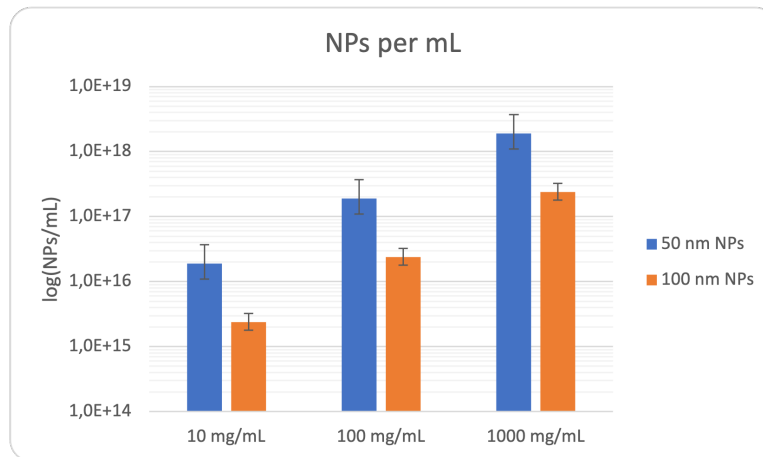


Figure 24: This figure shows the amount of NPs/mL which is calculated for the 3 concentrations and two sizes. These values were calculated using data provided by the manufacturer. The data was not proven using analytical methods.

Table 2: Values for the amount of NPs per mL of NP solution that was used for incubation with cells.

NPs size (nm)	Concentration NPs ($\mu\text{g/mL}$)	NPs/mL
50	10	1,9E+16
50	100	1,9E+17
50	1000	1,9E+18
100	10	2,4E+15
100	100	2,4E+16
100	1000	2,4E+17

Viability of A549 cells after exposure to NPs

Table 3: Values for the viability of A549 cells in channels after being exposed to NPs.

NPs size (nm)	Concentration NPs ($\mu\text{g/mL}$)	Mean viability (%)
50	10	96,5
50	100	86,5
50	1000	95,7
100	10	96,4
100	100	96,5
100	1000	95,5
Control	0	99,5

Table 4: Values for the viability of A549 cells in a well plate after being exposed to NPs.

NPs size (nm)	Concentration NPs (µg/mL)	Mean viability (%)
50	10	98,5
50	100	98,1
50	1000	97,1
100	10	97,9
100	100	96,1
100	1000	92,8
Control	0	99,0

Excitation wavelengths

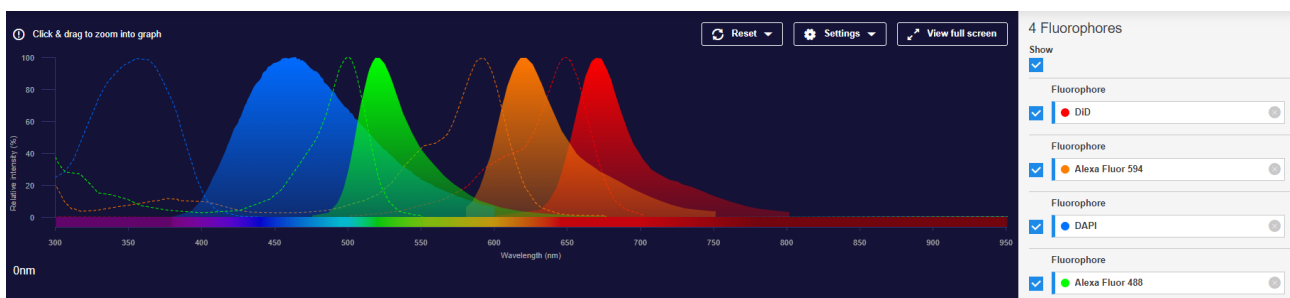


Figure 25: This figure shows the optimal wavelengths per stain, with the dashed line being the excitation wavelengths and the smooth line being the corresponding emitting wavelength. The red color stands for the cell membrane staining using DID, orange stands for the tight junctions staining using ZO-1 protein staining, blue is the nuclei staining using DAPI and the green colour are the NPs.

Translocation of nanoplastics

Chip

The colour coding for the confocal microscope images is as follows: blue (DAPI), green (NPs), red/yellow (DID + ZO-1).

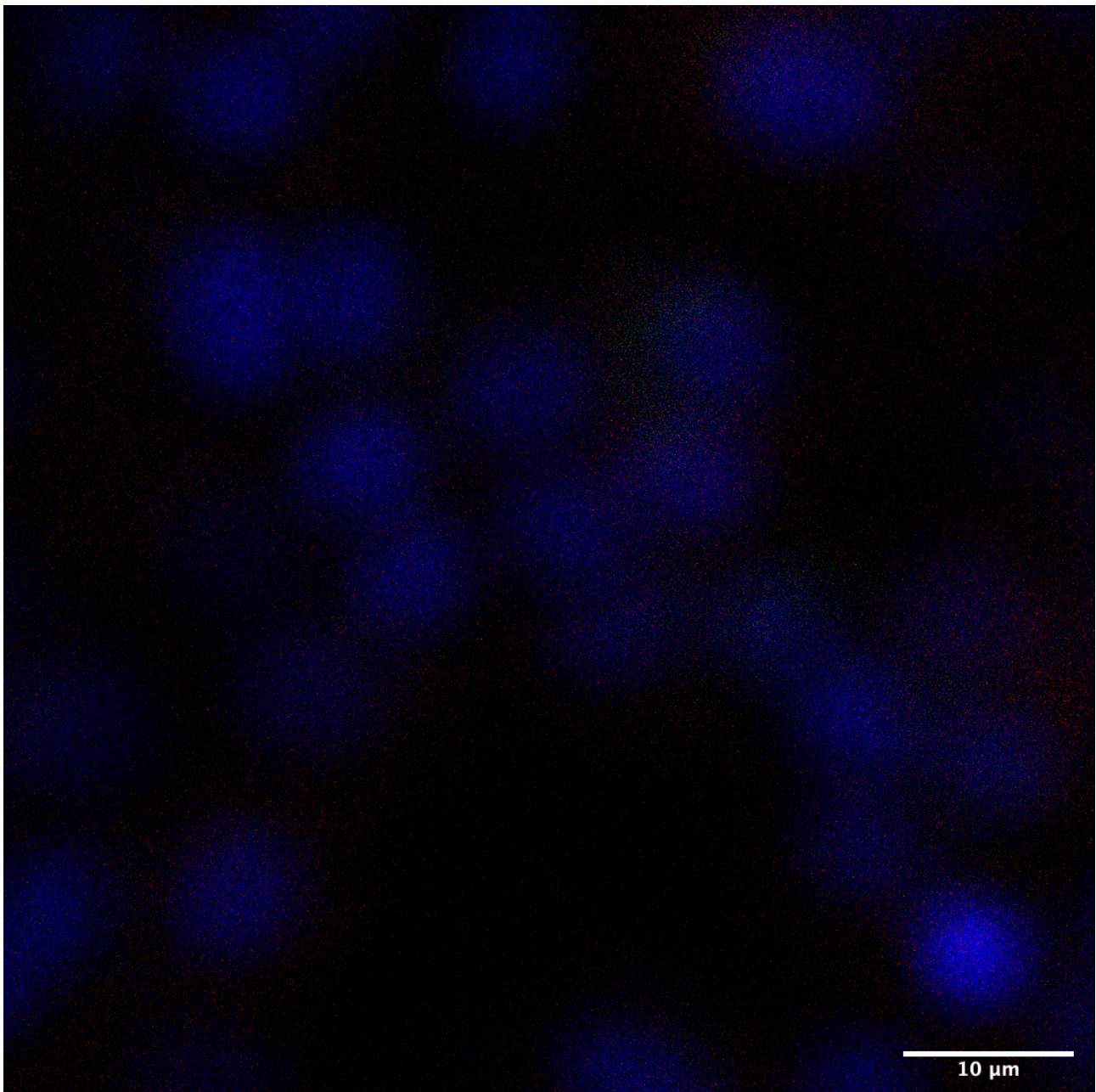


Figure 26: This figure presents 10 $\mu\text{g}/\text{mL}$ NPs with a size of 50 nm in a channel with A549 cells. The cells were incubated for 6 days after which the NPs were incubated for 24 hours. NPs were not visible in the collagen layer underneath the cells. This image was made using confocal laser microscopy Zeiss 880 and edited using Imagej.

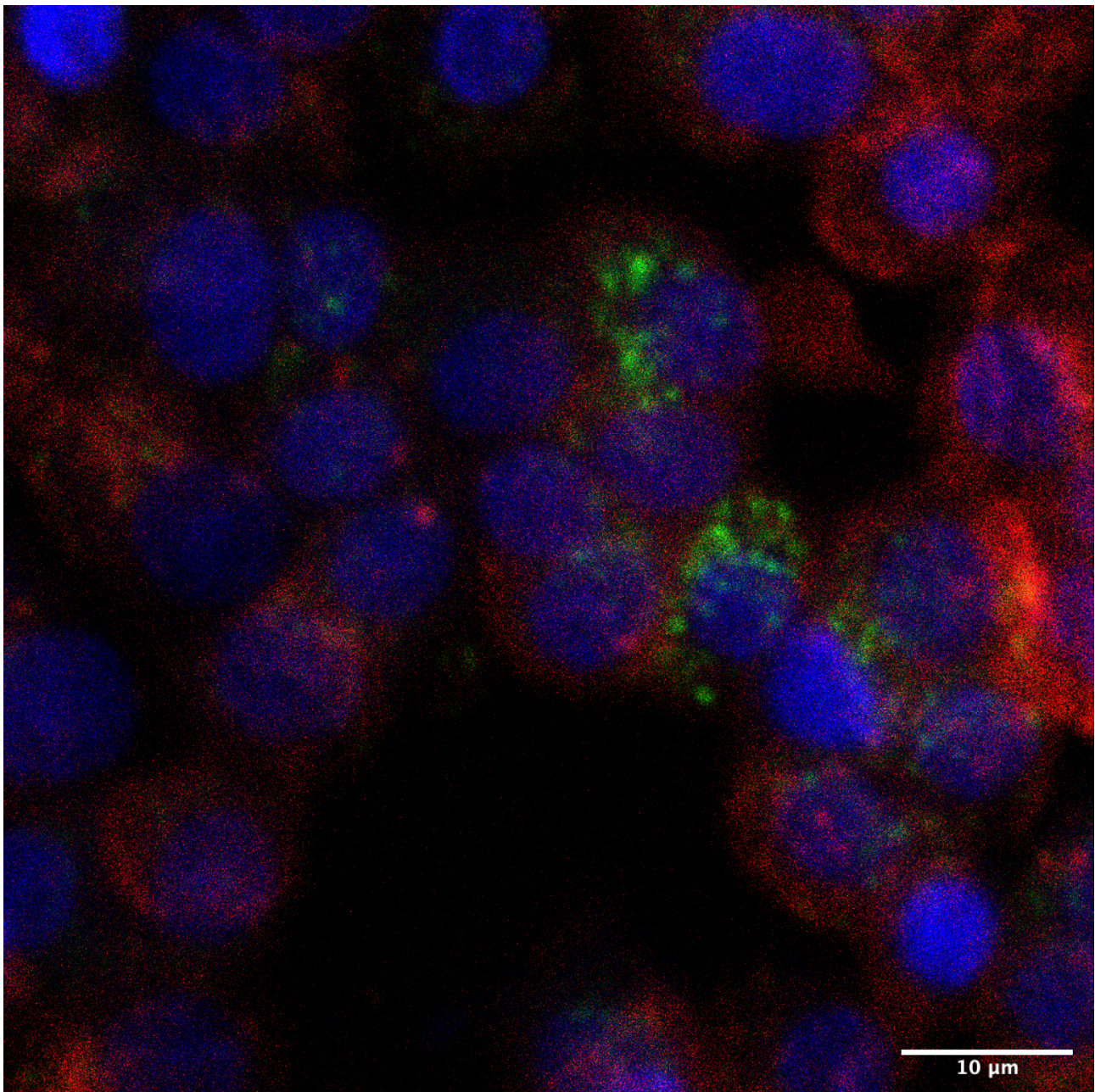


Figure 27: This figure presents 10 µg/mL NPs with a size of 50 nm in a channel with A549 cells. The cells were incubated for 6 days after which the NPs were incubated for 24 hours. NPs were visible in a few cells. This image was made using confocal laser microscopy Zeiss 880 and edited using Imagej.

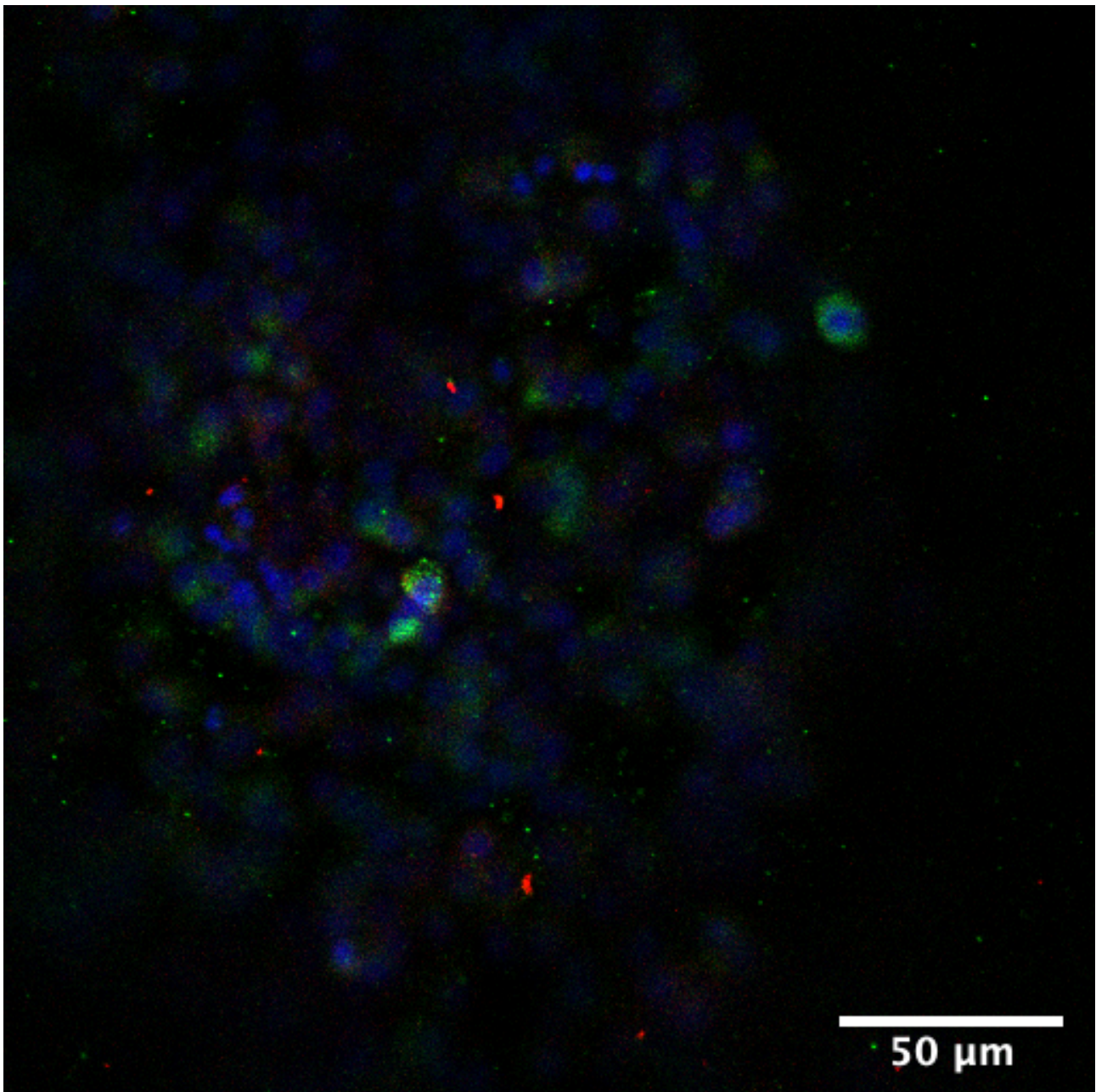


Figure 28: This figure presents 100 µg/mL NPs with a size of 50 nm in a channel with A549 cells. The cells were incubated for 6 days after which the NPs were incubated for 24 hours. A few NPs were visible in the collagen layer. This image was made using confocal laser microscopy Zeiss 880 and edited using Imagej.

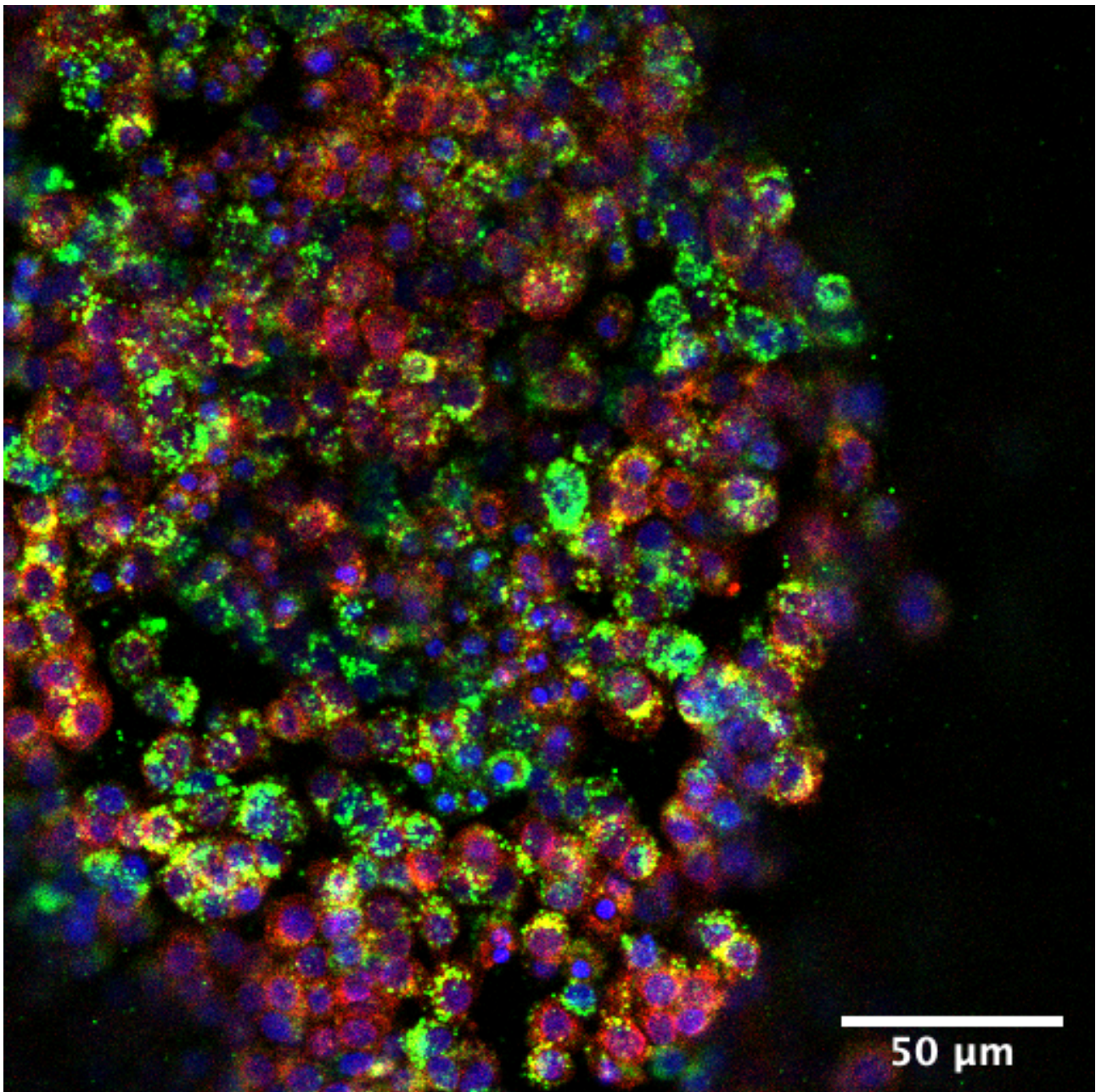


Figure 29: This figure presents 100 µg/mL NPs with a size of 50 nm in a channel with A549 cells. The cells were incubated for 6 days after which the NPs were incubated for 24 hours. NPs were visible in almost all cells. This image was made using confocal laser microscopy Zeiss 880 and edited using Imagej.

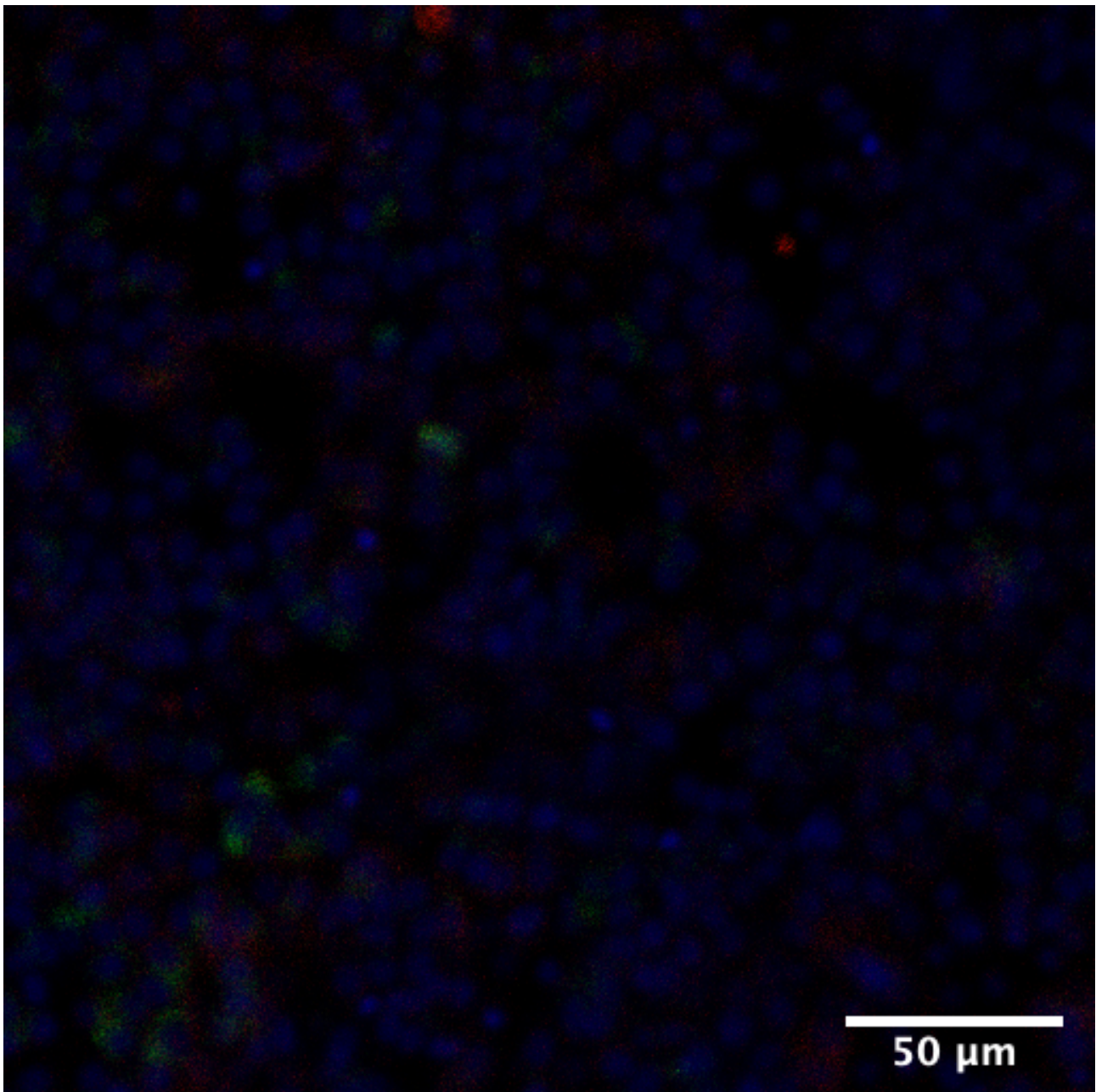


Figure 30: This figure presents 100 $\mu\text{g}/\text{mL}$ NPs with a size of 100 nm in a channel with A549 cells. The cells were incubated for 6 days after which the NPs were incubated for 24 hours. A few NPs were visible inside the collagen. This image was made using confocal laser microscopy Zeiss 880 and edited using Imagej.

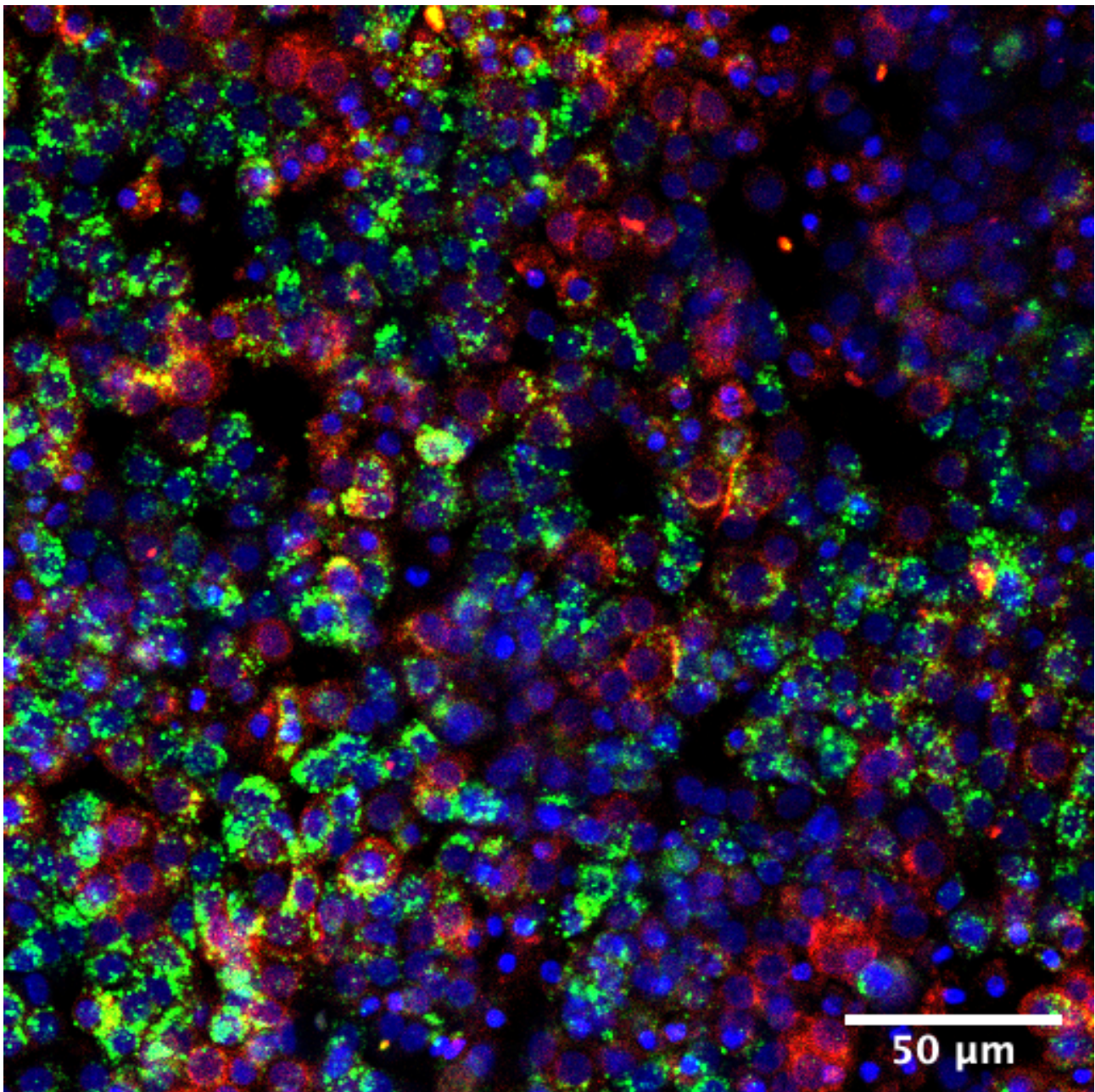


Figure 31: This figure presents 100 µg/mL NPs with a size of 100 nm in a channel with A549 cells. The cells were incubated for 6 days after which the NPs were incubated for 24 hours. NPs were visible in a lot of cells, however there were also a lot of cells which did not have NPs inside them. This image was made using confocal laser microscopy Zeiss 880 and edited using Imagej.

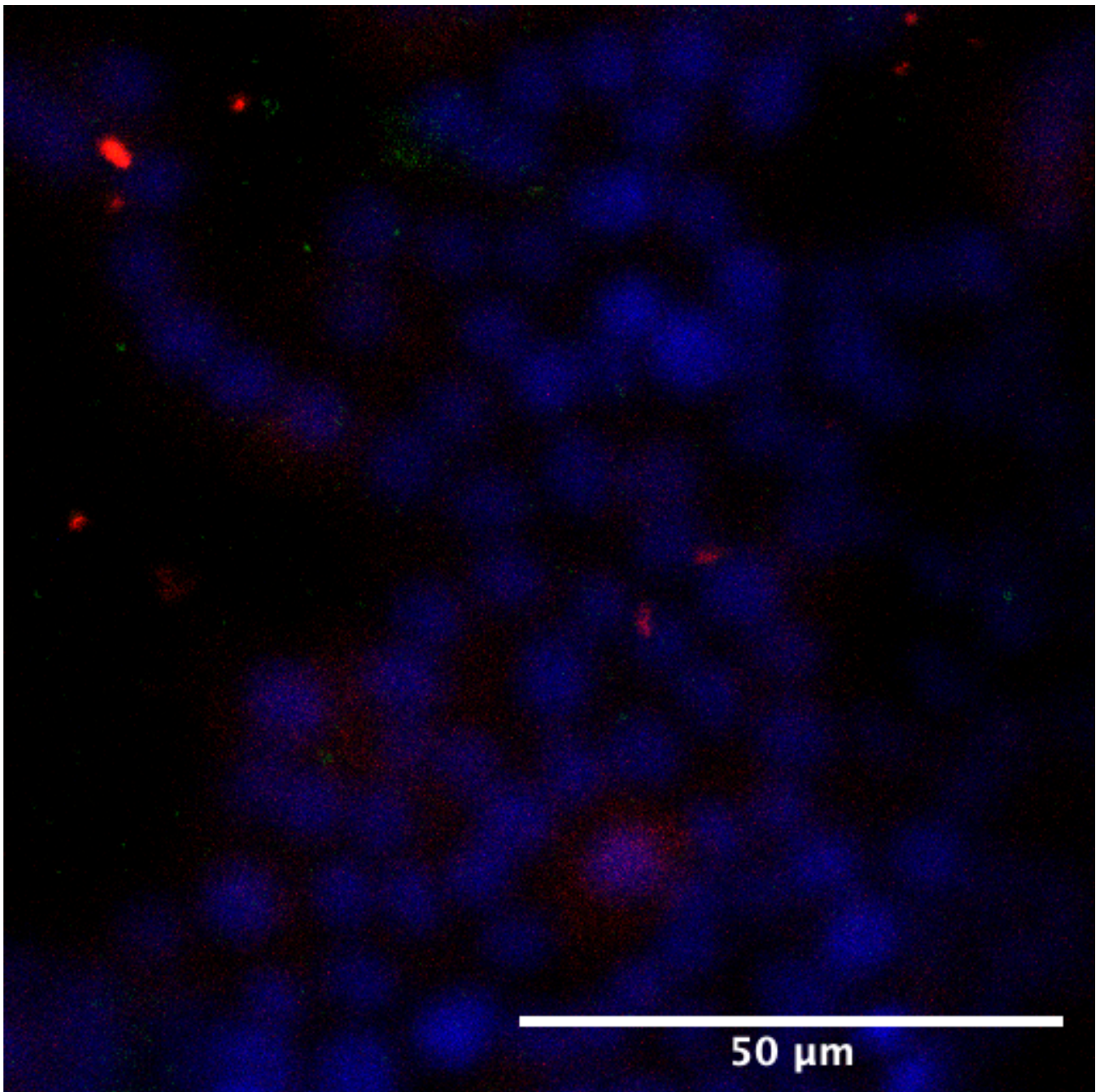


Figure 32: This figure presents 1000 µg/mL NPs with a size of 100 nm in a channel with A549 cells. The cells were incubated for 6 days after which the NPs were incubated for 24 hours. A few NPs were visible inside the collagen. This image was made using confocal laser microscopy Zeiss 880 and edited using Imagej.

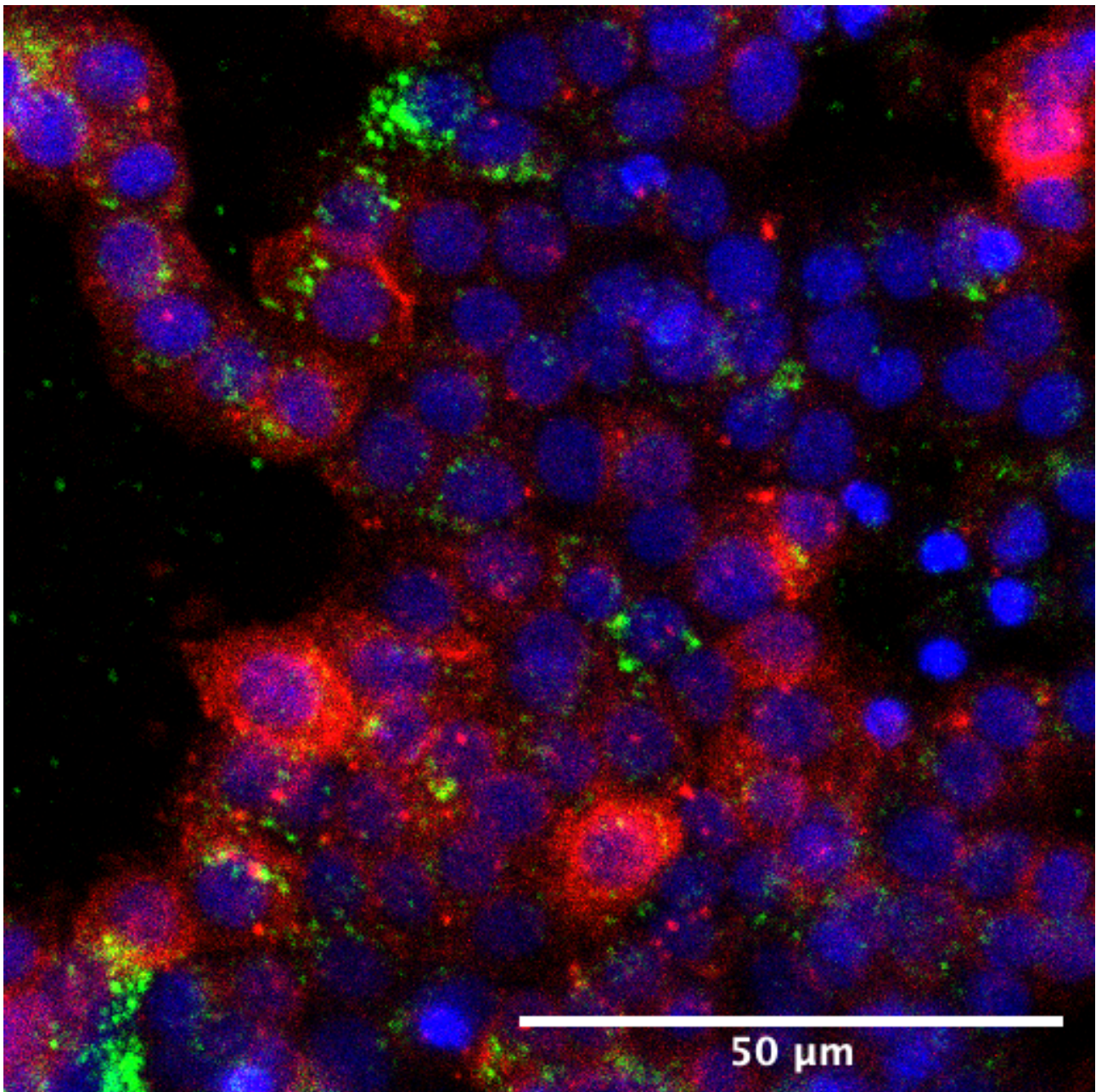


Figure 33: This figure presents 1000 µg/mL NPs with a size of 100 nm in a channel with A549 cells. The cells were incubated for 6 days after which the NPs were incubated for 24 hours. NPs were visible inside a lot of cells, however there were also a lot of cells which did not have NPs inside them. This image was made using confocal laser microscopy Zeiss 880 and edited using Imagej.

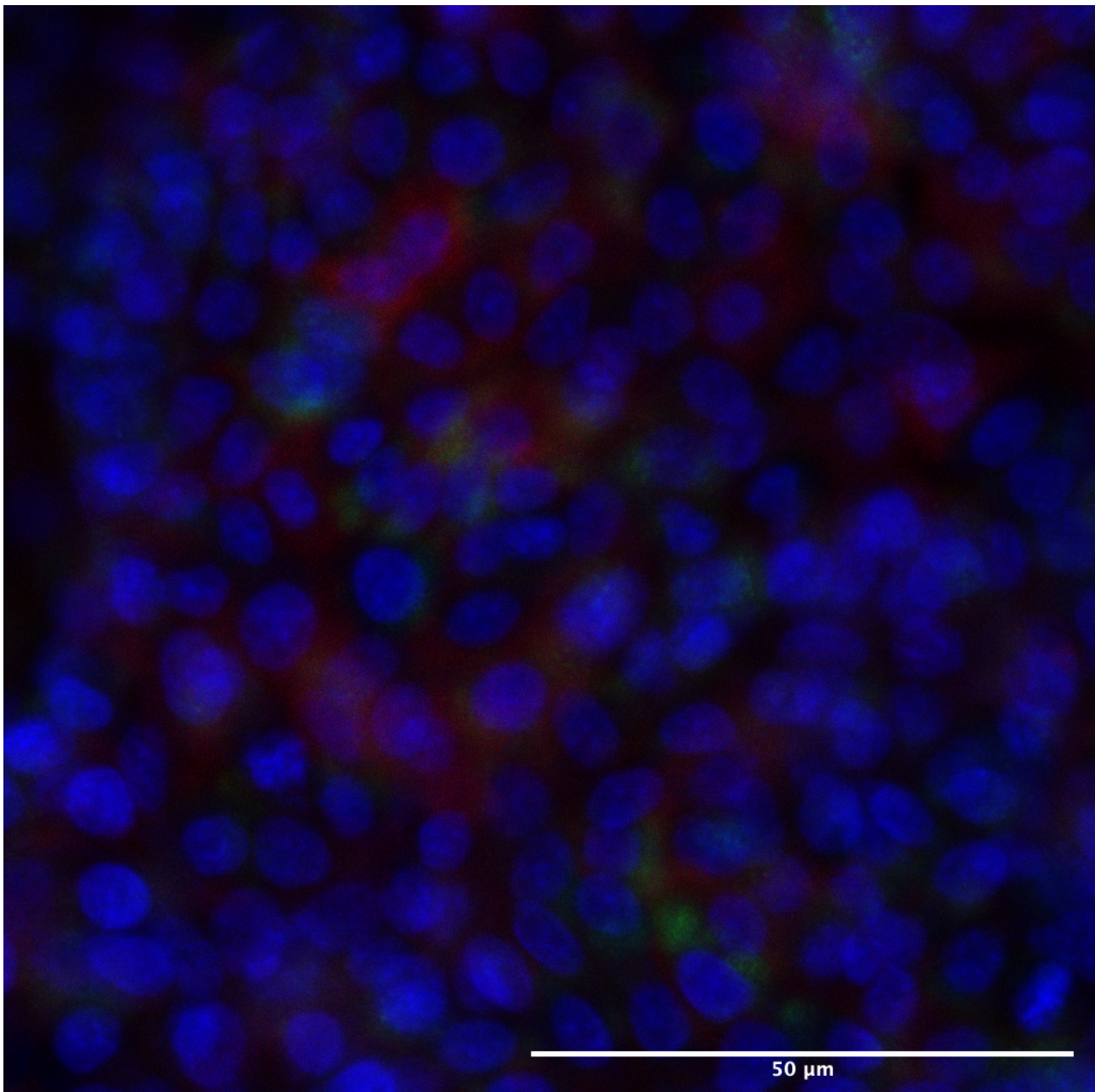


Figure 34: This figure presents 10 µg/mL NPs with a size of 50 nm in a channel with A549 cells. The cells were incubated for 6 days after which the NPs were incubated for 24 hours. No NPs were visible inside the collagen. This image was made using confocal laser microscopy Zeiss 880 and edited using Imagej.

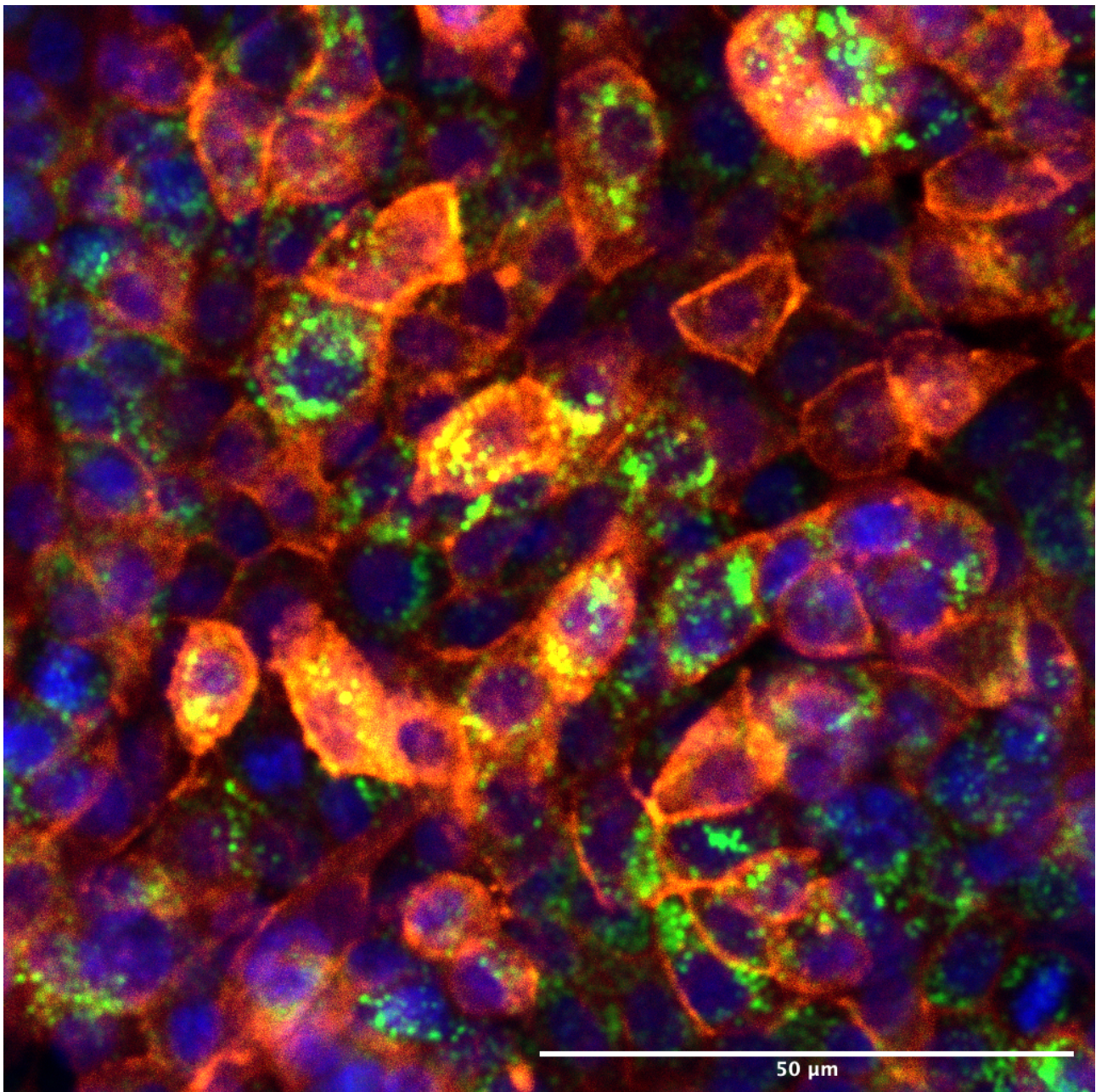


Figure 35: This figure presents 10 µg/mL NPs with a size of 50 nm in a channel with A549 cells. The cells were incubated for 6 days after which the NPs were incubated for 24 hours. NPs were visible inside a lot of cells, however there were also a lot of cells which did not have NPs inside them. This image was made using confocal laser microscopy Zeiss 880 and edited using Imagej.

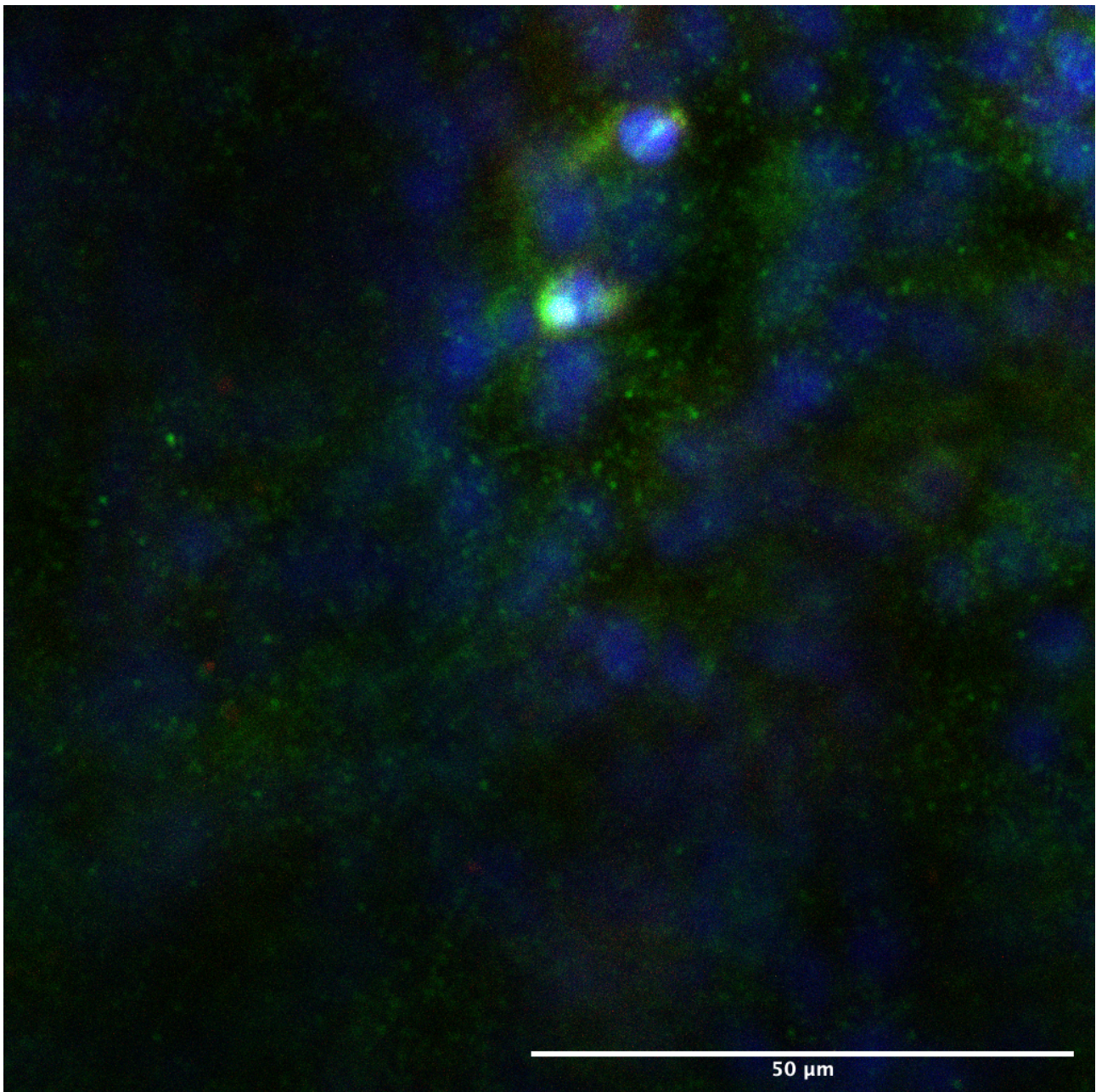


Figure 36: This figure presents 10 $\mu\text{g}/\text{mL}$ NPs with a size of 100 nm in the well plate with A549 cells. The cells were incubated for 3 days after which the NPs were incubated for 24 hours. No NPs were visible inside the collagen. This image was made using confocal laser microscopy Zeiss 880 and edited using Imagej.

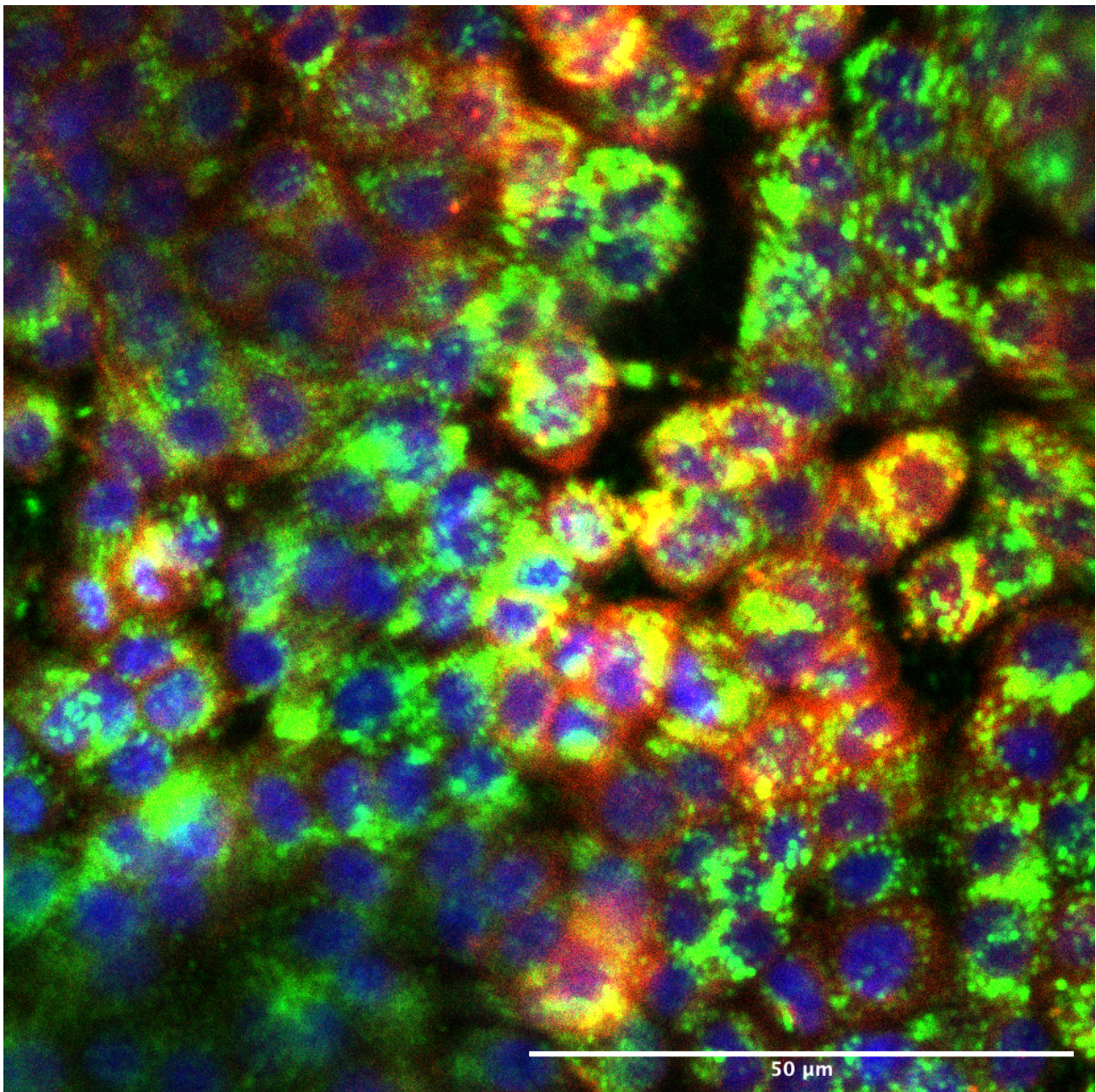
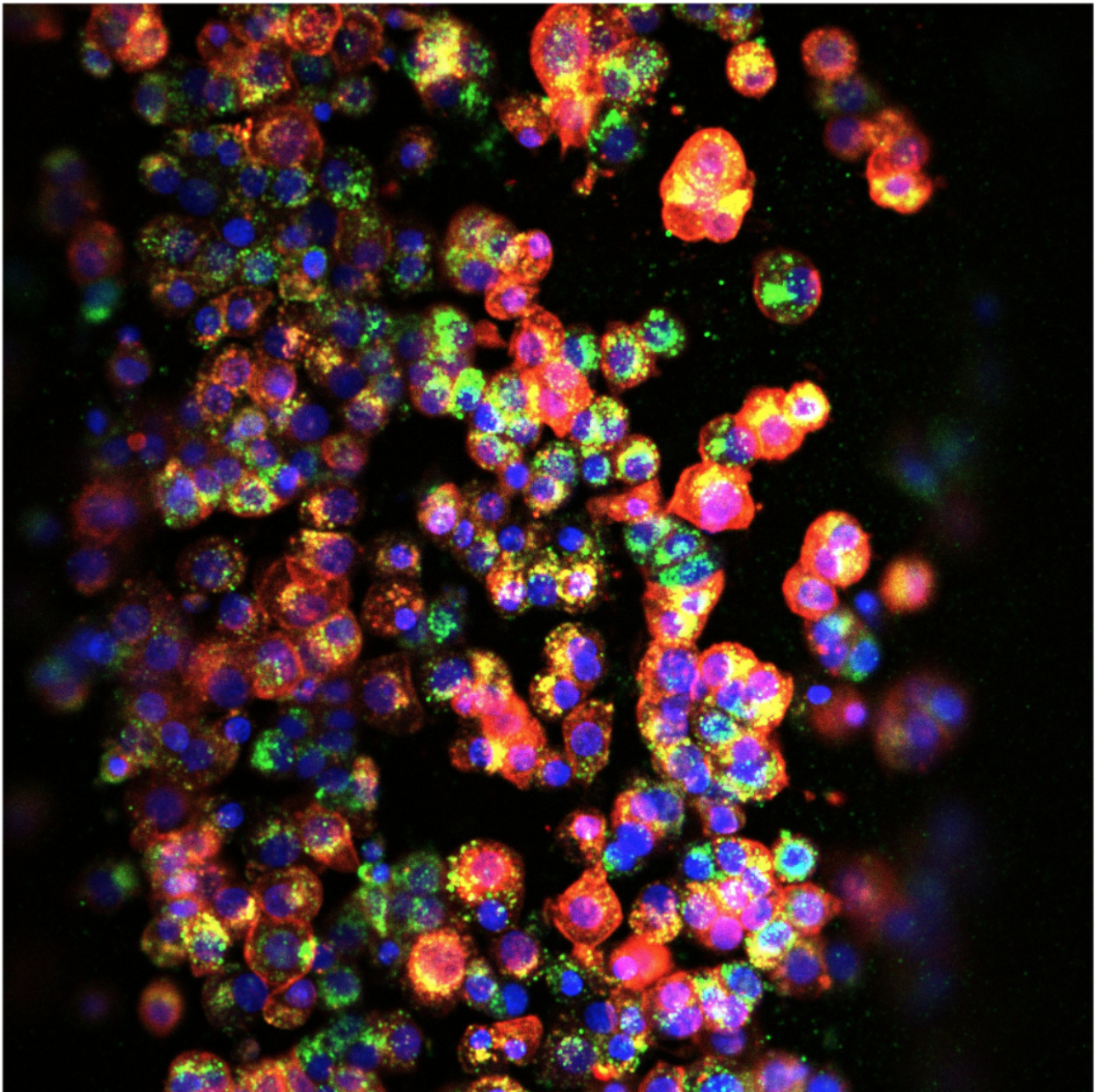
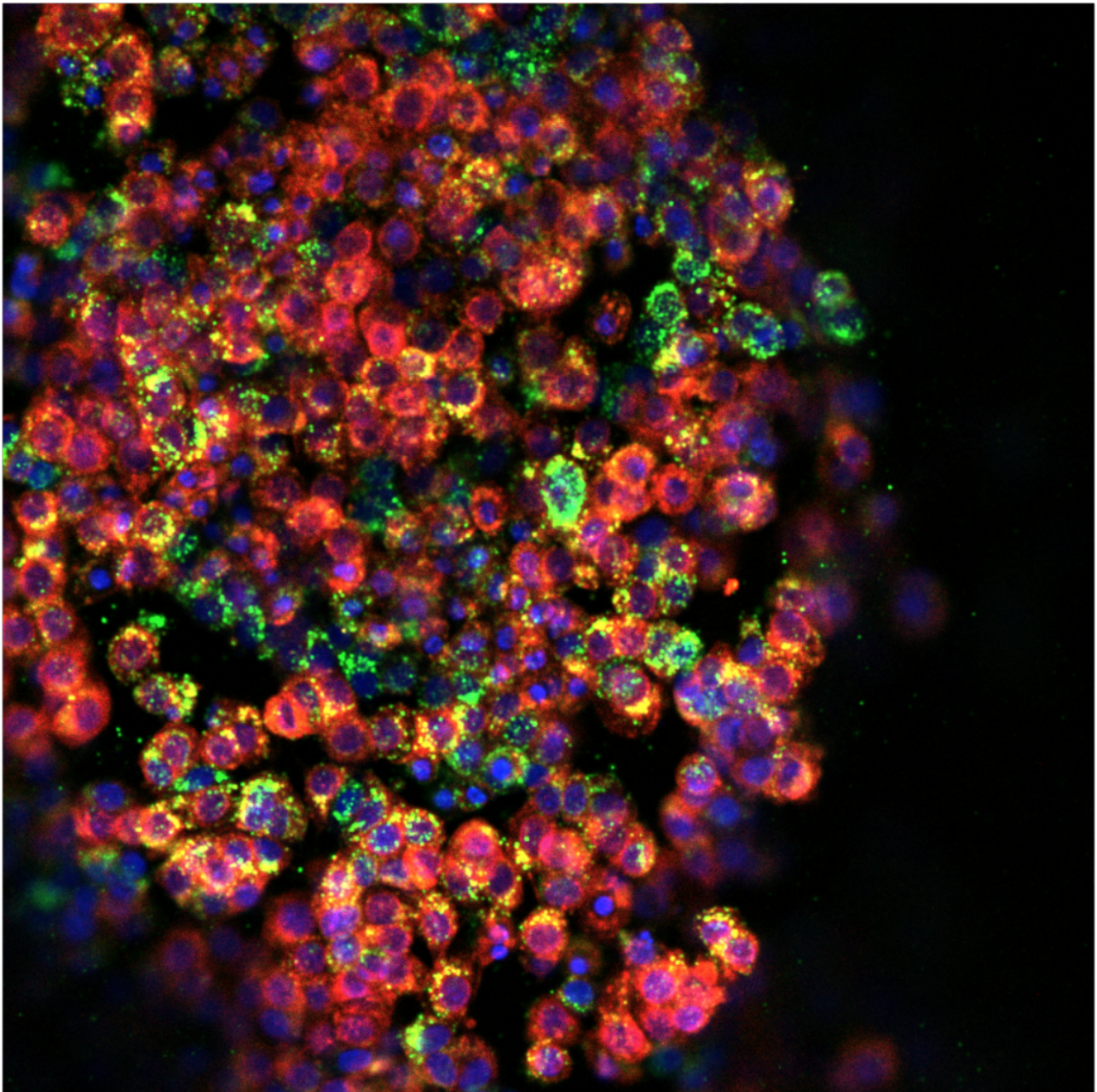


Figure 37: This figure presents 10 µg/mL NPs with a size of 100 nm in the well plate with A549 cells. The cells were incubated for 3 days after which the NPs were incubated for 24 hours. NPs were visible inside a lot of cells, however there were also a lot of cells which did not have NPs inside them. This image was made using confocal laser microscopy Zeiss 880 and edited using Imagej.



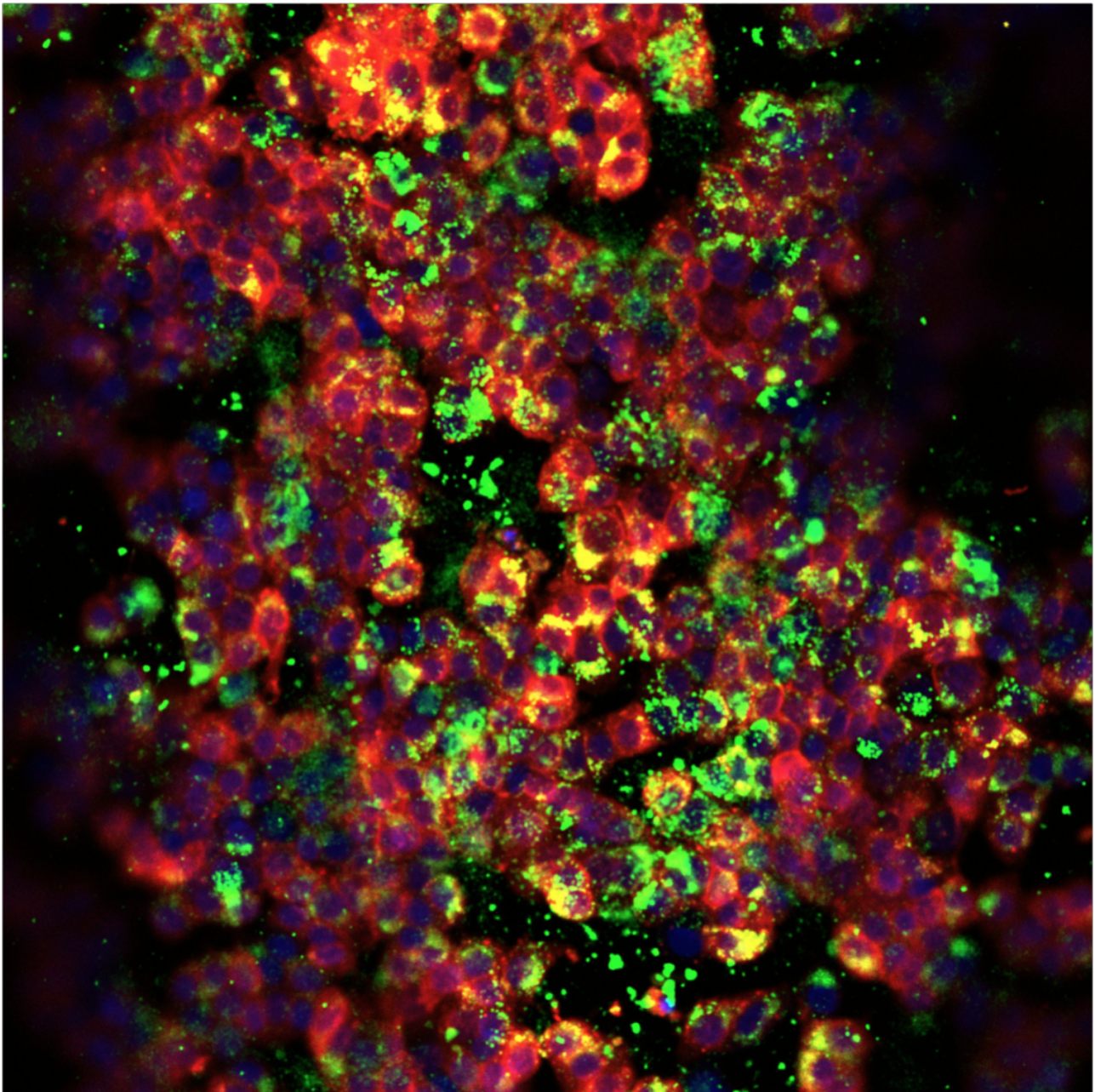
26 μm

Figure 38: This figure contains 10 $\mu\text{g}/\text{mL}$ NPs with a size of 50 nm in a channel with A549 cells. The cells were incubated for 6 days after which the NPs were incubated for 24 hours. NPs are translocated to almost every A549 cell. This image was made using confocal laser microscopy Zeiss 880 and edited using Imagej.



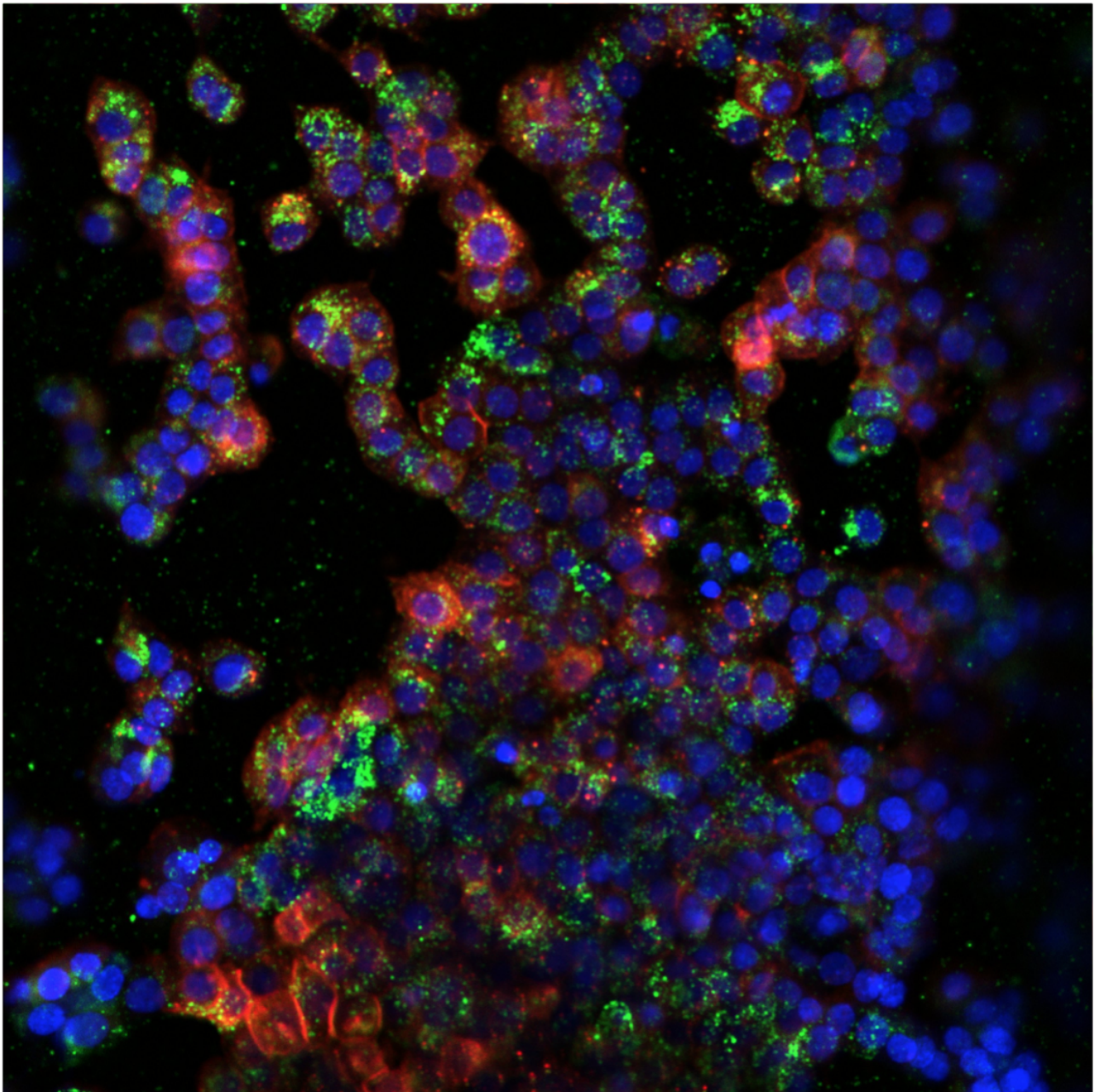
26 µm

Figure 39: This figure contains 100 µg/mL NPs with a size of 50 nm in a channel with A549 cells. The cells were incubated for 6 days after which the NPs were incubated for 24 hours. NPs are translocated to almost every A549 cell, however few NPs can be found outside the cells. This image was made using confocal laser microscopy Zeiss 880 and edited using Imagej.



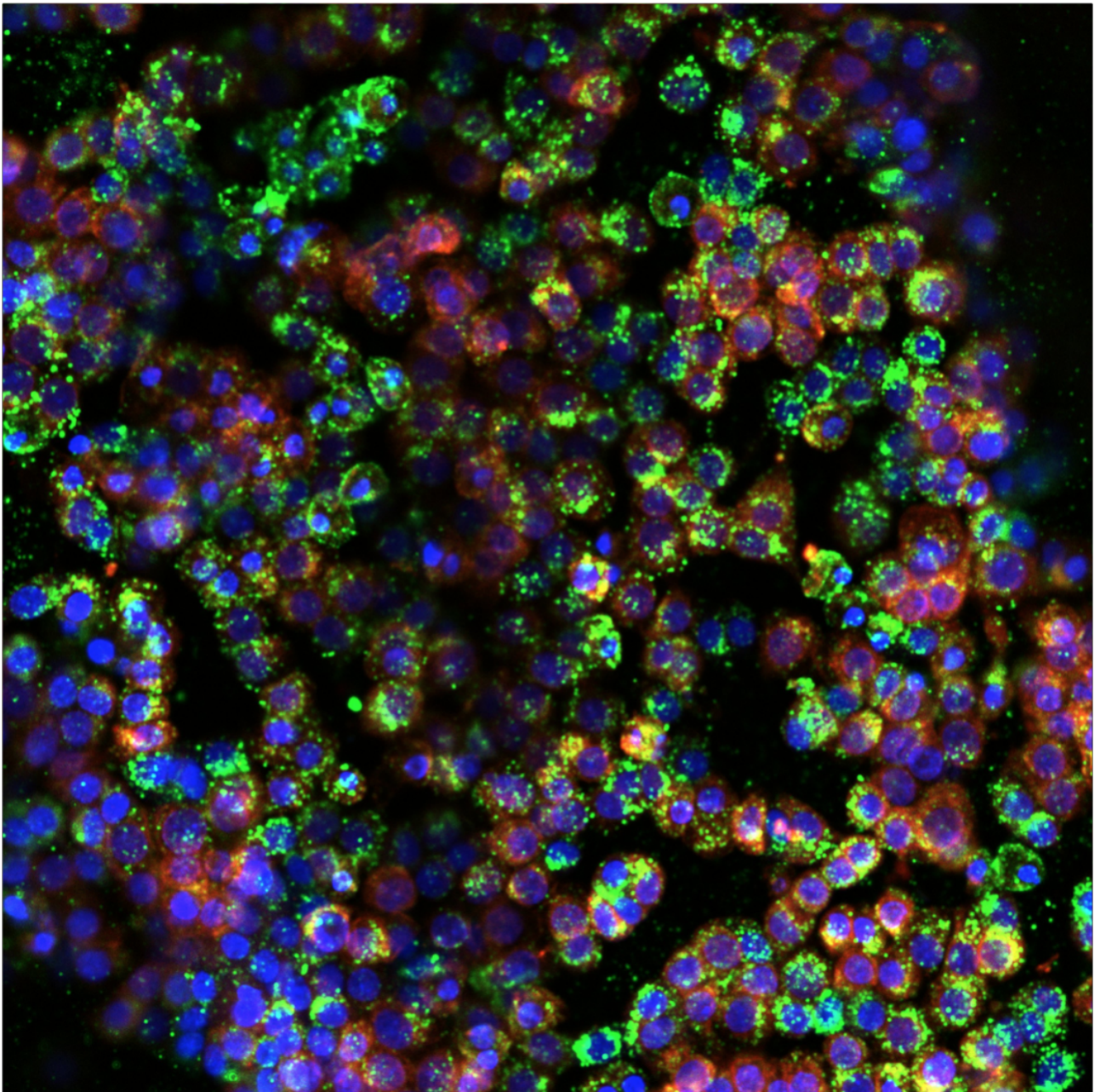
26 µm

Figure 40: This figure contains 1000 µg/mL NPs with a size of 50 nm in a channel with A549 cells. The cells were incubated for 6 days after which the NPs were incubated for 24 hours. NPs are translocated to many A549 cells, however NPs can also be found outside the cells. This image was made using confocal laser microscopy Zeiss 880 and edited using Imagej.



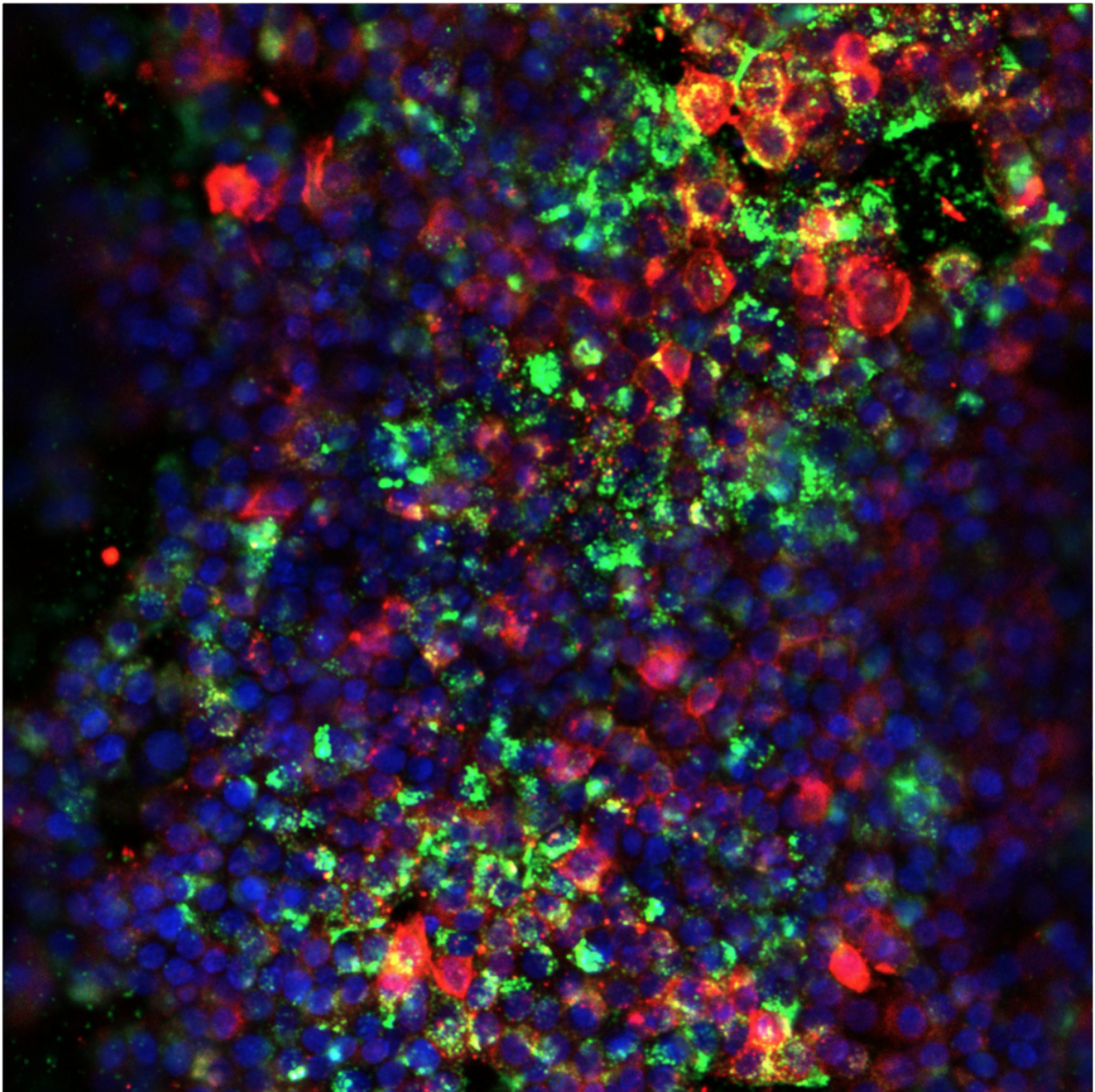
26 μm

Figure 41: This figure contains 10 $\mu\text{g}/\text{mL}$ NPs with a size of 100 nm in a channel with A549 cells. The cells were incubated for 6 days after which the NPs were incubated for 24 hours. NPs are translocated to almost every A549 cell. This image was made using confocal laser microscopy Zeiss 880 and edited using Imagej.



26 μm

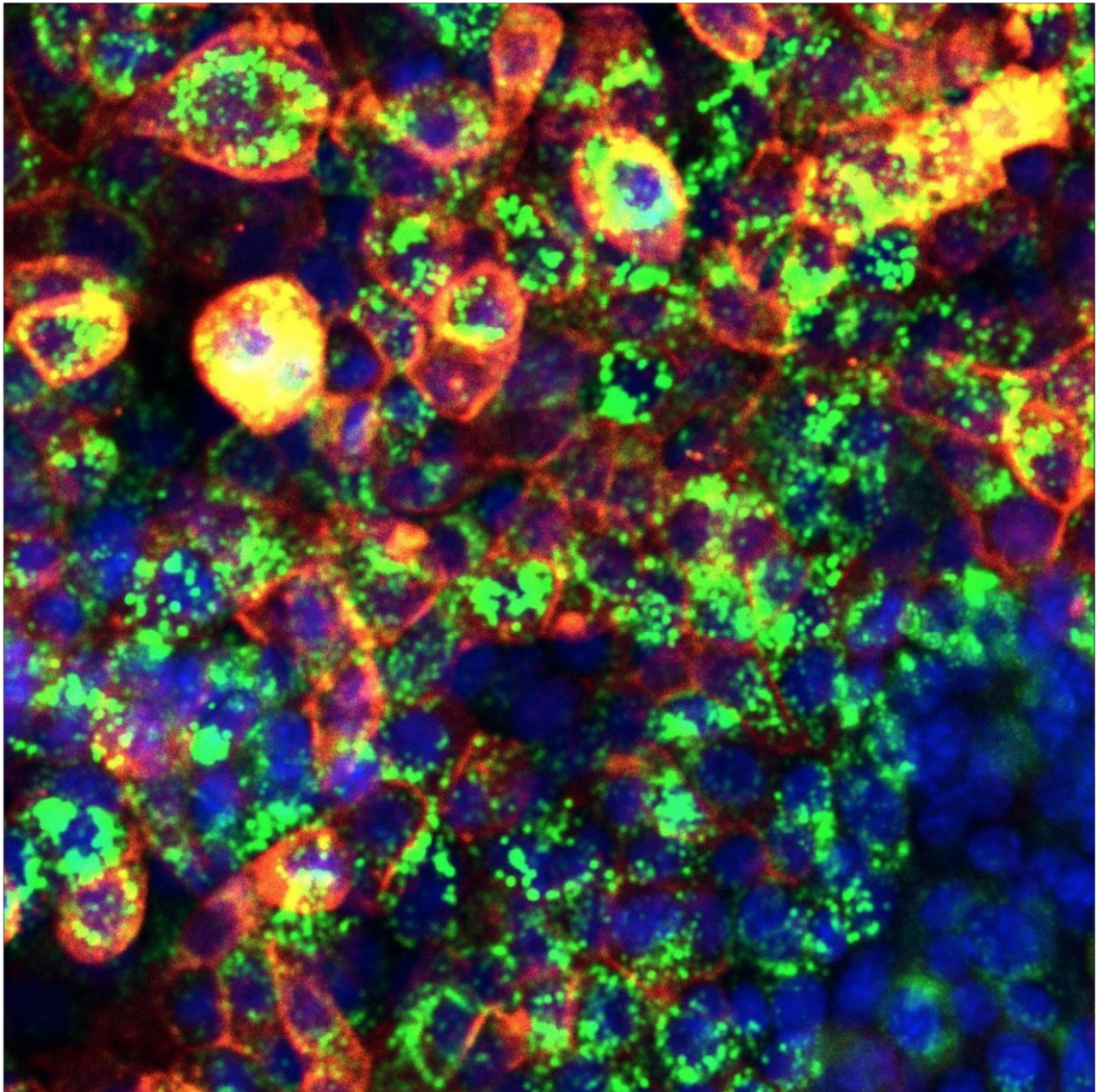
Figure 42: This figure contains 100 $\mu\text{g}/\text{mL}$ NPs with a size of 100 nm in a channel with A549 cells. The cells were incubated for 6 days after which the NPs were incubated for 24 hours. NPs are translocated to almost every A549 cell, however some NPs are visible outside the cells. This image was made using confocal laser microscopy Zeiss 880 and edited using Imagej.



26 µm

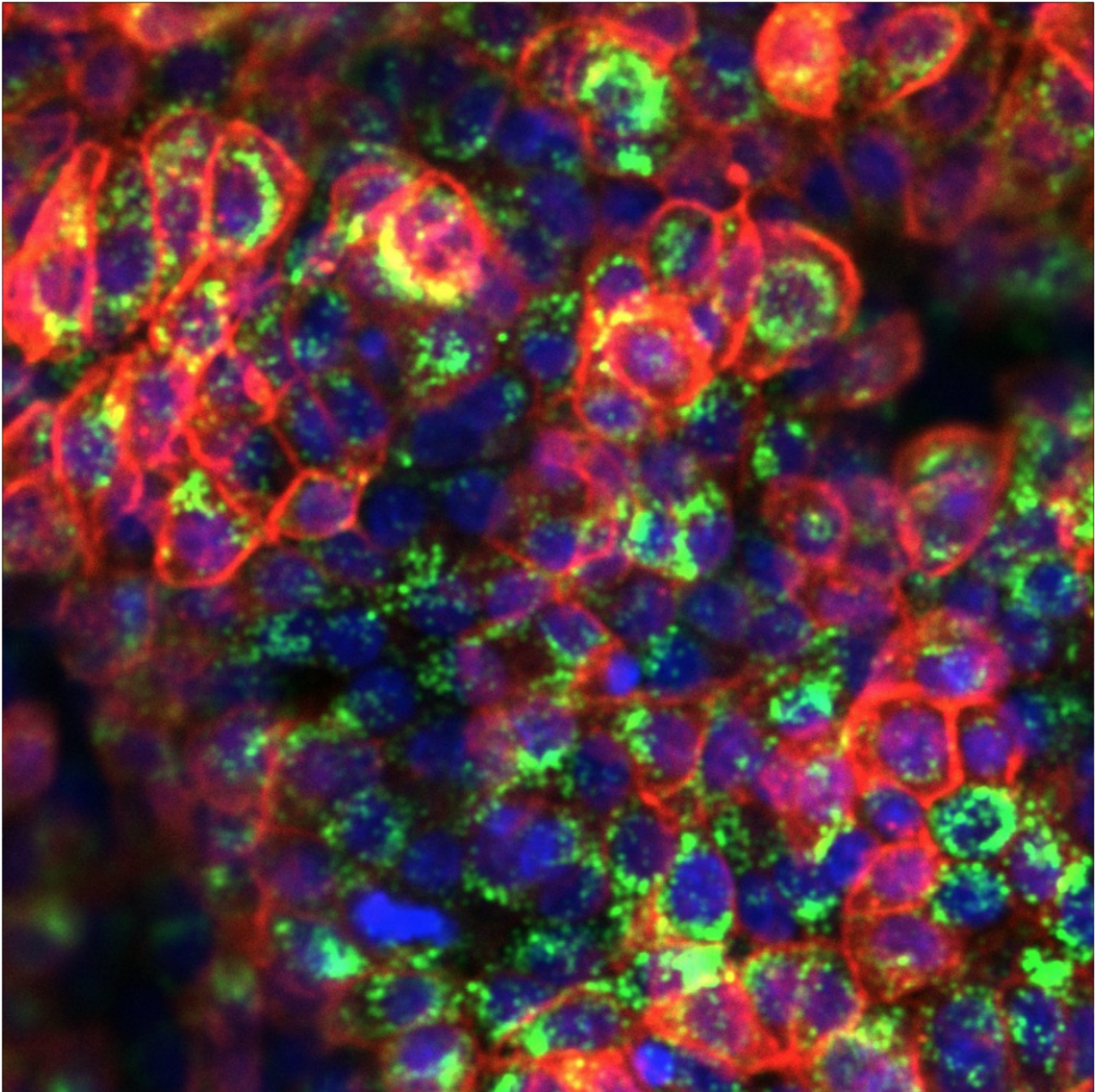
Figure 43: This figure contains 1000 µg/mL NPs with a size of 100 nm in a channel with A549 cells. The cells were incubated for 6 days after which the NPs were incubated for 24 hours. NPs are translocated to almost every A549 cell, however NPs are also visible outside the cells. Due to the high concentration and large size of NPs there is a bit of a haze visible. This image was made using confocal laser microscopy Zeiss 880 and edited using Imagej.

Well plate



13 µm

Figure 44: This figure contains 10 µg/mL NPs in the size 50 nm in a well with A549 cells. The cells were incubated for 3 days after which the NPs were incubated for 24 hours. NPs tend to stick to the outer cell membrane, however a lot of NPs can be found inside the cells. This image was made using confocal laser microscopy Zeiss 880 and edited using Imagej.



13 µm

Figure 45: This figure contains 100 µg/mL NPs in the size 50 nm in a well with A549 cells. The cells were incubated for 3 days after which the NPs were incubated for 24 hours. NPs tend to stick to the outer cell membrane, but are also taken up extensively by cells. This image was made using confocal laser microscopy Zeiss 880 and edited using Imagej.

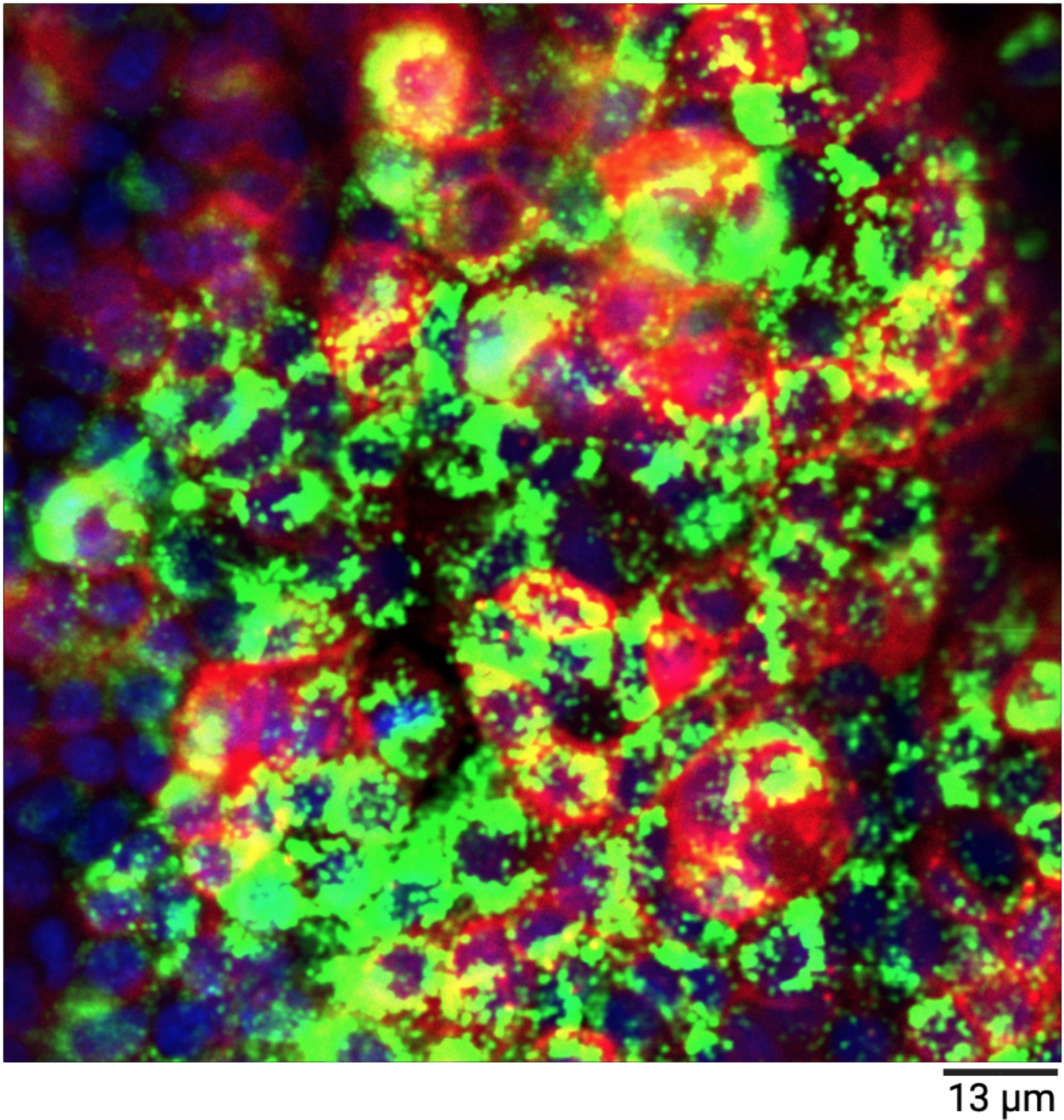
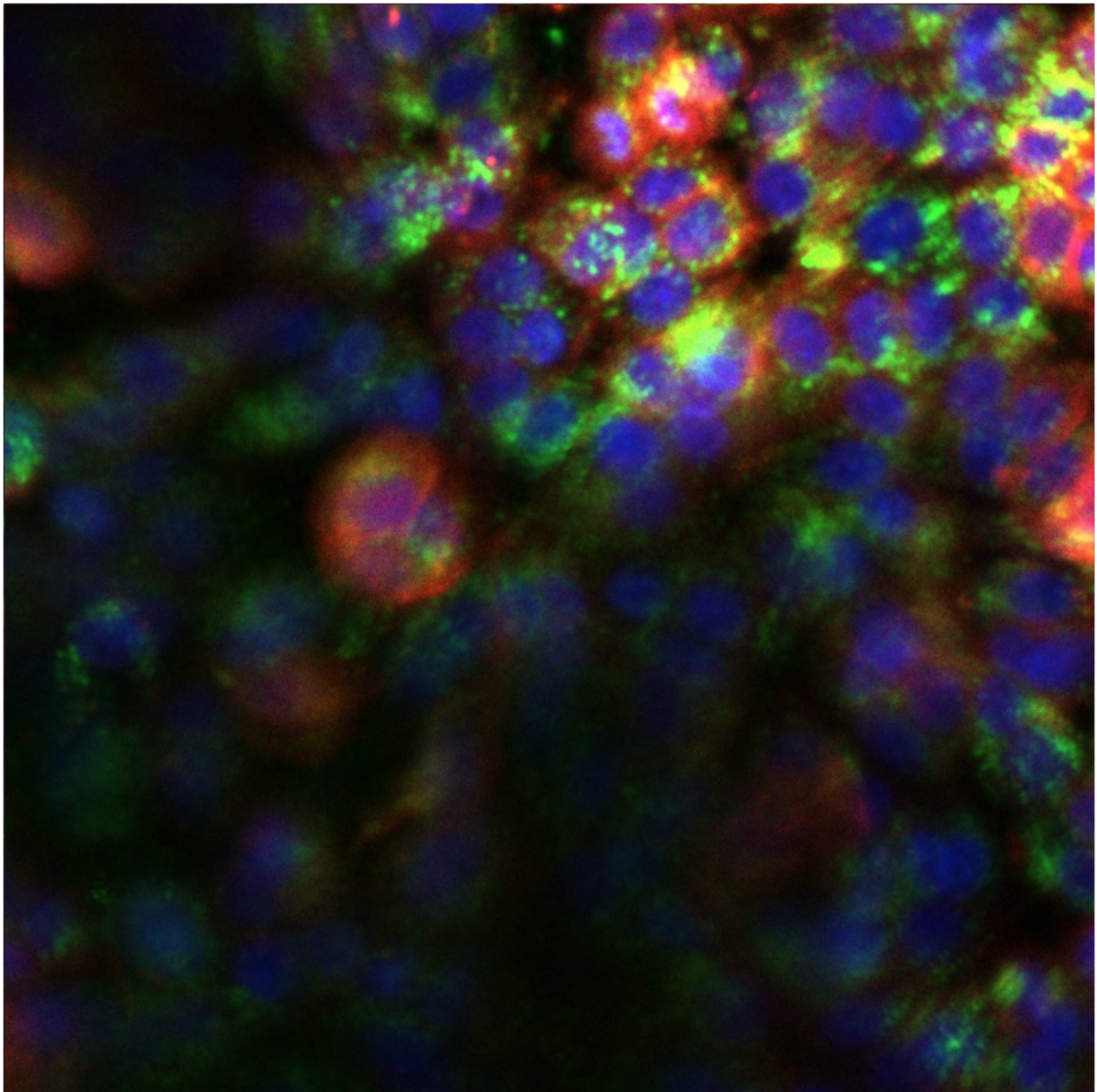
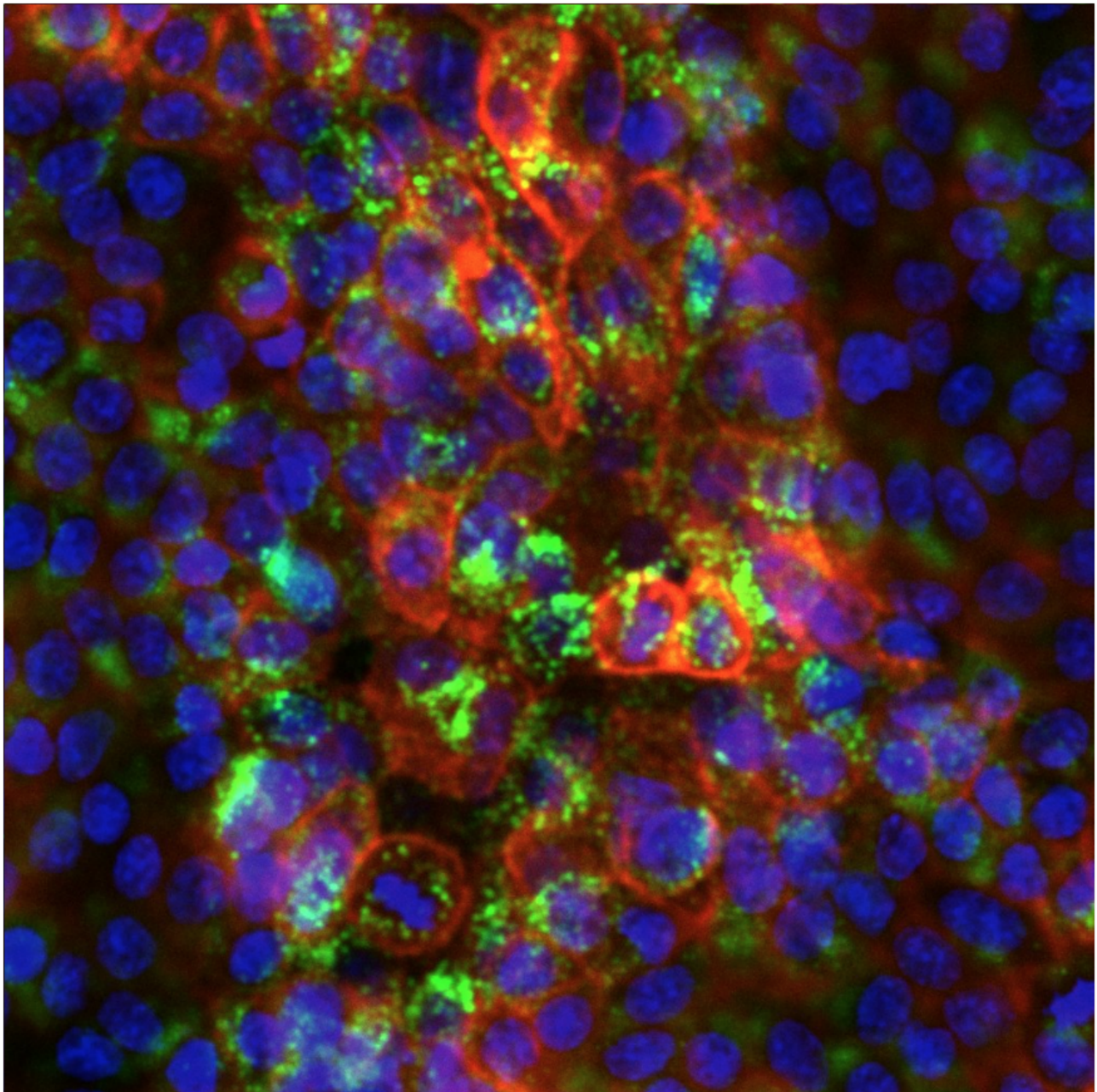


Figure 46: This figure contains 1000 µg/mL NPs in the size 50 nm in a well with A549 cells. The cells were incubated for 3 days after which the NPs were incubated for 24 hours. NPs are in abundance, also a greater amount tend to stick to the outer cell membrane. The NPs seem to have formed aggregates. This image was made using confocal laser microscopy Zeiss 880 and edited using Imagej.



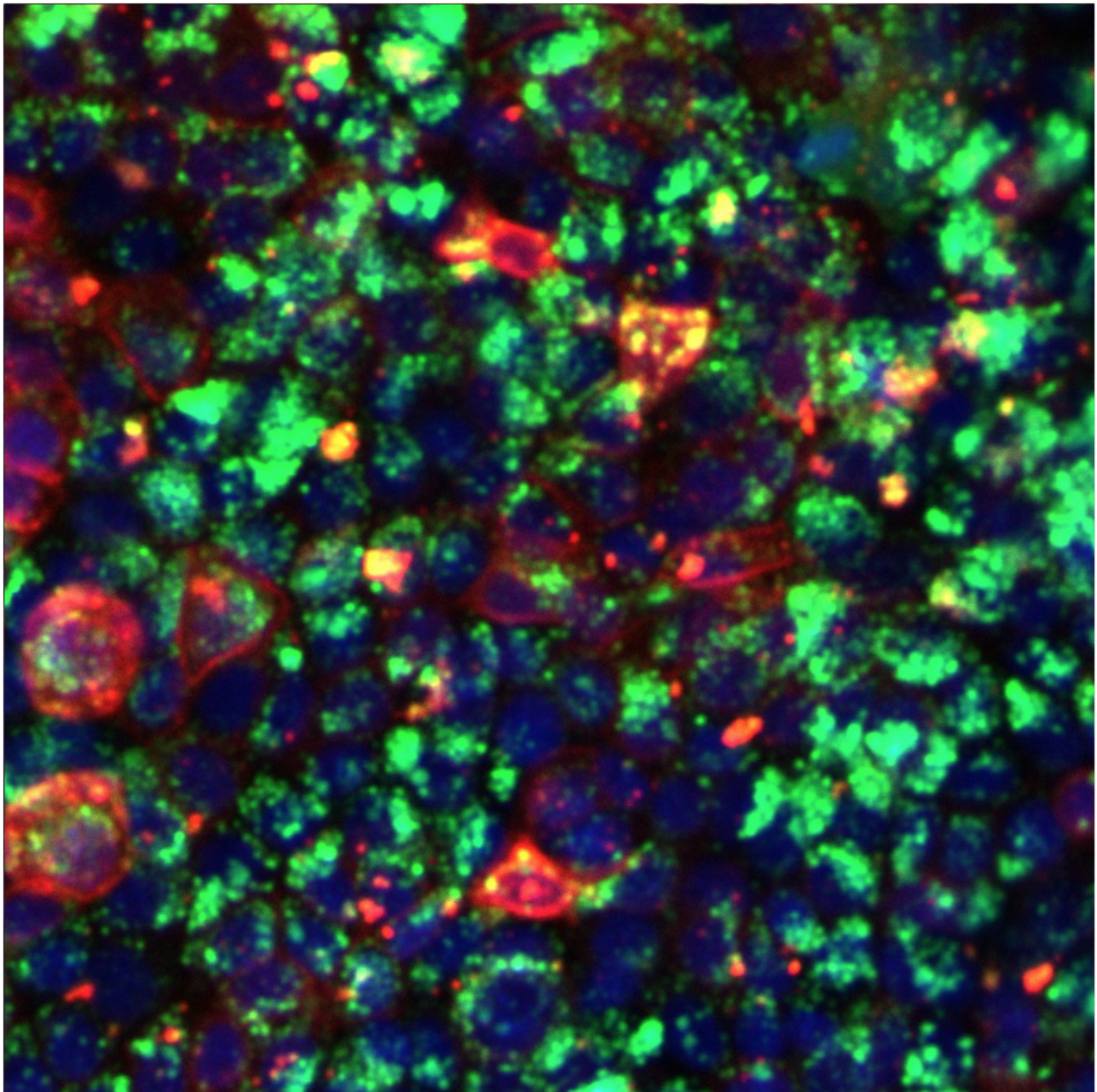
13 µm

Figure 47: This figure contains 10 µg/mL NPs in the size 100 nm in a well with A549 cells. The cells were incubated for 3 days after which the NPs were incubated for 24 hours. Most NPs are found in the cells, however it seems like some NPs stick to the outer cell membrane. This image was made using confocal laser microscopy Zeiss 880 and edited using Imagej.



13 µm

Figure 48: This figure contains 100 µg/mL NPs in the size 100 nm in a well with A549 cells. The cells were incubated for 3 days after which the NPs were incubated for 24 hours. Most cells have taken up NPs, however some NPs are visible outside the cells and sometimes NPs stick to the outside of the outer cell membrane. This image was made using confocal laser microscopy Zeiss 880 and edited using Imagej.



13 µm

Figure 49: This figure contains 1000 µg/mL NPs in the size 100 nm in a well with A549 cells. The cells were incubated for 3 days after which the NPs were incubated for 24 hours. NPs are present in abundance and tend to form aggregates. Due to the haze created by the high concentration of NPs cell membranes are hard to see, but it still looks like many cells have taken up NPs. This image was made using confocal laser microscopy Zeiss 880 and edited using Imagej.